Engineering Hypertrophic Chondrocyte-based Grafts for Enhanced Bone Regeneration

by

Jonathan C. Bernhard

Submitted in partial fulfillment of the
Requirements for the degree of
Doctor of Philosophy
in the Graduate School of Arts and Sciences

COLUMBIA UNIVERSITY

2016

ABSTRACT

Engineering Hypertrophic Chondrocyte-based Grafts for Enhanced Bone Regeneration

Jonathan C. Bernhard

Bone formation occurs through two ossification processes, intramembranous and endochondral. Intramembranous ossification is characterized by the direct differentiation of stem cells into osteoblasts, which then create bone. Endochondral ossification involves an intermediate step, as stem cells first differentiate into chondrocytes and produce a cartilage anlage. The chondrocytes mature into hypertrophic chondrocytes, which transform the cartilage anlage into bone. Bone tissue engineering has predominantly mimicked intramembranous ossification, creating osteoblast-based grafts through the direct differentiation of stem cells. Though successful in specific applications, greater adoption of osteoblast-based grafts has failed due to incomplete integration, limited regeneration, and poor mechanical maintenance. To overcome these obstacles, inspiration was drawn from native bone fracture repair, creating tissue engineered bone grafts replicating endochondral ossification.

Hypertrophic chondrocytes, the key cell in endochondral ossification, were differentiated from mesenchymal stem cell sources by first generating chondrocytes and then instigating maturation to hypertrophic chondrocytes. Conditions influencing this differentiation were investigated, indicating the necessity of prolonged chondrogenic cultivation and elevated oxygen concentrations to ensure widespread hypertrophic maturation. Comparing the bone production performance of differentiated hypertrophic chondrocytes to differentiated osteoblasts revealed that hypertrophic chondrocytes deposit significantly greater volume of bone mineral at a higher density than osteoblasts, albeit in a more juvenile form. When implanted subcutaneously, the hypertrophic chondrocytes stimulated turnover of this juvenile template into compact-like bone, whereas osteoblasts proceeded with processes similar to bone remodeling, generating spongy-

like bone. Implanting these tissue engineered constructs into an orthotopic, critical-sized femoral defect saw hypertrophic chondrocyte-based constructs integrate quickly with the femur and facilitate the creation of significantly more bone, resulting in a successful bridging of the defect. The success of hypertrophic chondrocyte-based grafts in overcoming the failures of tissue engineered bone grafts demonstrates the potential of endochondral ossification inspired bone strategies and prompts its further investigation towards clinical utilization.

TABLE OF CONTENTS

LIST OF TABLES

LIST OF FIGURES

ACKNOWLEDGMENTS

I would like to thank Dr. Gordana Vunjak-Novakovic for her fantastic mentorship, providing me the freedom to pursue my scientific whims and grow in my standing as an academic. Through I chased my research half way around the world; Dr. Vunjak-Novakovic was always there to provide support and a critical eye. I would also like to thank Dr. Sarindr "Ick" Bhumiratana, a great mentor during my first few years in the laboratory that was always willing to listen to my ideas and troubleshoot my concerns. I have enjoyed my time here in the Laboratory for Stem Cells and Tissue Engineering due to the excellence of these two mentors, and their ability to make me feel like an important member of the team.

A wonderful year of my dissertation research was completed in Vienna, Austria, as I split my presence between the Ludwig Boltzmann Institute for Clinical and Experimental Traumatology and the Institute for Biochemical Engineering at the University of Applied Sciences, Technikum Wien. For this amazing opportunity I have to thank Dr. Heinz Redl, who was willing to accommodate my extreme projects and has constantly offered excitement and support for my academic career. I would like to also thank Dr. Ruenzler, Dr. Teuschl, and Dr. Fuchs who provided space and expertise at the Technikum Wien, along with their constant positive attitudes, excitement for science, and acceptance into their research "family".

During my work in these two great cities, New York and Vienna, I have had the pleasure to work with some amazing people. I would like to personally thank all of the individuals that have had a direct impact on my research, and have helped me along the way: Susanna Betti, Dr. James Ferguson, Susan Halligan, Patrick Hiemel, Elizabeth Hulphers, Nathan Kim, Dr. Benjamin Lee, Dr. Gabriele Leinfellner, Dominika Lidinsky, Alessandro Marturano, Xavier Monteforte, Dr. Darja Morlat, Dr. Thomas Nau, Johnathan Ng, Dr. Sylvia Nuernberger, Bernhard Rieder, Sharon Shu, Dr. Paul Slezak, Dr. Stefan Tangl, Dr. Andreas Tueschl.

PART I

INTRODUCTION

1 Background

Bone is formed and maintained following an intricate and finely balanced set of processes that requires coordination and cooperation of various cell types, such as osteocytes, osteoblasts, and osteoclasts (1). These cells are sensitive to chemical and mechanical stimuli and actively communicate with one another (1, 2). Herein lays the greatest challenge for tissue engineers, as constructed bone grafts must adapt to the challenging environment and various cell types in order to be successful (3). Recently within tissue engineering, a "developmental paradigm" has gained popularity, attempting to closely mimic the native processes of tissue formation and repair to improve construct success (4). Therefore, native bone formation processes were used as inspiration to design new grafts with clinical potential.

1.1 Bone Biology:

Bone is a truly remarkable material, providing exceptional strength with minimal weight (5), which allows it to serve as the body's support structure. In this role, bone protects the vital internal organs, withstands load, and serves as levers for muscle contraction to produce movement (2, 6). Though commonly seen as inert, bone is a dynamic organ, constantly remodeling in response to stimuli, participating in metabolic activity as a mineral reservoir, and housing the bone marrow (3, 7, 8).

The skeleton is composed of a variety of bone types, geometries, and mechanical properties. Bone can be divided into two main types, cortical (80%) and cancellous bone (20%), which combine in different ratios to construct various bones (9). Cortical bone is compact, solid and strong (12-20 GPa stiffness) while cancellous bone forms in a honeycomb shape consisting of trabeculae filled with bone marrow (0.2-0.9 GPa stiffness) (9, 10). An example of the

combination of these two bone types is the femur, which contains an outer shell of cortical bone that surrounds an interior of bone marrow and cancellous bone (Figure 1.1 (11)).

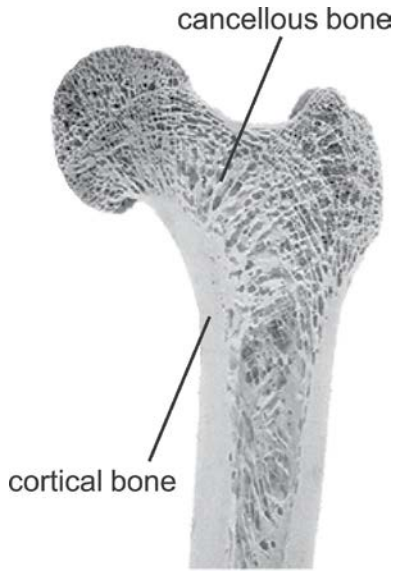

Figure 1.1: Cortical and cancellous bone in the adult, human femur*. The dense cortical bone forms a shell around the inner, porous cancellous bone. Within the pore space of the cancellous bone resides the bone marrow (11).*

1.2 BONE DEVELOPMENT

Bone formation occurs in humans about 4 weeks post-conception through the two ossification pathways, intramembranous ossification and endochondral ossification (2). In intramembranous ossification, osteoblasts directly differentiate from mesenchymal stem sources (MSC) and deposit bone within the existing fibrous matrix, with the formed bone often characterized by spicule formation (Figure 1.2) (12, 13). These spicules grow, fuse into trabeculae, and are later remodeled into mature bone (14, 15). Intramembranous ossification is responsible for the formation of the cranium and rib cage flat bones.

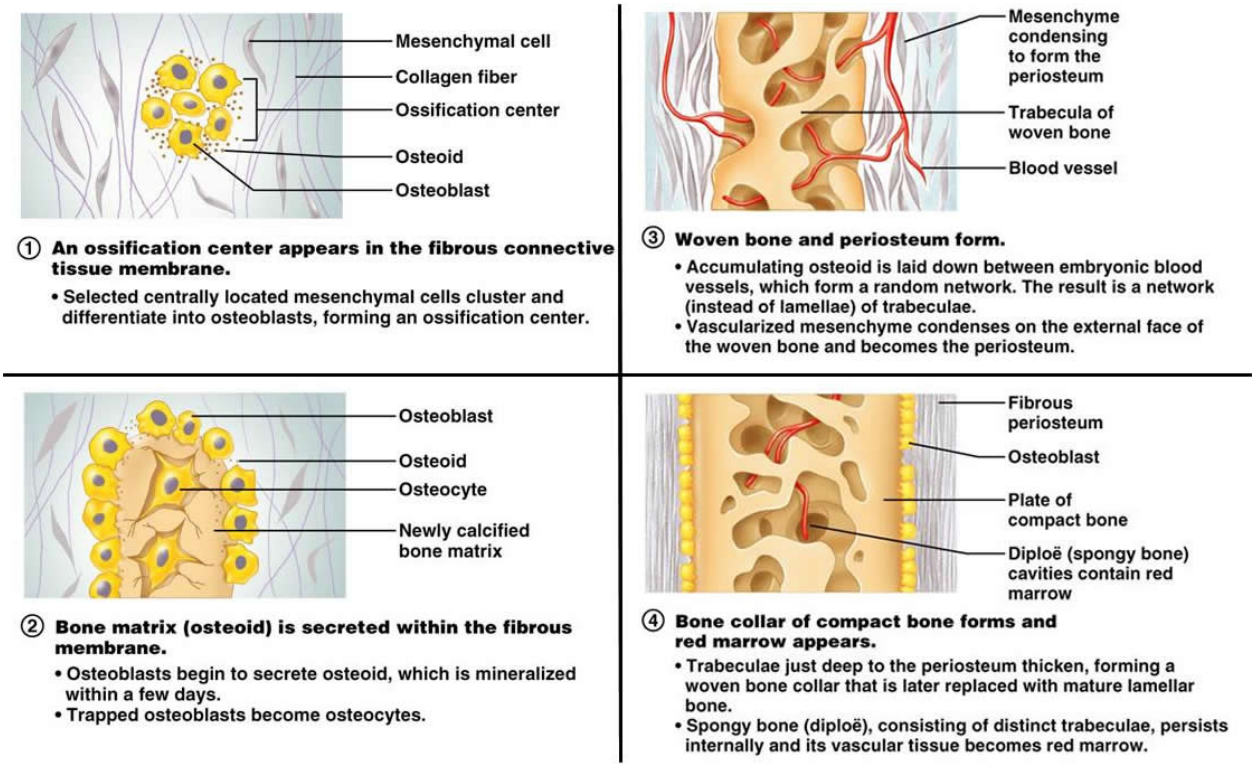

Figure 1.2: Bone development through intramembranous ossification. *Intramembranous ossification is initiated with mesenchymal stem cell condensation amid a fibrous environment. Within this cluster, osteoblasts differentiate to form an ossification center for bone formation (1). Within the ossification center, osteoblasts deposit bone matrix and expand the area of ossification. Osteoblasts that become entrapped within the deposited bone matrix differentiate into osteocytes (2). As the bone is being deposited, vascularization occurs within the ossification center causing a random deposition of bone and the formation of trabeculae (3). The external areas of the ossification center, with the help of the newly formed periosteum, become condensed cortical bone, as bone marrow is developed in the interstitial trabecular space (4). (16)*

Endochondral ossification is characterized by the formation of a cartilage intermediate that serves as the template for bone (Figure 1.3) (17). Endochondral ossification begins with the condensation of mesenchymal stem cells, and their subsequent differentiation into chondrocytes. After undergoing proliferation, these chondrocytes deposit matrix to form a cartilage anlage (18). After matrix production, the chondrocytes mature into an advanced state, hypertrophic chondrocytes, that orchestrate the breakdown of the cartilage anlage, the invasion of vasculature,

and the construction of bone (19, 20). After bone template deposition, osteoblasts and osteoclasts remodel the initial bone into mature bone (21). The source of these osteoblasts is under debate, as research has suggested that migration and differentiation of MSCs and the transdifferentiation of hypertrophic chondrocytes into osteoblasts are both feasible (22, 23). The majority of bones are developed through endochondral ossification and this process powers bone elongation through the growth plate (24). In addition, endochondral ossification has a primary role in the formation of bone marrow and hematopoiesis (25).

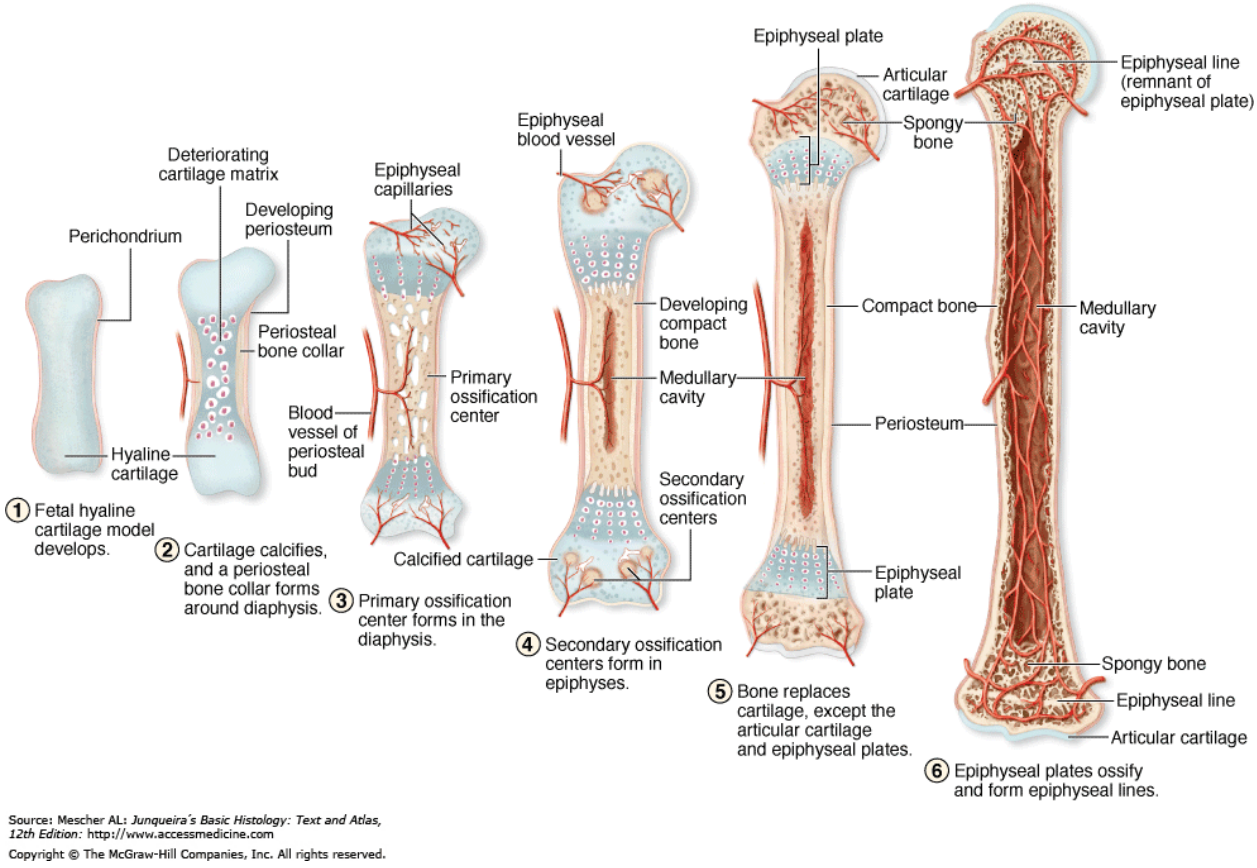

Figure 1.3: Bone development through endochondral ossification. *Endochondral ossification is initiated with the condensation of mesenchymal stem cells. These cells differentiate into chondrocytes, and create a cartilage anlage (1). The chondrocytes mature to hypertrophic chondrocytes, which orchestrate the growth of the cartilage anlage and its ossification (2). In long bone development, this ossification begins at the center of the anlage, which will later become the diaphysis of the bone (3). Similar to intramembranous ossification, the introduction of vascularization coincides with bone deposition, creating randomly distributed trabeculae within the middle of the future diaphysis (3). Compact bone forms on the exterior, aided by the formed, highly vascularized periosteum (3). As the ossification center progresses from the center out to the ends of the long bone, secondary ossification centers occur in the bone heads, following the same cartilage to bone transition that occurred initially (4). With the secondary ossification centers forming the bone ends, the primary ossification center in the diaphysis continues to progress towards this secondary ossification, lengthening the bone and diminishing the amount of remaining cartilage anlage (5). The remaining cartilage anlage persists through adolescence, and is referred to as the growth plate. In early adulthood, the last of the cartilage anlage is eventually ossified, resulting in the closure of the growth plates and skeletal maturity (6). (26)*

1.3 HYPERTROPHIC CHONDROCYTES

The crux of endochondral ossification is the transformation of the cartilage anlage into a bone template, making hypertrophic chondrocytes the key cell type of this pathway (27, 28). Hypertrophic chondrocyte maturation is marked by the swelling of the chondrocyte volume by almost 20 fold (19), and progresses through a combination of three main signaling pathways, IHH/PTHrP, Wnt/ ß-catenin, and BMP pathways, with possible crosstalk occurring (29-31).

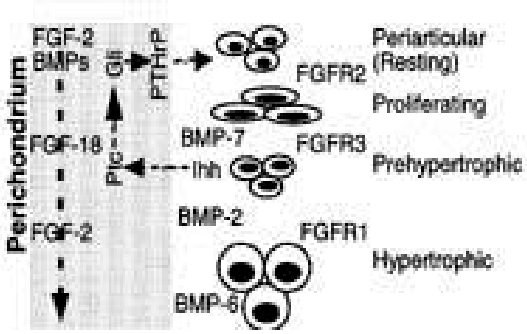

Figure 1.4: Chondrocyte maturation to hypertrophic chondrocytes*. This figure represents the various states of chondrocyte maturation, demonstrating the associated cytokines and interactions with the perichondrium necessary for progression. Chondrocyte maturation begins with the resting chondrocyte, which is then activated into a proliferating state. Upon chondrocyte proliferation, chondrocytes progress to a prehypertrohpic state that culminates with the increase in cell volume 10-15 fold, and the final hypertrophic chondrocyte maturation. (19)*

Hypertrophic chondrocytes straddle the in between of chondrocytes and osteoblasts, being surrounded by a cartilage matrix, but releasing mineral matrix vesicles and upregulating expression of important bone genes such as RUNX2, ALPL, and IBSP (32, 33). However, unique to the hypertrophic chondrocyte is the deposition of collagen type X, a special form of collagen that helps facilitate the mineralization of the cartilage anlage (34). Hypertrophic chondrocytes also express vascular endothelial growth factor (VEGF), and studies have

elucidated their pivotal role in stimulating vascularization, further accelerating turnover and providing a source of needed nutrients for bone formation (35-37).

1.4 Bone Fracture Repair

Bone is a unique tissue, as it is able to fully heal itself without scar formation (38). The highly vascular nature and proximity of stem cell sources allow seamless repair following the two main ossification pathways (Figure 1.5) (39). Computational modeling and animal studies have uncovered key variables that influence the ossification pathway followed. In a mechanically stable and well-perfused environment, intramembranous ossification is followed (20, 40-42). From a repair and regeneration standpoint, these situations occur with small breaks, as the direct reconnection of bone or a small gap can be easily overcome (43-45). In such small breaks, the general support structure of the bone is not compromised and the existing vasculature can provide the necessary factors and nutrients needed. Most broken bones are treated this way, through the common clinical practice of realignment and stabilization of the break.

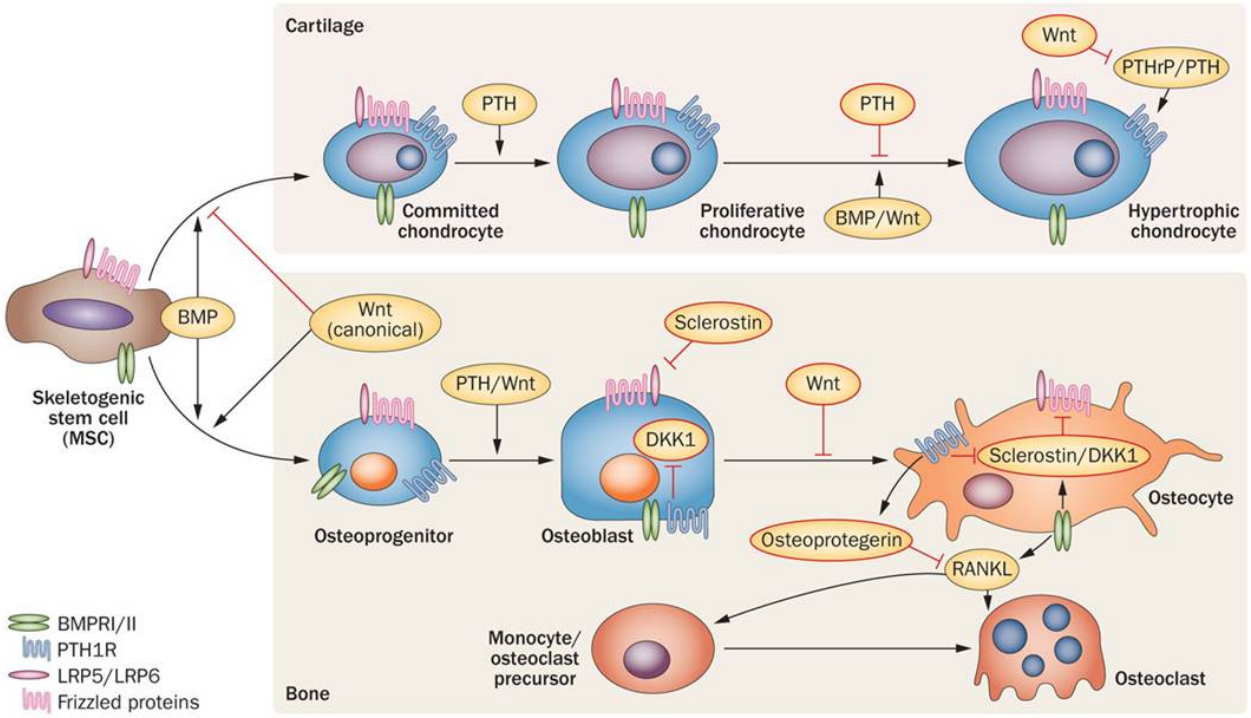

Figure 1.5: Differentiation of each key cell type in the ossification pathways*. Endochondral ossification (top) progresses from mesenchymal stem cell to chondrocyte, proliferating chondrocyte, and mature into hypertrophic chondrocytes. The figure demonstrates important cytokines (PTH, BMP/Wnt, PTHrP) that facilitate this maturation. Intramembranous ossification (bottom) begins with the mesenchymal stem cell advancing to an osteoprogenitor, which then differentiates into an osteoblast, the main bone producer in intramembranous ossification. In this pathway, PTH/Wnt, Sclerostin, and DKK1 are all essential for osteoblast differentiation. In formed bone, the osteoblasts can become osteocytes, which manage the bone, potentially recruiting osteoclasts for bone catabolism. (46)*

In contrast, if the defect is unstable, critical in size, or contains a nutrient-poor environment due to the destruction of the existing vasculature, endochondral ossification occurs (47, 48). Chondrocytes are able to survive in low-nutrient, mechanically intensive environments, which sways the differentiation of invading stem cells towards chondrocyte differentiation, cartilage callus formation and endochondral ossification (Figure 1.6). The cartilage callus provides stabilization that the hematoma cannot. Upon maturation, hypertrophic chondrocytes act as key drivers of bone vascularization, and with stability and increased nutrient presence, the

cartilage anlage is able to undergo transition into mature bone (49, 50). The processes used in fracture repair recapitulate the processes used in initial bone development (51).

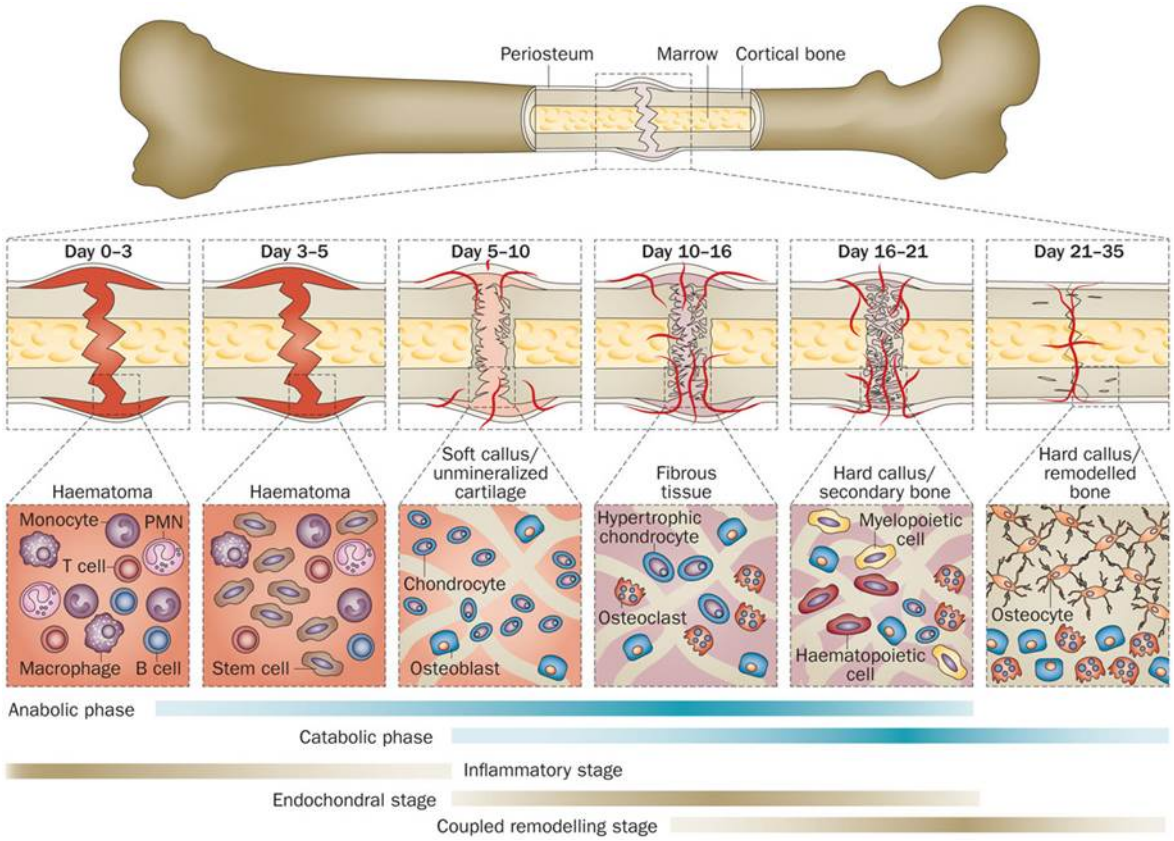

Figure 1.6: Long bone fracture repair. *After fracture, inflammation occurs and a hematoma is formed. From this hematoma, differentiated chondrocytes form a soft callus through the deposition of a cartilage anlage. With the maturation of the chondrocytes to hypertrophic chondrocytes, the soft callus is mineralized and vascularized into a hard callus. Osteoblasts and osteoclasts then remodel the hard callus into bone, complete with entrapped osteocytes. (46)*

1.5 BONE REMODELING

Throughout life, the skeletal system is constantly undergoing turnover, rebuilding the bodily framework for optimal structural support while using minimal material (6). Resorption of unwanted bone occurs through osteoclasts, giant multinucleated cells that are derived from hematopoietic cells. Osteoblasts balance this homeostasis by depositing new bone (52). A

majority of remodeling occurs in the same space, as osteoblasts deposit new bone into the osteoclast-mediated resorbed space, termed Howship's lacunae (53). Osteocytes, the mature bone cell that differentiates from osteoblasts trapped within the bone matrix, control bone remodeling (54). Osteocytes respond to various external cues by releasing a number of proteins, both systemically and locally, to recruit and activate the specialized anabolic and catabolic cells (7).

1.6 Clinical Problem and Treatments

The bone is a resilient organ, as it is one of the few structures in the body that is able to spontaneously regenerate without scar formation from the initial injury. However, the bone's ability to self-repair can be overwhelmed, resulting in a fibrous tissue filled defect in the bone, termed a nonunion (Figure 1.7). Without complete structural continuity, bone is not able to perform its primary support functions, and the patient is severely disabled. ~10% of all long bone fractures result in a nonunion (55-57), requiring external intervention. Even worse, up to 30% of surgical interventions result in failure, requiring further surgery and an extension of patient disability (56). Autografts are the gold standard; however the amount of bone required for long bone nonunion treatment is usually too large to sacrifice. Therefore, new alternatives are being pursued in order to improve patient outcomes and replace autografts as the premiere treatment solution. One area of prime interest is in bone tissue engineering.

***Figure 1.7: Long bone nonunion**. Improper healing of a long bone fracture results in the formation of a nonunion, as demonstrated by the disconnect in the humerus. This space is filled with fibrous tissue, instead of bone, compromising the support functions of the skeleton. (58)*

1.7 BONE TISSUE ENGINEERING

With the ease of harvest and multi-lineage potential of mesenchymal stem cells (MSC), coupled with the recent advances in induced pluripotent stem cells (iPSC), tissue engineering aims to provide autograft-like results without the necessity of donor tissue harvest or associated complications. Over the last 20 years, most bone tissue engineering strategies have followed an intramembranous pathway (59). The simple, well-established protocol for osteoblast derivation has been supplemented with osteoinductive scaffolds and mechanically-stimulating bioreactors to produce advanced grafts that attempt to meet important graft requirements: mechanical stabilization, integration with native bone, stimulation of regeneration and vascularization (3, 60). Despite heavy investment and the numerous variations studied, a viable, tissue engineered-solution for long bone fracture has yet to reach fruition.

One possibility for the widespread underwhelming performance of tissue engineered bone grafts could be the ossification pathway utilized. In native fracture repair, endochondral ossification ensures mechanical stabilization of the defect, quick integration with the healthy bone, wide-scale vascularization, and rapid turnover of the callus into mature bone. These numerous benefits suggest the appeal of an endochondral ossification pathway for bone tissue

engineered grafts (17). Recent advances have demonstrated the ability to derive hypertrophic chondrocytes, the key cell in endochondral ossification, from MSC sources (61, 62). These hypertrophic chondrocytes provide an enticing alternative pathway for bone tissue engineering (63). However, derived hypertrophic chondrocytes have not been extensively studied and require further investigation concerning their ability and suitability for bone tissue engineered grafts.

2 Objective

2.1 Hypothesis

The hypothesis is that the development of hypertrophic chondrocyte-based tissue engineered grafts enhances bone regeneration.

2.2 Specific Aims

The goal of this dissertation is to better understand the factors that influence hypertrophic chondrocyte derivation and utilize this knowledge for the creation of superior bone tissue engineered grafts. The first two aims focus on elucidating the biochemical factors that influence hypertrophic maturation and modulate bone template deposition. The final aim evaluates the performance of hypertrophic chondrocyte-based tissue engineered bone grafts in *in vivo* environments, elucidating mineral deposition and vascularization in a subcutaneous (ectopic) model and the stimulation of bone regeneration in a critical-sized long bone defect (orthotopic) model.

Aim 1: Elucidate the impact of oxygen concentration on the hypertrophic maturation of derived chondrocytes

A defining trait of cartilage is its hypoxic environment, as the lack of vasculature restricts oxygen and nutrient delivery. In endochondral ossification, the maturation of hypertrophic chondrocytes correlates with vascular invasion of the cartilage anlage and a rise in the local oxygen concentration (64). *In vitro* cultivation has demonstrated that culturing MSC-derived chondrocytes in hypoxic conditions, in essence replicating the native cartilage oxygen tension, enhances chondrogenesis and resists hypertrophic maturation (65-67). The goal of this aim was

to determine the effect that oxygen tension has on induced hypertrophic chondrocyte differentiation and to probe if an endochondral ossification-mimicking oxygen environment can enhance hypertrophic maturation by overcoming the resistive effects of hypoxia. The hypothesis stated that transitory application of hypoxia during chondrogenic differentiation suppresses induced hypertrophic maturation.

Aim 2: Measure the effect of advanced chondrogenic states on hypertrophic maturation and bone production

Endochondral ossification progresses along a defined pathway, progressing through various states from MSC condensation to final osteoblast-mediated bone remodeling (19). Hypertrophic chondrocytes are derived from advanced chondrocyte states, which have produced extensive cartilage matrix and have started to enlarge in cell size (68). The published work on hypertrophic chondrocyte differentiation of MSC sources *in vitro* does not include an extensive characterization of the chondrocyte state before hypertrophic maturation (61, 62, 69). The transient nature of MSC-derived chondrocytes allows the replication of various chondrocyte states through the duration of culture (70-72). The goal of this study was to characterize the chondrocyte state before induction of hypertrophic maturation, measuring the importance that chondrocyte state has on hypertrophic maturation and bone production. The hypothesis stated that advanced chondrocyte states, created by prolonged chondrogenic culture, results in superior hypertrophic maturation and bone template deposition.

Aim 3: Evaluate the ability of hypertrophic chondrocytes to mediate fast, vascularized bone deposition that integrates with host bone.

In long bone fractures, the mechanical instability and scarcity of nutrients within the bone regeneration environment favors endochondral ossification over intramembranous ossification (73-75). Until recently, bone tissue engineers have primarily utilized derived osteoblasts, despite the similarity in state of a freshly implanted bone graft to a long bone fracture environment: the mechanical instability caused by a native bone/ graft property mismatch and the nutrient scarce environment caused by a lack of mature vasculature (73-75). The goal of this aim was to study the performance of hypertrophic chondrocyte-based bone grafts, assessing their ability to stimulate bone formation and fracture repair through two studies. The first study investigated the bone template deposition and the incorporation of host vasculature in a subcutaneous, ectopic model, with the hypothesis stating that hypertrophic chondrocytes facilitate localized mineral deposition and promote widespread vascularization. The second study implanted hypertrophic chondrocyte-based bone grafts into a critical sized femoral defect and evaluated regeneration. The hypothesis of the second study stated that hypertrophic chondrocyte-based scaffolds rapidly enhanced long bone defect regeneration.

3 Motivation and Approach

Aim 1: Elucidate the impact of oxygen concentration on the hypertrophic maturation of derived chondrocytes

3.1 Motivation for Aim 1

Though referred to as normoxia, cell culture is usually conducted at the ambient oxygen concentration of ~21%, substantially higher than physiological levels in the developing cartilage. During the various developmental stages, the oxygen concentration in the cartilage anlage can vary between 2-10% (76, 77). Studies probing the impact of oxygen concentration on cell behavior have shown that these superoxic conditions elicit unusual activity, characterized by higher metabolic activity and acceleration in maturation that may cause mutagenesis (78, 79). Chondrogenically differentiated MSCs in a hypoxic environment that matched native cartilage, enhanced chondrogenesis and suppressed hypertrophic maturation (65, 80) despite the well-documented transient nature of MSC-derived chondrocytes (70-72). Hypoxic environments even repressed induced hypertrophic maturation with thyroid hormones (81), as it has been shown that low oxygen situations mediate the upregulation of hypertrophy resistive genes (82, 83).

In endochondral ossification, hypertrophic chondrocyte presence corresponds with vascular invasion (Figure 1.3), with hypertrophic chondrocytes locally preceding the infiltration of vasculature. The proximity of hypertrophic chondrocytes to new vasculature possibly suggests the requirement of elevated oxygen concentrations for chondrocyte hypertrophy. This study aimed to replicate the endochondral process with regards to oxygen tension, by chondrogenically differentiating in low oxygen concentrations and hypertrophically maturating in elevated oxygen

concentrations, to understand if the change in oxygen concentration influences hypertrophic differentiation and bone matrix production.

3.2 Approach and Rationale for Aim 1

To elucidate the impact of oxygen concentration on hypertrophic maturation, we differentiated mesenchymal cell pellets in either hypoxic (5%) or normoxic (21%) concentrations. To replicate endochondral ossification, an experimental group was created in which pellets were transferred from hypoxia to normoxia at the culmination of chondrogenic differentiation and the initiation of hypertrophic maturation. Hypertrophic maturation and bone deposition were evaluated through gene expression and matrix deposition, utilizing histology and μCT.

In this study, pellet cultures were utilized based on previous literature. Studies have validated the pellet culture as a satisfactory model of cartilage development (84), and a majority of the existing MSC, hypoxia literature was conducted in pellet culture (85-88). Another benefit of pellet culture is their relatively low cell number requirements, which allowed for fewer medium changes and thereby a more steady medium oxygen concentration. The hypertrophic induction protocol was based on published literature (61, 62).

Aim 2: Measure the effect of advanced chondrogenic states on hypertrophic maturation and bone production

3.3 Motivation for Aim 2

Endochondral ossification is utilized in situations requiring extensive bone formation and a lack of mechanical stability (89, 90). The progression of defined chondrocyte states in

endochondral ossification corresponds directly with this environment, as the differentiation of chondrocytes allows extensive, mechanically-stable matrix deposition within a nutrient scarce defect region (28, 91). It is after the deposition of this cartilage matrix that hypertrophic chondrocytes mature, utilizing the established matrix as a template to attract vasculature and create bone (28, 38, 51, 91).

Though native endochondral ossification occurs along a defined pathway, tissue engineered mimicking of this pathway does not need to faithfully match each progression. With the end goal being the development of translational technologies, bypassing certain steps of the native process provides multiple benefits, including specification of graft properties and faster graft generation. Published literature has already demonstrated this technique, removing the inflammatory and preparatory phases of endochondral ossification and beginning with the condensation of mesenchymal stem cells (69, 92, 93). However, these studies did not investigate the importance of the chondrogenic differentiation, routinely utilizing 3 weeks of chondrogenic culture before inducing hypertrophy (61, 62, 69, 93-95). Though native endochondral ossification would suggest the differentiation of late stage chondrocytes before inducing hypertrophic maturation, tissue engineered solutions can replace cartilage matrix deposition with a designed strategy. Therefore, tissue engineers only require the most beneficial chondrocyte state for hypertrophic chondrocyte differentiation and bone formation.

3.4 Approach and Rationale for Aim 2

To measure the effect of chondrogenic state on hypertrophic maturation, 16wt% silk fibroin scaffolds were created. Scaffolds were seeded with a standard concentration of MSCs, 30 million cells per milliliter. Progressive chondrocyte states were produced by increasing the

duration of chondrogenic culture, with 1, 2.5, and 4 weeks of chondrogenic culture chosen based on the experience of cartilage tissue engineers (96, 97). Upon completion of chondrogenic culture, a portion of the constructs were harvested and the remaining constructs were hypertrophically induced for three weeks. The chondrocyte state was determined through gene expression and matrix deposition, and the degree of hypertrophy and bone deposition was measured through similar means, utilizing histology and μCT for visualization of matrix deposition.

The transient nature of chondrogenically differentiated MSCs allowed the generation of various chondrocyte states by controlling the duration of chondrogenic culture (97). It has been shown that with increasing culture durations, chondrogenically differentiated MSCs will produce increasing amounts of hypertrophic markers, such as collagen type X (94, 97). Extended duration even results in bone formation when chondrogenically differentiated MSCs are implanted (71, 72). This differentiation regime was carried out in silk-based scaffolds due to the scaffold stiffness' similarity with values that promote chondrogenesis (98, 99). The non-human nature of silk and the lack of mineral in the scaffold allowed easy visualization and characterization of chondrocyte and hypertrophic markers and bone deposition.

Aim 3: Evaluate the ability of hypertrophic chondrocytes to mediate fast, vascularized bone deposition that integrates with host bone

3.5 Motivation for Aim 3

Natively, endochondral and intramembranous ossification are utilized in different circumstances (1). Endochondral ossification is utilized in situations requiring extensive bone deposition and mechanical stabilization (27). In contrast, intramembranous ossification occurs in

nutrient-rich environments and is responsible for the generation of mature bone (20, 40, 41). In line with the differing circumstances, the manner in which the key cell types of these two processes deposit bone and stimulate regeneration is also different. Hypertrophic chondrocytes deposit immature mineral containing excessive amounts of phosphate within a glycosaminoglycan-rich environment (100, 101), whereas polarized osteoblasts deposit mature mineral into a collagen-rich environment with deposition heavily influenced by the presence of mineral nucleators (102). Hypertrophic chondrocytes are responsible for the conversion of the cartilage template to bone, and multiple analyses have shown the importance of hypertrophic chondrocytes in prompting angiogenesis and creating a regenerative environment (103-105). Due to the nature of both key cell types, a characterization of the deposition tendencies and regenerative ability of these mimicked ossification pathways would allow tissue engineers further control in graft development.

One example of the importance of understanding the abilities of derived key cell types is the relative futility of osteoblast-based tissue engineered grafts in repairing long bone fractures (3). A critical sized long bone defect presents unique challenges, requiring strong integration into the native skeleton, the promotion of widespread vascularization, and rapid bone deposition to bridge the defect, all of this taking place in a challenging mechanical environment (regardless of the presence of fixators). Though osteoblast-based scaffolds have largely proven unsuccessful, the utilization of a hypertrophic chondrocyte-based graft might regenerate the defect. Endochondral ossification is the natural process for long bone fracture repair, and hypertrophic chondrocytes stimulate vascularization and robust mineral deposition (106, 107). Characterization of regeneration and long bone repair will demonstrate the attributes and potential of hypertrophic chondrocytes for bone tissue engineering.

3.6 Approach and Rationale for Aim 3.1

Characterization of the mineral deposition and bone regeneration mediated by hypertrophic chondrocytes and osteoblasts was performed in 16wt% silk fibroin scaffolds. Scaffolds were seeded with the standard concentration of MSCs, 30 million cells per milliliter and cultured in appropriate differentiation medium for a total of five weeks. At the end of culture, a portion of constructs were harvested to analyze deposition and cell behavior, with the remaining constructs implanted subcutaneously in nude mice. Constructs were harvested at regular time points to analyze bone regeneration.

Scaffolds were created from silk due to the non-human nature of silk and the lack of incorporated mineral, which allowed for easy visualization and characterization of the deposited bone matrix both after *in vitro* culture and *in vivo* implantation. No external stimuli were applied to the scaffolds, as it would have distorted the baseline ability of the differentiated cells. Implantations were conducted in the subcutaneous model, as this location provides a nutrient-rich, stress-free environment that promotes bone formation (108, 109).

3.7 Approach and Rationale for Aim 3.2

Bone tissue engineered constructs were created by seeding adipose derived stem cells (ADSCs) within decellularized bone scaffolds at the standard concentration, 30 million cells per milliliter, and then cultured in the appropriate medium for five weeks. External stimuli were applied to optimize the constructs according to published literature, with hypertrophic chondrocyte-based constructs statically cultured and osteoblast-based constructs cultured in perfusion bioreactors (93, 110). Constructs were implanted into a 5 mm femoral defect in nude

rats, and stabilized with an internal fixator. Defect regeneration was evaluated *in vivo* by μCT over twelve weeks, with complete defect evaluation completed upon harvest.

The study was conducted as an analysis of critical sized defect repair, but to also evaluate the clinical feasibility of hypertrophic chondrocyte-based grafts. Therefore, clinically relevant ADSCs were utilized, as their ease of harvest and rapid doubling makes them an attractive source for translated tissue engineered technologies. Before use, multiple donors of ADSC were evaluated in comparison to various MSC donors for their ability to undergo hypertrophic chondrocyte differentiation (Appendix). ADSCs showed a similar ability to undergo hypertrophic chondrocyte differentiation. In the defect model, mechanical stress is still applied to the implanted graft despite the internal fixation; therefore, decellularized trabecular bone was utilized due to its ability to match the properties of native bone.

PART II

ELUCIDATE THE IMPACT OF OXYGEN CONCENTRATION ON THE HYPERTROPHIC MATURATION OF DERIVED CHONDROCYTES

4 Transitory application of hypoxia during chondrocyte differentiation stunts induced hypertrophic maturation

4.1 ABSTRACT

Objective: The study investigated the temporal importance of hypoxia in preventing hypertrophic maturation of chondrogenically derived bone marrow stem cells (BMSC) for tissue engineering. We hypothesized that initial, transitory hypoxic chondrogenic differentiation was sufficient to delay induced hypertrophic maturation and suppress bone template formation.

Methods: BMSC were pelleted and chondrogenically differentiated in either hypoxia (5% O_2) or normoxia (~21% O_2) for two weeks. After chondrogenic differentiation, a group of hypoxic pellets were transferred to normoxia, noted as the Switch group. All pellet groups were then cultured for an additional three weeks in medium that promotes hypertrophic maturation. Hypertrophic maturation and bone template formation were analyzed through gene expression and histology.

Results: Chondrogenic differentiation of pellets in hypoxia resulted in reduced gene expression and matrix deposition of key cartilage markers compared to normoxia; however, sufficient chondrogenesis was achieved. The switch and hypoxia groups delayed hypertrophy and prevented bone template formation at similar levels. Gene expression of important hypertrophic (COL10A1, MMP13, IHH) and bone formation (IBSP, ALPL, BGLAP, SPP1) markers for both groups were similar, and significantly less than the normoxia group. Histological analysis of the normoxia group showed immediate, widespread deposition of collagen type X, bone formation

markers, and mineral, whereas the switch and hypoxia groups had delayed and reduced deposition.

Conclusion: The switch group's ability to delay hypertrophy and prevent bone template formation after transitory hypoxic differentiation confirms the temporal importance of hypoxia in cartilage tissue engineering.

4.2 INTRODUCTION

The characteristic inability of cartilage to repair itself has driven significant research into the development of cartilage tissue engineered grafts. The unique properties of cartilage have provided a difficult challenge, and in response, a number of biomaterials, cell sources, and stimulation techniques have been developed and utilized (111, 112). In particular, stem cells derived from bone marrow (BMSC) have been extensively studied due to their widespread availability and their potential for generating patient-specific treatments (113). Differentiation protocols have long been established that produce chondrocytes, and with the right combination of elements, cartilage grafts that mimic native morphology and approach physiological properties have been produced (114). However, one significant drawback of BMSC use is the tendency for derived chondrocytes to undergo hypertrophy while in culture (61, 72, 115). Upon implantation, hypertrophic chondrocyte presence facilitates endochondral ossification and ectopic bone formation.

To mitigate hypertrophic maturation, researchers have investigated controlling the oxygen tension at which BMSCs are cultured. Providing a more physiologic oxygen tension, termed hypoxia (1-5% (77)), has shown to delay hypertrophic maturation *in vitro* and provide a more stable cartilage graft (65, 80). Though debate still exists concerning hypoxia's benefit to

chondrogenic differentiation and matrix production, hypoxia's success in limiting hypertrophic maturation has seen it extensively used in BMSC-based tissue engineered cartilage grafts (116).

Due to ambient oxygen concentration, termed normoxia (~21%), maintaining long-term hypoxia for cartilage development can prove challenging and expensive. Recent work in our lab has demonstrated that a transient exposure of embryonic stem cells (ESC) to hypoxia during preparation had a significant, positive effect in the ESCs ability to chondrogenically differentiate and produce a cartilage-like matrix (88). In addition, this short-term exposure to hypoxia diminished hypertrophic maturation and stifled collagen type X deposition (a key hypertrophic chondrocyte marker). In response, the objective of this study was to determine the temporal importance of hypoxia in preventing BMSC hypertrophic maturation and bone template deposition via endochondral ossification. To address this objective, cell pellets were cultured for two weeks in chondrogenic medium under hypoxic (5%) or normoxic (21%) conditions. After chondrogenic differentiation, a group of pellets were transferred from hypoxia to normoxia, and the newly created group (Switch), plus the original two groups (Hypoxia and Normoxia), were cultured for an additional three weeks in hypertrophic maturation medium. Based on our laboratory's recent work, we hypothesized that the initial two weeks of chondrogenic differentiation in hypoxia was sufficient to delay induced hypertrophic maturation and suppress bone template formation.

4.3 METHOD

All reagents were purchased from Sigma Aldrich (St. Louis, MO) unless otherwise specified.

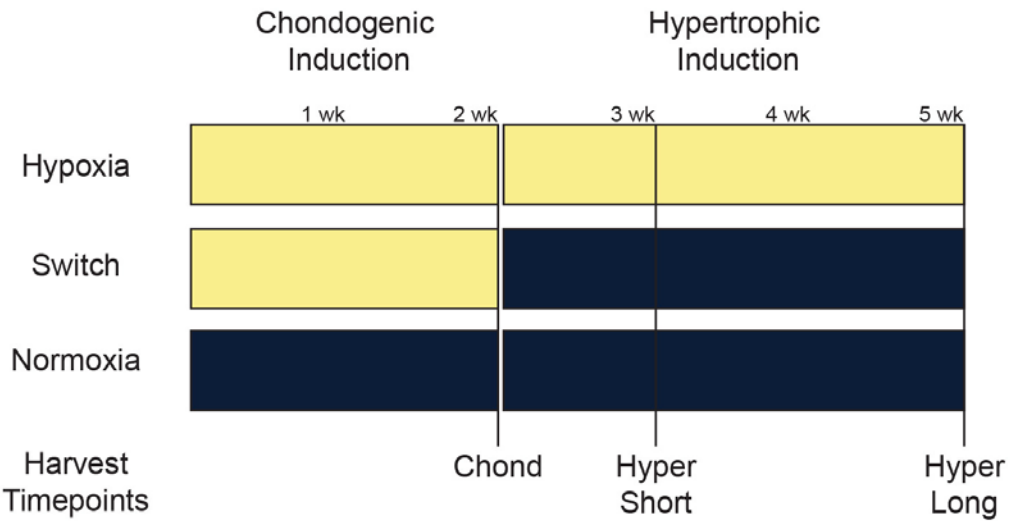

Figure 4.1: Pellet culture regime to determine the role of temporal hypoxia on induced hypertrophic maturation*. Hypertrophy was induced by first deriving chondrocytes from bone marrow stem cells (BMSC) during two weeks in chondrogenic medium, then switching to a hypertrophy inducing medium for the last three weeks of culture. Two oxygen tensions were utilized to create the three experimental groups, 5% (hypoxia, yellow) and ~21% (normoxia, blue). The Hypoxia group was entirely cultivated in hypoxia, the Normoxia group entirely cultivated in normoxia, and the Switch group underwent chondrogenic differentiation in hypoxia, and then was transferred to a normoxic environment for the remaining three weeks of hypertrophic induction. Pellets were harvested at the end of chondrogenic differentiation (Chond), one week into hypertrophic induction (Hyper Short) and at the culmination of cultivation (Hyper Long).*

Cell expansion and pellet formation

Fresh human bone marrow aspirates were obtained from Lonza (Allendale, NJ) and bone marrow stem cells (BMSC) were isolated and characterized following previously described protocols (117). Expansion of the isolated BMSCs occurred in high-glucose Dulbecco's Modified Eagle Medium (DMEM, ThermoFisher, Waltham, MA) supplemented with 10% FBS (Atlanta Biologicals, Flowery Branch, GA), 1% penicillin streptomycin (ThermoFisher, Waltham, MA), and 1 ng/mL basic fibroblast growth factor (ThermoFisher, Waltham, MA).

Cells were pelleted at the fifth passage by aliquoting 250,000 cells into 96 U-bottom well plates (ThermoFisher, Waltham, MA), and centrifuging at 300g for 5 minutes.

Culture regime

A specific culture medium regime was followed to induce hypertrophy (Figure 4.1). During the first two weeks, pellets were cultured in chondrogenic medium consisting of high glucose DMEM, 1% penicillin streptomycin, 1% ITS+ (Corning, Corning, NY), 100 nM dexamethasone, 50 µg/mL L-proline, 100 µg/mL sodium pyruvate, 10 mM HEPES buffer (Corning, Corning, NY) 50 µg/mL ascorbic acid 2-phosphate, 10 ng/mL TGF-β3 (Peprotech, Rocky Hill, NJ) at one of two oxygen tensions. After two weeks of chondrogenic differentiation, pellets were cultured in hypertrophic medium for three additional weeks. Hypertrophic medium had a similar recipe as chondrogenic medium, except for the reduction in dexamethasone concentration to 1 nM, removal of TGF-β3, addition of L-thyroxine at 50 ng/mL, and the addition of 5 mM sodium β-glycerophosphate.

After pelleting, chondrogenic medium culture was initiated and the pellets were split into three experimental groups based on oxygen tension and duration (Figure 4.1). The three groups were referred to as Hypoxia, Switch (hypoxia to normoxia), and Normoxia. Hypoxia culture was maintained at 5% oxygen concentration through the use of a New Brunswick Galaxy incubator (Eppendorf, Hauppauge, NY). Normoxia culture was maintained at ambient oxygen concentrations, ~21%. At the initiation of hypertrophic medium culture, the Switch group was removed from hypoxic culture and transferred to normoxia. The Hypoxia and Normoxia groups were maintained at their respective oxygen concentration throughout culture. As medium exchange occurred at normoxic conditions, medium was changed once a week for a total

duration less than 10 minutes to minimize any effect caused by the temporary increase in oxygen tension.

Samples were harvested from each experimental group at three distinct time points: after two weeks of culture and the culmination of chondrogenic differentiation ("Chond"), one week after the initiation of hypertrophic maturation culture (3 weeks total, "Hyper Short"), and three weeks after the initiation of hypertrophic maturation culture (5 weeks total, "Hyper Long").

Quantitative biochemical analysis

Pellets were digested with papain (40 Unites/ mg) in digest buffer (0.1M sodium acetate, 10 mM cysteine HCl and 50 mM EDTA, pH 6.0) at 60 ^{o}C overnight. DNA content per pellet was measured from the digest using Quant-iT PicoGreen assay kit and the supplied lambda DNA standard (ThermoFisher, Waltham, MA). Sulfated glycosaminoglycan (GAG) content was measured using the dimethylmethylene blue assay with chondroitin 6 sulfate as a control. Each sample was run in duplicate, with n=4 for each experimental group and time point.

RNA isolation and real time polymerase chain reaction (RT-PCR)

Total RNA was extracted from pellets using the TRIzol method (ThermoFisher, Waltham, MA). Contaminating DNA was removed from the extracted RNA through the use of DNase I treatment for ten minutes at 37 ^{o}C. cDNA was transcribed using the High Capacity cDNA Reverse Transcription kit (ThermoFisher, Waltham, MA) according to the manufacturer's instructions. Quantitative RT-PCR was performed using Fast Sybr Green mix (ThermoFisher, Waltham, MA). Expression levels were quantified applying the ΔCt method, with the Ct of GAPDH subtracted from the Ct of the gene of interest. Forward and reverse primers for each

gene of interest are presented (Table 4.1). Samples were run in duplicate, with n=5 for each experimental group and time point.

Histology and Immunohistochemistry

Pellets from each experimental group and time point were fixed in 10% formalin, dehydrated, embedded in paraffin, and sectioned at 6 µm. Pellets were stained with alcian blue and von Kossa following publicly available protocols. Antigen retrieval was required for bone sialoprotein (BSP) immunohistochemistry. Slides were placed in a container filled with citrate buffer (1.8 mM citric acid, 8.2 mM sodium citrate, pH 6.0), and the container was submerged in boiling water for 20 min. Slides were blocked with 0.3% hydrogen peroxide in absolute methanol for 20 minutes before following the Vectastain Elite Universal staining kit (Vector Laboratories, Burlingame, CA). The primary antibody for BSP (EMD Millipore, 1/500 dilution, AB1854, Bilerica, MA) was incubated on the samples overnight at 4 ^{o}C. The slides were counterstained with Hematoxylin QS (Vector Laboratories, Burlingame, CA). Slides for collagen type X immunohistochemistry followed the previously described protocol (118). The primary antibody was obtained from Abcam (1/1000 dilution, AB49945, San Francisco, CA), and Hematoxylin QS was used as a counterstain.

Micro-computed tomography

Samples were scanned and reconstructed using a Scanco VivaCT 40 micro-computed tomography system (Scanco Medical, Bassersdorf, Switzerland). Scans were performed using 55 kVp, 109 µA, and 200 ms integration time, and resulted in images with 21 µm isotropic voxel size. Reconstructed images were smoothed using a Gaussian filter (Sigma 0.8, support 1),

segmented using a global threshold of 22% maximum gray-scale value, and three-dimensional images were captured using the built in visualization software.

Statistical Analysis

Statistical analysis was performed using GraphPad Prism 5 (GraphPad, La Jolla, Ca). Analysis of the chondrogenic state was performed using Student's t-tests, when only two experimental groups were analyzed. The remaining statistical analysis was performed using analysis of variance with factors of time (Chond, Hyper Short, Hyper Long) and experimental group (Hypoxia, Switch, Normoxia). Tukey post-tests for comparison between the groups were utilized. Data is presented as mean ± standard deviation, with significance denoted by $p<0.05$.

Table 4.1: List of RT-PCR primers.

Gene	Forward (5' – 3')	Reverse (5' – 3')
GAPDH	AAGGTGAAGGTCGGAGTCAAC	GGGGTCATTGATGGCAACAATA
COL2A1	AGACTTGCGTCTACCCCAATC	GCAGGCGTAGGAAGGTCATC
ACAN	CCCCTGCTATTTCATCGACCC	GACACACGGCTCCACTTGAT
SOX9	AGCGAACGCACATCAAGAC	CTGTAGGCGATCTGTTGGGG
COL10A1	CATAAAAGGCCCACTACCCAAC	ACCTTGCTCTCCTCTTACTGC
MMP13	CCAGACTTCACGATGGCATTG	GGCATCTCCTCCATAATTTGGC
IHH	AACTCGCTGGCTATCTCGGT	GCCCTCATAATGCAGGGACT
COL1A1	GATCTGCGTCTGCGACAAC	GGCAGTTCTTGGTCTCGTCA
IBSP	GAACCTCGTGGGGACAATTAC	CATCATAGCCATCGTAGCCTTG
ALPL	GGGACTGGTACTCAGACAACG	GTAGGCGATGTCCTTACAGCC
BGLAP	GGCGCTACCTGTATCAATGG	GTGGTCAGCCAACTCGTCA
SPP1	GTTTCGCAGACCTGACATCCA	GCTTTCCATGTGTGAGGTGAT

4.4 RESULTS

Influence of Oxygen Environment on Chondrogenic Differentiation

Two oxygen tensions were utilized during cultivation of the hBMSC pellets, hypoxia (5% O_2) and normoxia (~21% O_2). Evaluation at the culmination of two weeks of chondrogenic differentiation demonstrated differences between the two groups (Figure 4.2). Expression of key chondrocyte-related genes, COL2A1 and SOX9, were significantly higher in the normoxia group (Figure 4.2A). Despite aggrecan (ACAN) gene expression not being significantly different between the groups, the amount of glycosaminoglycans (GAGs) deposited was significantly higher for the normoxia group (Figure 4.2A). Histological staining and immunohistochemistry of deposited matrix proteins confirms the quantification, with the intense alcian blue staining of the normoxia group depicting an increase in the amount of GAGs present in the pellet (Figure 4.2B). The intensity and spread of collagen type 2, the cartilage-specific collagen, was also increased in the normoxia group (Figure 4.2B). Hypoxia promoted increased cellularity, as DNA content was significantly increased in hypoxic culture. In total, the increase in chondrocyte-specific genes and cartilage-specific matrix deposition suggests that the normoxia group had enhanced chondrogenic differentiation.

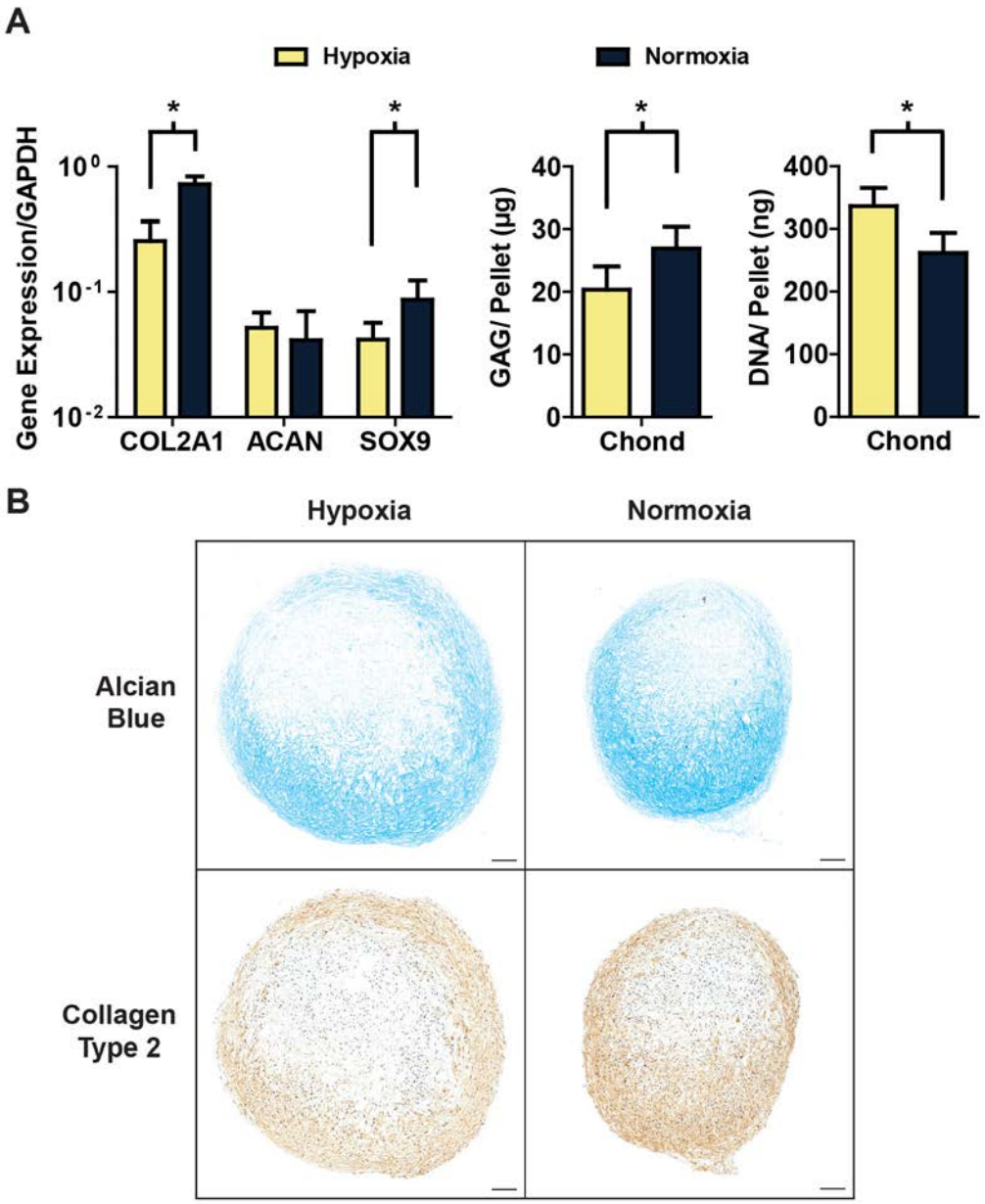

Figure 4.2: Enhanced chondrogenic state of pellets cultured in normoxia based on increased expression of key chondrogenic genes and superior cartilage matrix deposition. *(A) Gene expression of important chondrogenic genes relative to the GAPDH housekeeping gene and quantitation of the glycosaminoglycan (GAG) and DNA content per pellet. All data is presented as mean ± standard deviation with n=4-5 and * denoting significance of $p<0.05$. (B) Staining and immunohistochemistry for important cartilage matrix elements, GAG and collagen type 2. Scale bars = 100 µm.*

Induced Hypertrophic Maturation of Pellet Cultures

To determine pellet maturation, expression of key hypertrophic chondrocyte-related genes was measured across all time points (Figure 4.3).

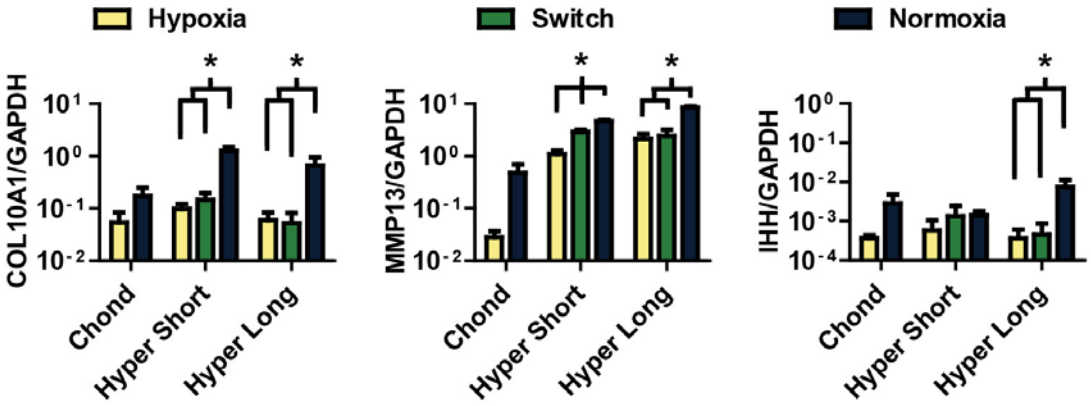

Figure 4.3: The Switch group suppressed key genes of hypertrophic maturation across all time points, which was similar to Hypoxia expression and significantly less than Normoxia*. Progressive expression of collagen type X (unique hypertrophic chondrocyte protein), MMP13 (key enzyme for cartilage callus turnover), and IHH (key signaling protein for hypertrophic maturation) normalized to GAPDH (housekeeping gene) across all three time points, data is presented as mean ± standard deviation, n=5 and * denotes significance of p<0.05.*

Collagen type X is a unique marker of hypertrophic chondrocytes, and significant upregulation was seen in the normoxia group upon hypertrophic induction. Both the hypoxia and switch groups repressed collagen type X expression, with no significant differences between the two groups across all time points. Matrix Metalloprotease 13 (MMP13), utilized in cartilage turnover during endochondral ossification, is an early indicator of hypertrophic maturation. Upon induction, all experimental groups had increased MMP13 expression. Once again, the normoxia group had significantly higher MMP13 expression compared to the other two groups. At the earlier time point, the switch group had a significantly higher expression compared to the hypoxia group; however, by the Hyper Long time point, the hypoxia expression had risen to

match the switch group. Indian Hedgehog (IHH) is a cell signaling protein for maturation and is a late indicator of hypertrophic chondrocytes. At the final time point, the hypoxia and switch groups had significantly reduced expression compared to the normoxia group, with minimal change compared to the initial Chond time point. By the final time point, the normoxia group had a significant increase in IHH expression compared to the two earlier time points and the other groups.

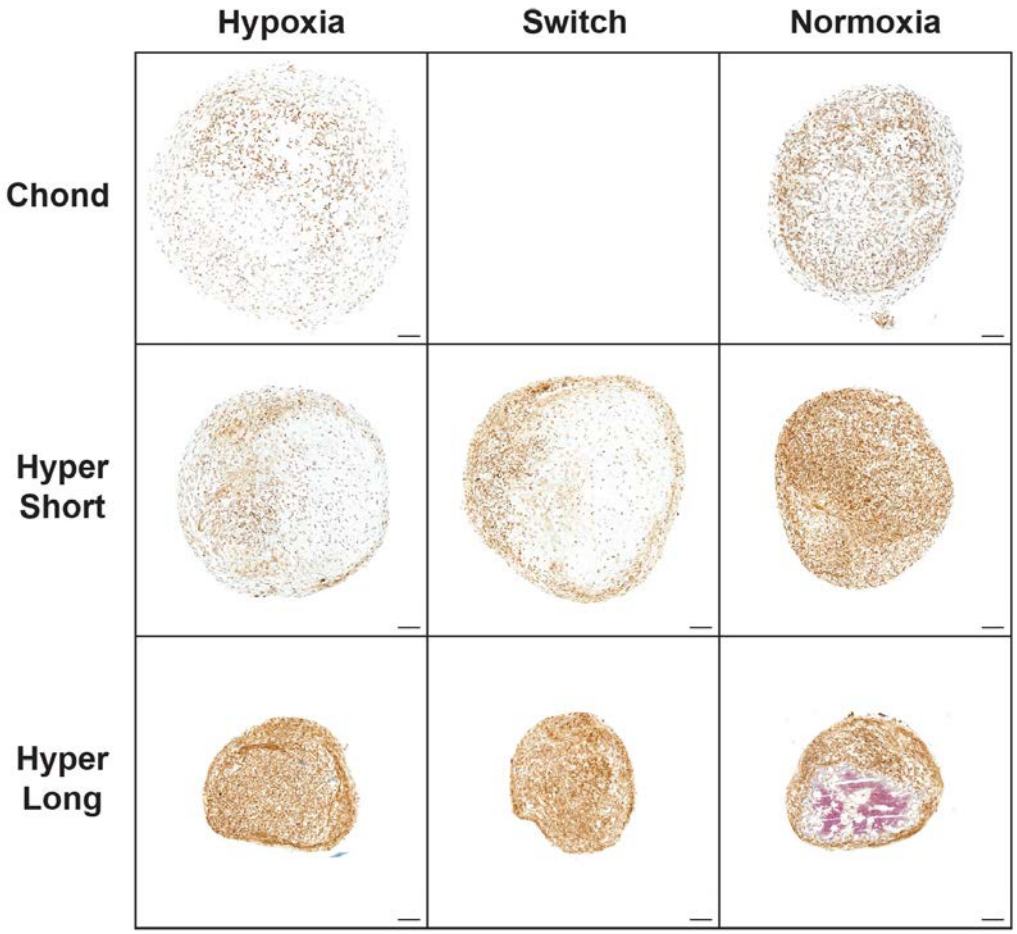

Figure 4.4: Delayed deposition of collagen type X by the Switch and Hypoxia groups*. Immunohistochemistry of collagen type X to demonstrate hypertrophic maturation within cell culture pellets, scale bars = 100 µm.*

Immunohistochemical staining of collagen type X demonstrated the repressed hypertrophic maturation of the two experimental groups conditioned in a hypoxic environment (Figure 4.4). In agreement with the collagen type X gene expression data, the hypoxia and switch groups had reduced deposition of collagen type X at the Chond and Hyper Short time points. The normoxia group appeared to have more collagen type X deposition during chondrogenic differentiation and had widespread collagen type X deposition at the Hyper Short time point, shortly after hypertrophic induction. Extensive collagen type X staining wasn't demonstrated until the Hyper Long time point in the hypoxia and switch groups. An advanced hypertrophic state was reached at the Hyper Long time point within the normoxia group, as mineral deposition can be seen by the intense purple staining present within the center of the pellet.

Pellet GAG content, shown with alcian blue staining (Figure 4.5), showed a quick turnover in matrix content that mirrored the collagen type X deposition. At the earliest time point after induction, the normoxia group was almost absent of stained GAG. This lack of GAG was in stark contrast to the intensely stained GAG present in the normoxia group at the Chond time point. At the late time point, alcian blue staining was present in the normoxia group, but associated with mineral deposition. In both the hypoxia and switch groups, GAG is still very much present at the Hyper Short time point, as shown by the intense blue staining present within the pellets. It is not until the Hyper Long time point that the hypoxia and switch groups are absent of GAG and resemble the normoxia group. The delayed disappearance of GAG in the hypoxia and switch groups matches that of the delayed appearance of collagen type X.

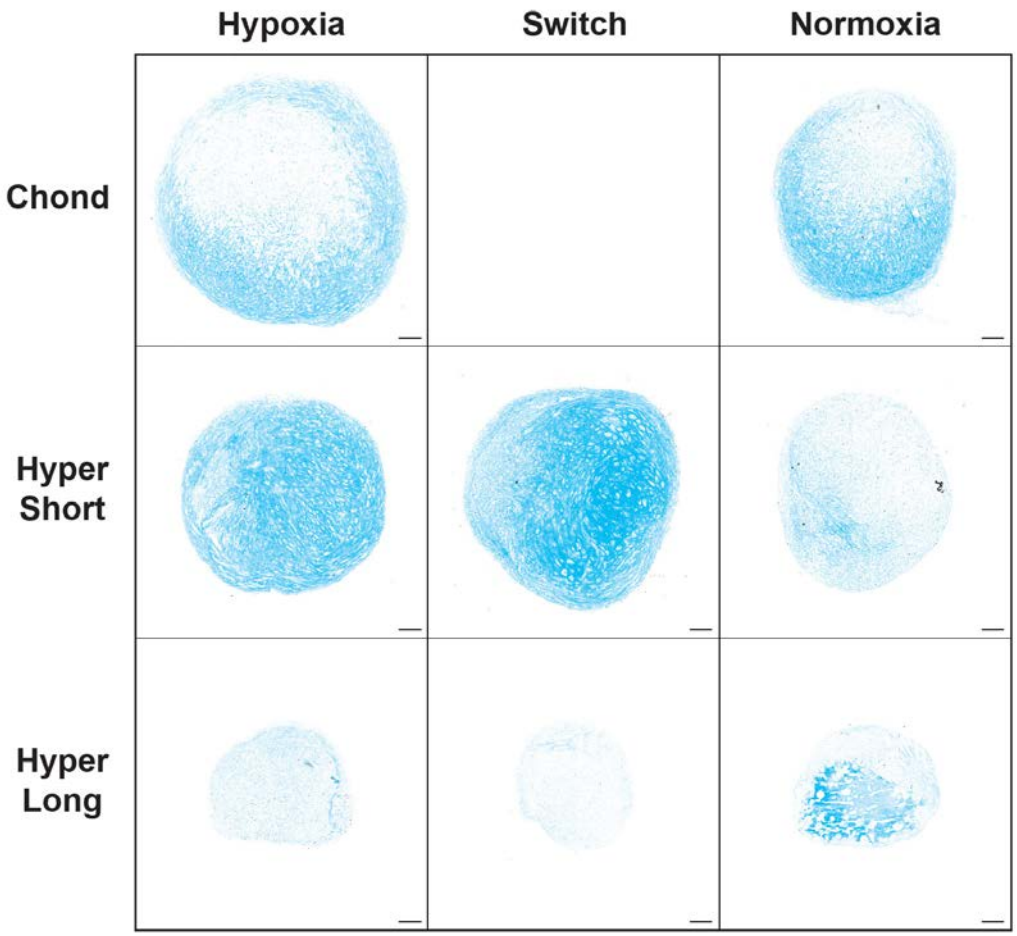

Figure 4.5: Prolonged GAG presence and delayed cartilage matrix turnover in the Switch and Hypoxia groups*. Alcian blue staining to portray GAG content, and its progressive change, within the cell culture pellets, scale bars = 100 µm.*

Bone Template Matrix Production and Mineralization

Upon maturation, hypertrophic chondrocytes produced a bone template (Figure 4.6). Analysis of bone forming genes at the final time point consistently showed reduced expression in the hypoxia and switch groups. Normoxia demonstrated significantly elevated levels of IBSP, ALPL, BGLAP, and SPP1 expression (Figure 4.6A). Deposition of Bone Sialoprotein (BSP), a key noncollagenous protein in the construction and mineralization of bone, was limited to the external surface in both the hypoxia and switch groups, but was deposited broadly in the

normoxia group, especially in connection with the deposited mineral (Figure 4.6B). von Kossa staining depicts the phosphate in deposited mineral, and was heavily present in the normoxia group, indicating mineral location in the same internal position as the heavy GAG and BSP presence was seen in the previous stains (Figure 4.5, 4.6B). Similar to the lack of BSP deposition, the hypoxia and switch groups were negative for von Kossa staining, demonstrating a lack of bone template deposition. Mineral deposition was investigated more extensively using micro computed tomography (μCT) (Figure 4.6B). Scanning and 3D reconstruction of the pellets showed a complete lack of mineral formed in both the hypoxia and switch pellets, but extensive deposition in the normoxia group.

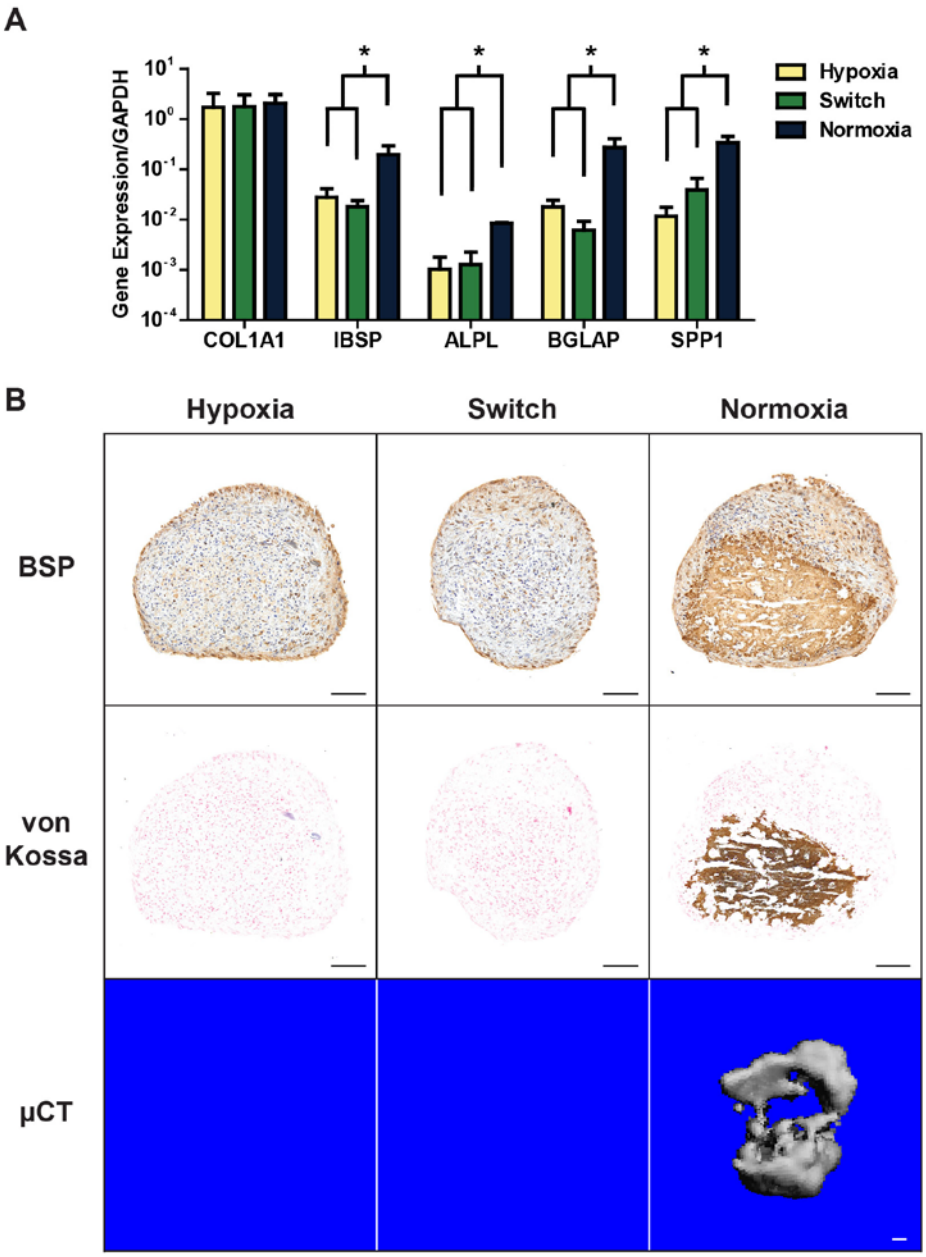

Figure 4.6: The Switch group prevented bone template production and mineralization analogous to the Hypoxia group and in stark contrast to the template produced by the Normoxia group*. (A) Expression of genes involved in bone production relative to the GAPDH housekeeping gene. Data is presented as mean ± standard deviation, n=5 and * denotes significance of p<0.05. (B) Immunohistochemistry for bone sialoprotein (BSP), a key non-collagenous protein for bone formation, followed by von Kossa staining of the phosphate groups in deposited mineral. Micro-computed tomography (µCT) scan and three-dimensional reconstruction of the deposited mineral within the cell pellet. Scale bars = 100 µm.*

4.5 DISCUSSION

Hypertrophic maturation of chondrocytes in tissue engineered cartilage grafts eventually leads to the unwanted recapitulation of endochondral ossification and ectopic bone formation. Traditionally, tissue engineered cartilage derived from mesenchymal stem cells has been plagued by this hypertrophic maturation (61, 83). Hypoxia has been shown to effectively delay the initiation of hypertrophy, reducing gene expression and deposition of the unique hypertrophic chondrocyte marker, collagen type X (81, 116). Recent work has shown that transitory pre-conditioning of cells in a hypoxic environment before differentiation improves chondrogenic differentiation and matrix production and can limit hypertrophic maturation when in normoxic culture (88, 119). As other important chondrogenic induction and maintenance factors have shown a temporal aspect to their activity (120, 121), it was hypothesized that there is also a temporal importance of hypoxia for cell culture. In the current study, hypoxic culture of cell pellets during chondrogenic differentiation suppressed chemically-induced hypertrophic maturation, even after the pellets were transferred to a normoxic environment. The switching of pellets from hypoxia to normoxia at the time of hypertrophic induction had minimal impact on maturation, as Switch pellets displayed reduced gene expression and limited matrix deposition of key hypertrophic markers similar to pellets cultured exclusively in hypoxia. Whereas normoxia pellets had extensive endochondral ossification, demonstrated by bone template deposition and mineralization, the groups initially cultured in hypoxia both did not produce bone template matrix. This study confirmed the hypothesis and clarified the temporal importance of hypoxia for cartilage tissue engineering, indicating that hypoxic conditioning during the initial chondrogenic differentiation was sufficient to hinder hypertrophic maturation.

There is an ongoing debate concerning the benefit of hypoxia to chondrogenic differentiation and MSC-derived chondrocyte matrix production (122, 123). During the initial chondrogenic differentiation of this study, normoxic pellets had broader chondrogenic differentiation and greater cartilage matrix deposition. These results agree with the literature that suggests that the availability of oxygen mediates matrix production and that hypoxia can result in diminished differentiation and matrix production (124-126). Despite significantly lower gene expression and significantly less GAG, the degree of cartilage matrix deposition of GAG and collagen type 2 by the hypoxic pellets does suggest chondrogenic differentiation. In agreement with established literature, the hypoxia group also experienced reduced expression and matrix deposition of key hypertrophic markers, specifically collagen type X.

After chondrogenic culture, cell pellets were subjected to an altered culture medium composition, containing a thyroid hormone (L-Thyroxine) and a reduction in dexamethasone concentration, to induce hypertrophic maturation. This specific cell culture medium composition produces an advanced hypertrophic chondrocyte state and replicates endochondral ossification (62, 93). By initiating hypertrophic maturation through this medium composition, as opposed to the general hypertrophic progression of chondrogenically differentiated MSCs, it was shown that hypoxia not only delayed hypertrophic maturation, but also suppressed endochondral ossification. These findings are in agreement with existing literature, as hypoxia-mediated delay in maturation has been shown in a number of cell sources and cartilage tissue engineering manifestations (81, 127, 128). In explant cultivation of embryo forelimbs and fetal mouse tibia (66, 129), hypoxia prevented endochondral ossification-mediated bone formation.

To address, the temporal importance of hypoxia, the primary objective of the study, pellets chondrogenically differentiated in hypoxia were transferred to a normoxic environment

concurrently with the initiation of hypertrophic induction. Across almost all measures of hypertrophic maturation and endochondral ossification conducted in this study, Switch pellets were not significantly different than pellets maintained exclusively in hypoxia. However, the Switch pellets were significantly different than the Normoxia group that clearly underwent hypertrophy and endochondral ossification. These results suggest that hypoxia provides initial cues that affect chondrocyte differentiation and pellet formation, and that prolonged hypoxic cultivation is not necessary to delay hypertrophic maturation. This temporal importance of hypoxia has been alluded to in other studies (88, 119); however, these studies have not uncovered the specific mechanisms triggered by hypoxia. Therefore, knowledge gained during hypoxic chondrogenesis may allude to the initial effect hypoxia provides. In specific studies, hypoxia alone promoted chondrogenesis and the stabilization of a stable cartilage phenotype through the upregulation of important factors such as HIF-1Alpha, HDAC4 and Nkx3.2 (67, 129-131). However, the explanation that temporal hypoxia cultivation upregulated chondrogenic factors and created a permanent chondrocyte state is not viable for this study, as expression of these important stable cartilage genes, HIF-1alpha, HDAC4, CHM-1, and MEF2C produced no significance difference or noticeable trends amongst the three pellet groups (data not shown). In support of this data, it was obvious that a stable chondrocyte state was not reached in either hypoxia-related group, due to the substantial collagen type X deposition and the removal of matrix GAG over time, key processes undertaken by hypertrophic chondrocytes. Further studies are required to determine the exact impact of hypoxic culture in the first two weeks of chondrogenesis, and how this leads to the delay of hypertrophic maturation regardless of oxygen tension.

In conclusion, the results of this study demonstrate that hypoxia is sufficient to delay induced hypertrophic chondrocyte maturation and suppress downstream bone template production and mineralization via endochondral ossification. Of particular novelty, the transfer of hypoxia derived pellets to a normoxic environment did not alter behavior compared to pellets maintained solely in hypoxia. This confirms the hypothesis and indicates that only initial hypoxic cultivation is necessary for delaying induced maturation and suppressing endochondral ossification. With the knowledge that only initial hypoxic conditioning is necessary, intensive studies can be conducted to further understand the mechanisms that delay hypertrophy and develop strategies to prolong this delay. Armed with this knowledge, researchers will be able to overcome ectopic bone formation and develop stable tissue engineered cartilage.

PART III

MEASURE THE EFFECT OF ADVANCED CHONDROGENIC STATES ON HYPERTROPHIC MATURATION AND BONE PRODUCTION

5 Increased Duration of Chondrogenic Differentiation Enhances Hypertrophic Maturation and Bone Production

5.1 Abstract

Endochondral ossification-based strategies for bone tissue engineering have demonstrated enhanced deposition of mature, vascularized bone. A key component of these strategies is the differentiation of hypertrophic chondrocytes from mesenchymal stem cell sources. In native endochondral ossification, a progression of chondrocyte states leads to the maturation of hypertrophic chondrocytes. However, current strategies have not evaluated the importance of the chondrocyte state preceding hypertrophic induction. The aim of this study was to evaluate the impact of the derived chondrocyte state on the differentiation and performance of hypertrophic chondrocytes. The chondrocyte state was controlled through the duration of chondrogenic differentiation, with the hypothesis stating that increased duration of chondrogenic culture will create an advanced chondrocyte state that will enhance hypertrophic maturation and bone production. Chondrogenic differentiation of human mesenchymal stem cells within porous silk scaffolds occurred for 1, 2.5, and 4 weeks, before being hypertrophically induced for 3 weeks. At the culmination of chondrogenesis, increased culture duration produced advanced chondrogenic states as seen with enhanced cartilage gene expression and matrix deposition and the initial presence of hypertrophic markers. Induced maturation resulted in widespread hypertrophic differentiation within the prolonged culture groups and corresponding bone template deposition. Though all groups produced similar volume of bone, the prolonged cultures contained small clumps spread across the scaffold. The similarity in bone template production of the 2.5 and 4 week chondrogenic culture groups suggests a minimum threshold of chondrogenesis needed for

hypertrophic chondrocyte maturation and bone production in endochondral ossification-based strategies.

5.2 INTRODUCTION

Endochondral ossification, the process used in skeletal development, progresses along a defined pathway to produce bone (132). This pathway is initiated with the proliferation and condensation of mesenchymal stem cells and their subsequent differentiation into chondrocytes (133). These chondrocytes deposit a collagen type II and glycosaminoglycan (GAG)-rich cartilage matrix that will serve as the template for bone formation (133). After cartilage component deposition, the chondrocytes undergo maturation into hypertrophic chondrocytes, as noted by the increase in cell volume (19). Hypertrophic chondrocytes serve as the key cell type in endochondral ossification by orchestrating the progression of the cartilage template into bone (133). The hypertrophic chondrocyte mediates the breakdown of the cartilage matrix through MMP-13 production, the construction of the bone template through collagen type X and mineral deposition, and the vascularization of the template (24, 51, 132). Osteoblasts utilize this deposited bone template to complete this sequential process and generate mature bone.

A recent tissue engineering paradigm has utilized this natural process as inspiration (4, 134), recapitulating endochondral ossification to generate bone grafts. The paradigm was developed based on observations of cartilage tissue engineered constructs derived from mesenchymal stem cell sources. These cartilage constructs demonstrated hypertrophic markers during *in vitro* culture and formed bone when implanted, indicating the transient nature and the various, distinct states of stem cell derived chondrocytes (70-72). Bone tissue engineers have utilized this information and recreated many of the steps of endochondral ossification by

initiating condensation of mesenchymal stem cells, differentiating chondrocytes through TGFß stimulation, and enhancing hypertrophic maturation with the addition of thyroid hormones, the results of which produced vascularized bone in vivo (61, 62, 93). Interestingly, these studies maintained a three week duration of chondrogenic culture without characterization of the chondrocyte state. Therefore, the aim of this study was to investigate the impact of the derived chondrocyte state on hypertrophic differentiation and performance. Due to the transient nature of these stem cell derived chondrocytes, it is known that the duration of chondrogenic culture correlates with the chondrogenic state, as increasing cultivation time results in a greater presence of advanced state chondrocytes (94).

In this study, the chondrocyte state was controlled by the duration of chondrogenic culture. After chondrogenic culture, the scaffolds were switched to medium that induced hypertrophic maturation. To depict varying chondrocyte states before induced maturation, chondrogenic culture was established for one, two and a half, and four weeks, corresponding to condensed MSC/ early stage chondrocyte, cartilage producing chondrocytes, and early hypertrophic chondrocytes. We hypothesized that increased duration of chondrogenic culture, and hence an advanced chondrocyte state, will enhance hypertrophic maturation and bone production. The results demonstrated that the chondrocyte state was important, as varying durations of chondrogenic cultivation modulated the deposition pattern and amount of key bone proteins.

5.3 MATERIALS AND METHODS

All materials were obtained from Sigma-Aldrich (St. Louis, MO, USA) unless otherwise noted.

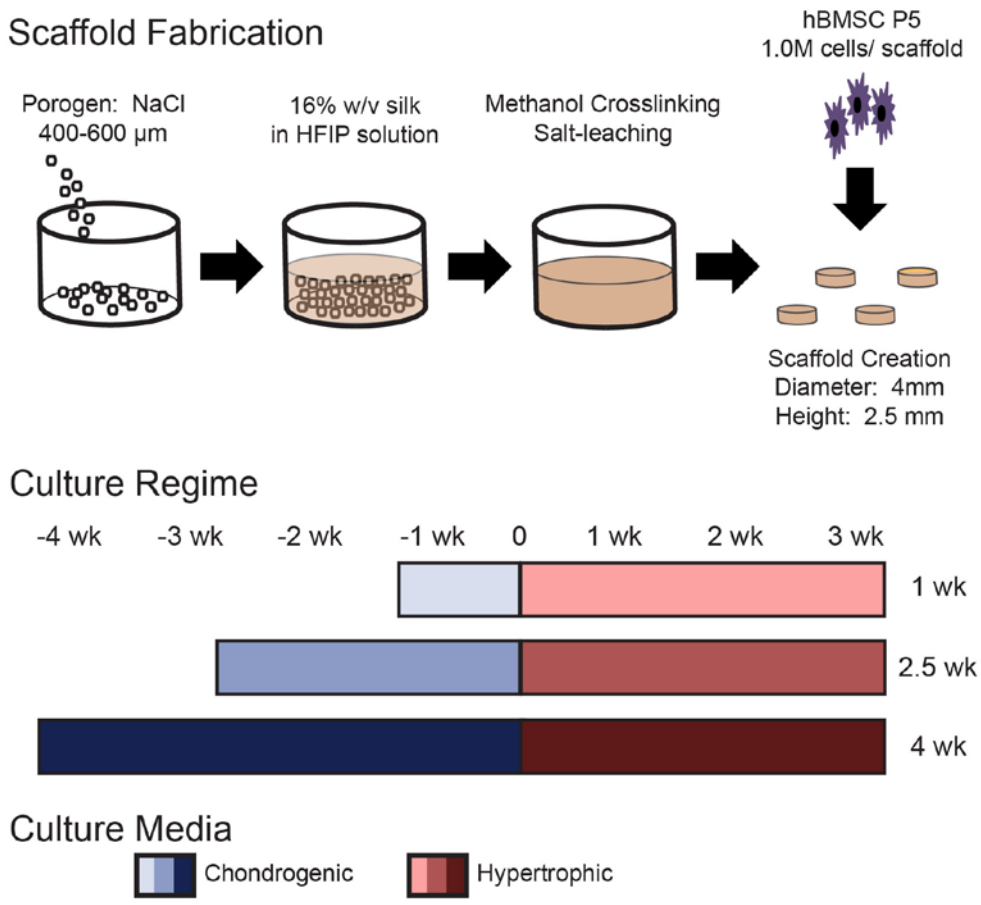

Figure 5.1: Scaffold creation and cell culture regime to produce various chondrocyte states. *Silk scaffolds were prepared following the published protocol (68). 16% w/v bombyx mori silk fibroin in HFIP solution was poured over NaCl salt porogens 400-600 µm in diameter and allowed to dry. β-sheet formation was induced by submerging the constructs in methanol for 1-2 days. After formation, constructs were subjected to incubation in multiple changes of deionized water to remove the salt porogen. After porogen removal, scaffolds were sized into cylinders of 4 mm diameter and 2 mm height. Human bone marrow stem cells were seeded into the scaffolds, and the scaffolds were cultured based on the specified regime. Experimental groups were determined based on the duration of chondrogenic pre-culture, either 1 wk, 2.5 wks, or 4 wks. After chondrogenic culture, all scaffolds were induced to hypertrophic maturation through cultivation in hypertrophic medium for three weeks. After cultivation, all scaffolds were analyzed for matrix content, gene expression, and histology.*

Scaffold fabrication:

Porous silk scaffolds were fabricated based on published methods (135), Figure 5.1. Briefly, 16% w/v bombyx mori silk fibroin in HFIP solution was poured over NaCl salt porogens 400-600 µm in diameter and allowed to dry. ß sheet formation was induced by submerging the constructs in methanol for 1-2 days. After formation, constructs were subjected to incubation in multiple changes of deionized water to remove the salt porogen. After porogen removal, scaffolds were sized into cylinders of 4 mm diameter and 2 mm height. Scaffolds were disinfected in sterile-filtered 70% ethanol prior to use.

Mesenchymal stem cell expansion, seeding, and cultivation:

Human bone marrow stem cells (hBMSCs, Lonza, Basel, CH) were expanded until passage five in expansion medium consisting of high glucose medium with L-glutamine, 10% fetal bovine serum, and 1% penicillin/ streptomycin. Cells were trypsinized, resuspended in culture medium at a concentration of 30M cells/ mL, and were drip seeded into the scaffolds. Seeded scaffolds were incubated in expansion medium for an additional day to promote cell stabilization within the constructs. Cells were then switched to chondrogenic medium consisting of high glucose DMEM (ThermoFisher, Waltham, MA) supplemented with 100 nM dexamethasone, 50 µg/mL ascorbic acid, 50 µg/ mL proline, 100 µg/mL sodium pyruvate, 1% ITS+, 1% P/S, 10 ng/mL BMP6 and 10 ng/mL TGF-β3. The duration of chondrogenic culture dictated the three different experimental groups, with constructs cultured for 1, 2.5, and 4 weeks (Figure 5.1). The names of the experimental groups matched the duration of chondrogenic culture. At the culmination of chondrogenic culture at the specified duration, a portion of constructs were harvested, while the remaining constructs were incubated for three weeks in

hypertrophic medium with the same base composition as chondrogenic medium but without TGF-β3, a dexamethasone concentration of 1 nM, 50 ng/mL of L-thyroxine, and 5mM of β-glycerophosphate. After three weeks of hypertrophic culture, constructs were harvested and analyzed.

Construct matrix biochemical quantitation:

At harvest, constructs were weighed and then digested with papain (40 units/ mg) in digest buffer (0.1M sodium acetate, 10 mM cysteine HCl and 50 mM EDTA, pH 6.0) at 60 ^{o}C overnight. DNA content was measured using the Quant-iT PicoGreen assay kit (ThermoFisher, Waltham, MA) following the manufacturer's instructions, with content normalized by the construct wet weight. Construct glycosaminoglycan (GAG) content was determined using the dimethylmethylene blue assay (136). Collagen quantitation through hydroxyproline (OHP) concentration was conducted per the author's instructions (137). Samples were run in duplicate for each analysis, with n=4 for each experimental group.

RNA isolation and RT-PCR:

Construct RNA was extracted using provided TRIzol-based methods (ThermoFisher, Waltham, MA), with total RNA content measured using NanoDrop spectrophotometric quantitation (ThermoFisher, Waltham, MA). DNase incubation was utilized to remove any contaminating DNA and cDNA was transcribed from the isolated RNA using the High Capacity cDNA Reverse Transcription kit (ThermoFisher, Waltham, MA) according to the manufacturer's instructions. Once cDNA was obtained, quantitative RT-PCR was performed using Fast Sybr Green mix (ThermoFisher, Waltham, MA). Quantitation was normalized using the ΔC_t, with the C_t of GAPDH subtracted from the C_t of the gene of interest. Forward and reverse primers for

each gene are present in Table 5.1. Samples were run in duplicate, with n=4 for each experimental group.

Table 5.1: Primers used in RT-PCR

Gene	Forward	Reverse
GAPDH	AAGGTGAAGGTCGGAGTCAAC	GGGGTCATTGATGGCAACAATA
RUNX2	CCGTCTTCACAAATCCTCCCC	CCCGAGGTCCATCTACTGTAAC
COL1A1	GATCTGCGTCTGCGACAAC	GGCAGTTCTTGGTCTCGTCA
MMP13	CCAGACTTCACGATGGCATTG	GGCATCTCCTCCATAATTTGGC
IHH	AACTCGCTGGCTATCTCGGT	GCCCTCATAATGCAGGGACT
ALPL	GGGACTGGTACTCAGACAACG	GTAGGCGATGTCCTTACAGCC
IBSP	GAACCTCGTGGGGACAATTAC	CATCATAGCCATCGTAGCCTTG
COL10A1	CATAAAAGGCCCACTACCCAAC	ACCTTGCTCTCCTCTTACTGC
BGLAP	GGCGCTACCTGTATCAATGG	GTGGTCAGCCAACTCGTCA
SPARC	CCCAACCACGGCAATTTCCTA	CGTCTCGAAAGCGGTTCC
SOX9	AGCGAACGCACATCAAGAC	CTGTAGGCGATCTGTTGGGG
AGC	AGACTTGCGTCTACCCCAATC	GCAGGCGTAGGAAGGTCATC

Histology and Immunohistochemistry:

At harvest, constructs were preserved in 10% formalin for 24 hours then dehydrated through serial ethanol solutions. After dehydration, constructs were embedded in paraffin and sectioned at 6 µm per slice. Constructs were stained with alcian blue for construct-immobilized GAG and von Kossa for phosphate presence in deposited mineral following established protocols. Collagen type X and bone sialoprotein (BSP) presence were visualized through immunohistochemistry. For collagen type X, the protein was exposed by first subjecting samples to hyaluronidase treatment (2 mg/mL, type IV) for 60 minutes at 37^{o}C, then treated with Pronase E (1 mg/mL) for 60 minutes at 37^{o}C. In contrast, BSP underwent antigen retrieval, with slides submerged in citrate buffer within a container of boiling water and allowed to incubate for 20 minutes. After these preparation steps, both sets of stains were blocked through incubation of samples in 0.3% hydrogen peroxide for 30 minutes and then the Vectastain Elite Universal staining kit (PK-6200, Vector Laboratories, Burlingame, CA) was utilized to prepare and detect

the primary antibody (Vector Laboratories, Burlingame, CA). Primary antibodies for collagen type X (AbCam, 1/1000 dilution, AB49945, San Francisco, CA) and BSP (EMD Millipore, 1/500 dilution, AB1854, Bilerica, MA) were incubated on the slides overnight at 4 ^{o}C. Samples were counterstained with Hematoxylin QS (Vector Laboratories, Burlingame, CA).

Micro-computed tomography (µCT):

Constructs were scanned on a vivaCT 40 (Scanco Medical, Bruttisellen, Switzerland) system using a modified protocol by Liu, X.S. et al (138). Scanner settings were as follows: voltage 55 kV, current 0.109 mA, slice thickness 21 µm. Scans had a 21 µm isotropic resolution. Three dimensional reconstructions and quantitation was performed by using thresholding set at 200 mg HA/ cubic centimeter. Bone Volume, bone mineral density (BMD), and bone surface to bone volume ratio (BS/BV) were calculated for the scanned samples. n=4 for each experimental group.

Mechanical testing:

The equilibrium and Young's modulus were determined for each construct (n=6) following previously published methods (102). An initial compressive load of 0.2N was applied to all samples, followed by a stress-relaxation step with compression occurring at a ramp velocity of 1% per second to 10% total strain, which was then held at 10% strain for 1800 s. The Young's and equilibrium modulus were calculated based on the forces measured during this step. n=5 for each experimental group.

Statistics:

All data is presented as mean ± standard deviation. Statistical significance of analyses were analyzed by using a one-way analysis of variance (ANOVA) followed by Tukey's post-test, with significance determined by $p<0.05$ for each chondrogenic duration (Prism Software, GraphPad, La Jolla, CA, USA).

5.4 Results

Constructs were harvested after their respective chondrogenic cultivation durations (1, 2.5, or 4 weeks) and were evaluated for their chondrocyte state (Figure 5.2). Over the additional three weeks of culture, the 4 wk constructs had significantly greater DNA and GAG content compared to the 1 wk group, suggesting a transition through a chondrocyte proliferation and matrix production stage (Figure 5.2A,B) (19). A state of enhanced matrix production was confirmed with gene expression, as the 4 wk group had significantly higher gene expression of important cartilage matrix proteins collagen type 2 (gene: COL2A1) and aggrecan (gene: AGC) (Figure 5.2C). Histological staining of sulfated GAGs through the use of alcian blue dye provides a good representation of the associated aggrecan present in the matrix. In agreement with the gene expression data, positive staining with alcian blue increased with increasing duration. The broadened deposition of GAG and the higher intensity of the blue staining suggest the varied states of chondrogenesis, with the early state chondrocytes depositing little aggrecan and the progression to mature states corresponding with broader and more plentiful deposition (Figure 5.2D, Alcian Blue). The maturation towards a hypertrophic chondrocyte state in these constructs was also shown in this gene expression data, as prolonged chondrogenic culture corresponded with a significant increase in gene expression of the unique hypertrophic

chondrocyte marker collagen type X (19) (gene: COL10A1) amongst all groups, and of one of the key signaling proteins for hypertrophic maturation, Indian hedgehog (139) (gene: IHH) for the longer cultivated groups compared to 1 wk. The presence of deposited collagen type X increased with prolonged cultivation, and hypertrophic-like chondrocytes were even present, as noted by their increased cell volume and pericellular staining of collagen type X (Figure 5.2D, Collagen Type X). Prolonged duration did correspond with advanced chondrocyte states, as evidenced by the significantly higher gene expression and widespread protein deposition.

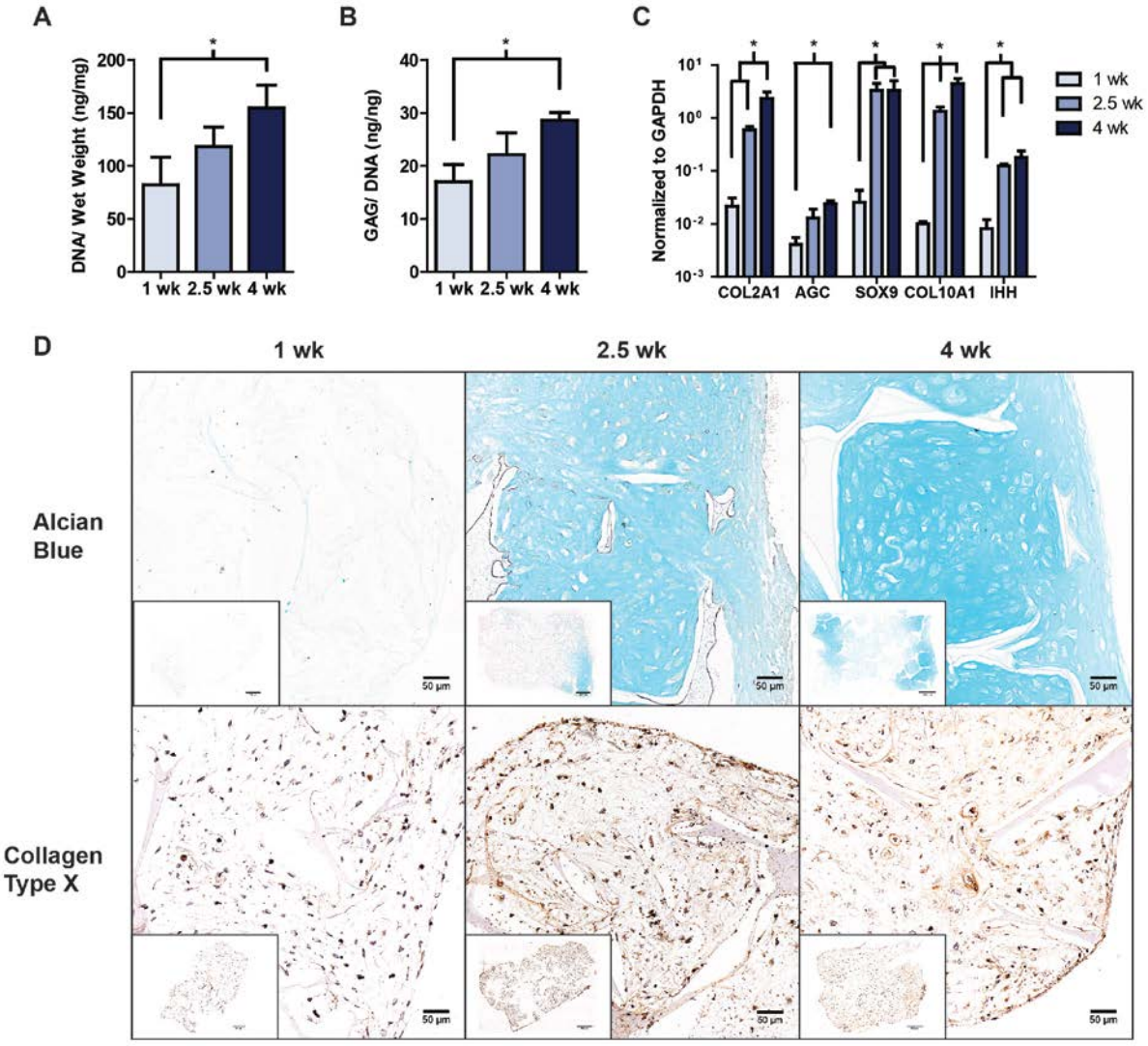

Figure 5.2: Chondrocyte state determined by the duration of chondrogenic culture. *Prolonged chondrogenic culture corresponded to an increase in cartilage matrix production and a more advanced chondrocyte state. Prolonged culture resulted in increased DNA and GAG present within the scaffolds, with 4 wks having significantly more DNA and GAG/ DNA compared to the 1 wk group (5.2A,B). Gene expression of key cartilage-related genes saw enhanced expression with increased duration across all genes studied, both in the chondrocyte-specific and in the more mature, hypertrophic genes (5.2C). Increased GAG deposition and collagen type X staining corresponded to increased duration of chondrogenic culture, with 4 wk demonstrating widespread GAG and collagen type X within the construct (5.2D). [n=4 and * denotes significance of $p<0.05$ (5.2A-C), Scale Bar = 50 µm, Insert Scale Bar = 500 µm (5.2D)]*

After chondrogenic culture, all groups were incubated in hypertrophic medium for three weeks to induce maturation. After culture, constructs from each experimental group were harvested, and analyzed for their degree of hypertrophy. Expression of genes essential for hypertrophic chondrocyte performance were analyzed (19, 140): collagen type X (COL10A1), a unique collagen produced only by hypertrophic chondrocytes, RUNX2, a master regulatory for bone formation, IHH, a signaling protein to induce maturation, and matrix metalloprotease 13 (MMP13), a cartilage degrading protease expressed during turnover (Figure 5.3A). The expression of COL10A1, RUNX2, and IHH all increased significantly with each experimental group and MMP13 was enhanced in the 2.5 wk group.

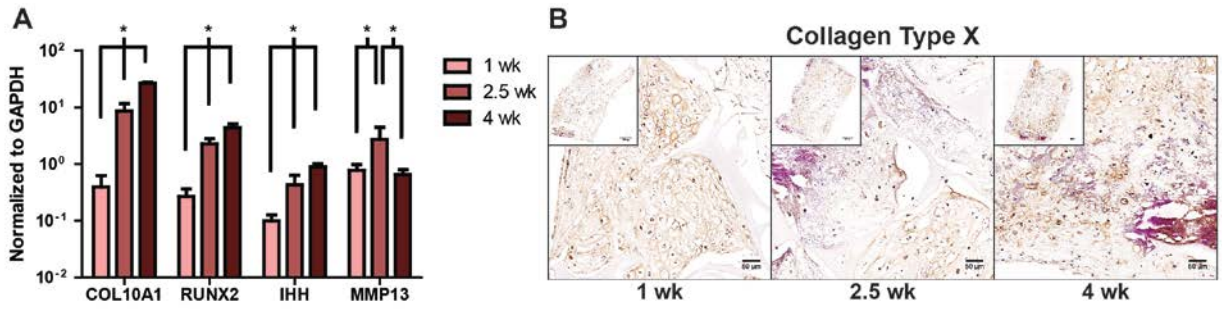

Figure 5.3: Enhanced hypertrophic maturation of constructs with increasing chondrogenic culture duration. *At the culmination of the three week hypertrophic induction, the constructs with a prolonged chondrogenic culture demonstrated enhanced hypertrophic chondrocyte maturation. Gene expression of hypertrophic markers significantly increased with increased chondrogenic culture (5.3A). All three groups contained cells with the trademark hypertrophic chondrocyte markers of an enlarged lacunae surrounded by collagen type X; however, a greater presence of collagen type X was seen with increased duration (5.3B). [n=4 and * denotes significance of $p<0.05$ (5.3A), Scale Bar = 50 µm, Insert Scale Bar = 500 µm (5.3B)]*

Immunohistochemistry showed the collagen type X deposition followed the gene expression trends, with broader deposition and deeper intensity seen throughout the longer cultivated constructs (Fig3B, inset). Unlike the samples harvested after chondrogenic cultivation, all constructs contained the enlarged lacunae and pericellular collagen type X staining that are

hallmarks of hypertrophic chondrocytes (Figure 5.3B), but there was a clear increase in hypertrophic chondrocyte numbers with each increase in chondrogenic cultivation duration.

The induced maturation did not have a dramatic effect on cell viability amongst the groups, as the DNA content per construct was not significantly different (Figure 5.4A). The maturation did initiate the deposition of a bone matrix within each construct. Genes related to bone formation were analyzed, and the two prolonged chondrogenic cultivations had enhanced expression in all genes studied, with collagen type I, bone sialoprotein (IBSP), and alkaline phosphatase (ALPL) were significantly higher than 1 wk (Figure 5.4B). Despite similarity in COL1A1 gene expression between 2.5 wk and 4 wk constructs, the 4 wk constructs had significantly more collagen at the end of the hypertrophic culture (Figure 5.4C). Immunohistochemistry for presence of the mineral nucleator bone sialoprotein (BSP) revealed similar deposition profiles between the 2.5 wk and 4 wk constructs, which had stronger staining than the 1 wk constructs.

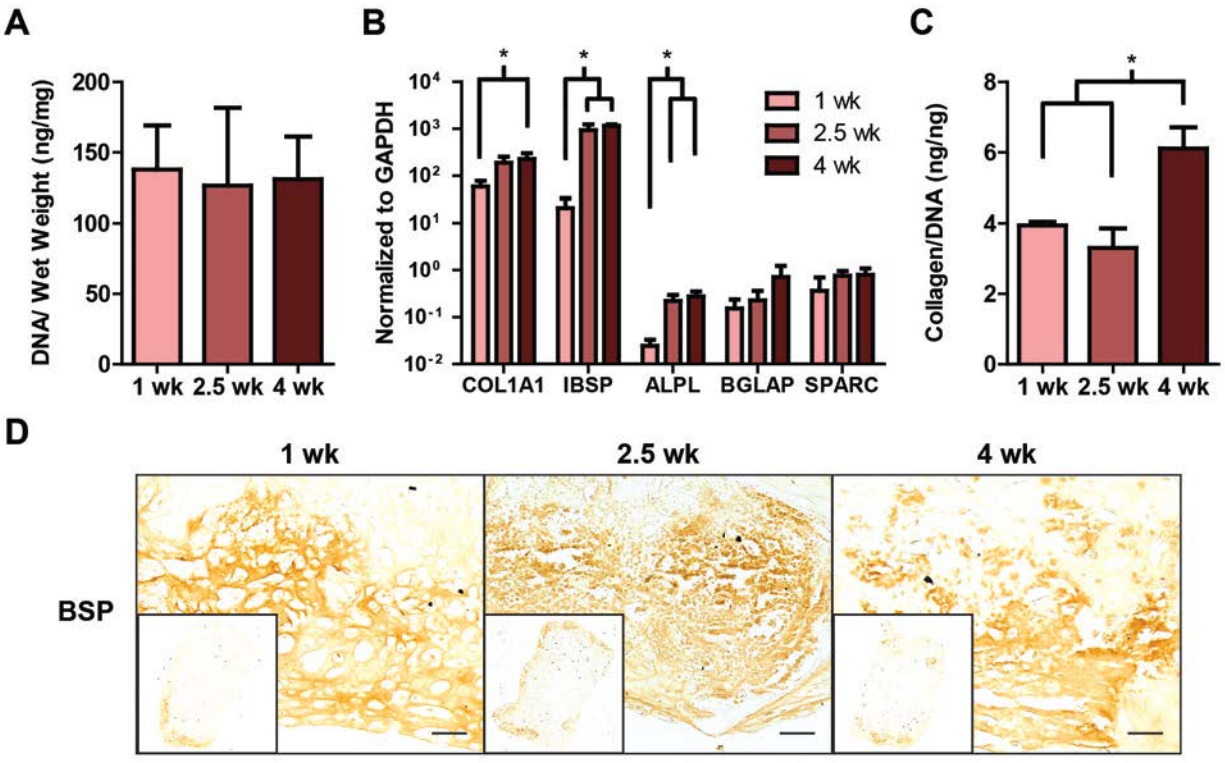

Figure 5.4: Advanced chondrocyte states corresponded to increased hypertrophic chondrocyte deposition of bone template matrix. *Hypertrophic chondrocytes induced after prolonged chondrogenic culture deposited an enhanced bone template. After hypertrophic induction, there was no significant difference amongst the groups in the cellularity of the constructs (5.4A). Gene expression of key bone genes, COL1A1, IBSP, and ALPL, were all significantly higher with increasing chondrogenic culture (5.4B), and there was significantly more collagen content in the 4 wk group, compared to the others (5.4C). Presence of bone sialoprotein was apparent in all three groups, but the longer durations showed increased and more widespread deposition across the construct. [n=4 and * denotes significance of $p<0.05$ (5.4A-C), Scale Bar = 50 µm, Insert Scale Bar = 500 µm (5.4D)]*

The trends seen in BSP deposition matched the mineral deposition, as shown through von Kossa histological staining (Figure 5.5A). The 2.5 wk and 4 wk constructs had depositions at various points along the periphery of the construct, whereas the 1 wk constructs concentrated mineral at both ends of the scaffold. Three dimensional reconstructs of the µCT scans clearly demonstrated the differences in mineral deposition seen in the histological stains (Figure 5.5B).

The widespread mineral depositions seen in histology of the 2.5 and 4 wk constructs correlated with extensive mineral deposits, with many small, concentrated bundles of mineral. In contrast, the 1 wk constructs, with sparse histological staining for mineral except at the scaffold ends, had two large sheets of deposited mineral located on either side of the scaffold. Quantitation of the μCT scans demonstrated no significant difference in the amount or density of the deposited mineral (Figure 5.5C). The differences in deposition pattern were elucidated by quantitation, with the bone surface to bone volume ratio was significantly lower for the 1 wk constructs, agreeing with the observation of 1 wk constructs' concentrated location for mineral deposition.

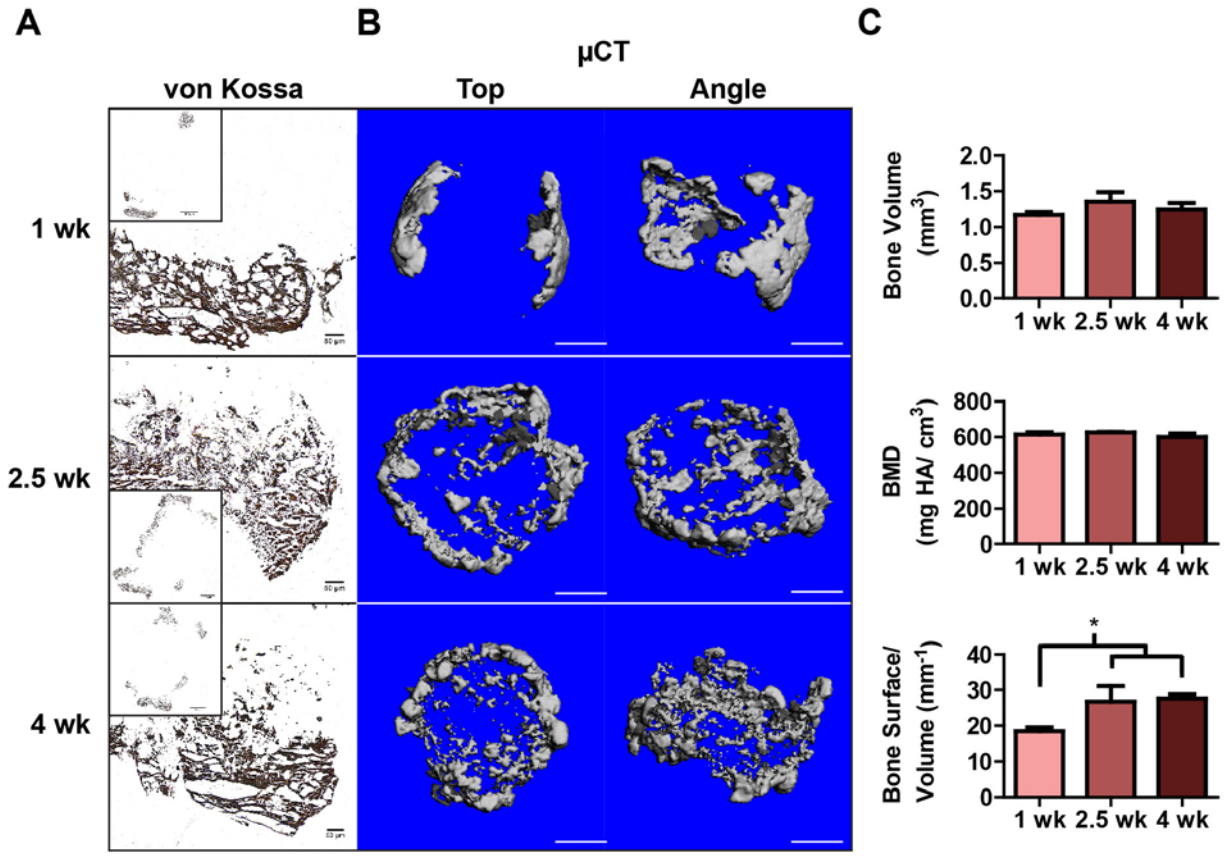

Figure 5.5: Hypertrophic chondrocyte mineral deposition varies based on chondrocyte state. *Prolonged chondrogenic culture resulted in a significantly different pattern of mineral deposition. Von Kossa staining demonstrated widespread mineral deposition throughout the 2.5 wk and 4 wk constructs while the mineral deposition in the 1 wk constructs was localized to the scaffold edges (5.5A). Three dimensional reconstruction of μCT scans showed widespread deposition of small clumps of mineral for the two prolonged culture constructs. In contrast, the 1 wk constructs deposited sheet-like mineral in a continuous manner (5.5B). The μCT scans were quantified, with the bone volume and bone mineral density (BMD) not significantly different amongst the different constructs (5.5C). The bone surface/ volume ratio was significantly higher for 2.5 and 4 wk constructs, elucidating the deposition pattern differences. [Scale Bar = 50 μm, Insert Scale Bar = 500 μm (5.5A), Scale bar = 1 cm (5.5B), n=4 and * denotes significance of $p<0.05$ (5.5C)]*

The mechanical properties of the constructs were evaluated upon harvest at the two essential time points (Figure 5.6). After chondrogenic culture, the 4 wk construct had a significantly higher elastic modulus than the 1 wk group. Induction of hypertrophic maturation

and bone matrix deposition did increase the stiffness of the constructs, as the 1 wk construct after hypertrophic culture still had a higher mechanical stiffness than the 4 wk construct after chondrogenic culture. Despite the increase in mechanical stiffness, the same trends held after hypertrophic cultivation, with the 4 wk construct significantly stiffer than the other constructs.

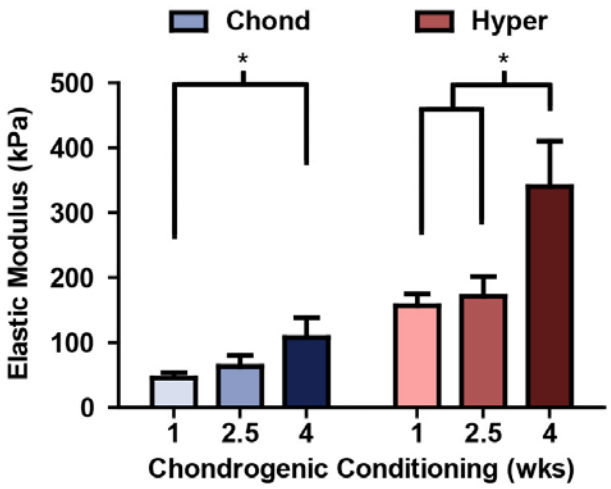

Figure 5.6: Elastic modulus of constructs at various stages of differentiation. *The elastic modulus is presented of constructs harvested at the culmination of both chondrogenic and hypertrophic cultivation. Prolonged chondrogenic culture resulted in enhanced mechanical properties, as the 4 wk constructs had a significantly greater elastic modulus than the 1 wk constructs for both the chondrogenic and hypertrophic harvests, and a significantly greater elastic modulus than the 2.5 wk constructs for the hypertrophic harvest. [n=5 and * denotes significance of $p<0.05$]*

5.5 DISCUSSION

Endochondral ossification-based strategies show promise for bone tissue engineering by facilitating rapid bone deposition and vascularization of constructs (62, 69, 93). These strategies hinge on the ability to derive hypertrophic chondrocytes, the cells that orchestrate key events for bone formation (132). In native endochondral ossification, hypertrophic chondrocyte

differentiation is the culmination of a progression through various chondrocyte states (19). The aim of this study was to investigate the importance of replicating this progression, to determine if advanced chondrogenic states result in an enhanced maturation to hypertrophic chondrocytes.

The various chondrogenic states of endochondral ossification were replicated by controlling the cultivation duration of constructs in chondrogenic medium. By culturing for 1, 2.5, and 4 weeks in chondrogenic medium, clear construct characteristics were developed that allow an approximation of the chondrogenic state. The 1 wk constructs were clearly at an early chondrogenic state as they had significantly lower cartilage gene expression and matrix deposition, and the DNA content of the constructs was significantly lower than the 4 week group, suggesting that the chondrocyte proliferation and matrix deposition hadn't yet taken place (4). The 2.5 wk constructs were more similar to the matrix-producing chondrocyte state seen natively. The constructs contained noticeable deposition of GAG, had strongly upregulated chondrocyte-specific genes, and even contained some pre-hypertrophic and hypertrophic cells, as referenced by hypertrophic gene expression and collagen type X deposition. The 4 wk constructs were firmly in the advanced chondrocyte state. These constructs had the highest expression of hypertrophic genes, and had trademark collagen type X deposition surrounding the increased lacunae of the derived hypertrophic chondrocytes.

TGF-ß and dexamethasone are strong promoters of chondrogenesis (141), and their removal, coupled with the addition of a thyroid hormone (142, 143), progressed hypertrophic maturation. Over the three week hypertrophic culture, cells in all three experimental groups underwent maturation, as shown by the trademark hypertrophic chondrocyte lacunae surrounded by collagen type X. The elevation in expression of hypertrophic genes confirms this analysis, as each group experienced a significant increase from the chondrogenic culture to hypertrophic

culture. Though research suggests various states of hypertrophic chondrocytes (140, 144, 145), the differences in elevated gene expressions between groups is most likely related to the number of matured hypertrophic chondrocytes within each construct. This point is further validated through collagen type X staining, with each increase in chondrogenic cultivation duration corresponding to more extensive staining of collagen type X.

The importance of the chondrogenic state in facilitating hypertrophic maturation is evident, as the constructs with the most advanced, widespread chondrocyte differentiation resulted in the highest concentration of hypertrophic chondrocytes. Interestingly, the 1 wk constructs that represented early chondrogenesis, with reduced chondrocyte gene expression and minimal cartilage deposition, still contained hypertrophic chondrocytes at the end of cultivation. The delivery and accessibility of growth factors plays an integral role in differentiation. TGFß, the powerful growth factor utilized in chondrogenic medium (70), has been shown to stimulate small clusters of chondrogenic differentiation within just 1 week of cultivation, even though prolonged culture produced widespread differentiation (146). In addition, mesenchymal stem cells are heterogeneous, with various subpopulations behaving differently in response to stimuli (147, 148). The ability of TGFß to stimulate localized differentiation coupled with the known effects of MSC heterogeneity, suggests that various chondrogenic states existed even within the constructs. In the 1 wk group, it is likely that more advanced chondrocytes had differentiated in specific locations during the one week of cultivation, and were subsequently matured into hypertrophic chondrocytes.

The lack of chondrocytes and hypertrophic chondrocytes in the interior of the constructs was also due to growth factor accessibility. Exogenously added TGFß is readily confined to the exterior of constructs due to cell activity, preventing growth factor penetration to the interior of

the construct and mitigating chondrocyte differentiation in these parts (149). Recent work demonstrated that the utilization of a latent phase of TGFß was able to bypass the exterior cells and localize to the interior of the constructs, and upon activation, stimulated chondrogenic differentiation (150). Therefore, the limited diffusion of TGFß restricted chondrocyte differentiation to the exterior of the construct. The sole localization of hypertrophic chondrocytes within the areas of chondrocyte differentiation demonstrates the importance of the chondrocyte differentiation in successful hypertrophic chondrocyte differentiation.

Similar to the presence of hypertrophic chondrocyte markers, bone formation markers increased with increasing duration of chondrogenic culture. The deposition of BSP correlated with collagen type X deposition, indicating that it was in fact the matured hypertrophic chondrocytes that contributed to the bone template formation (140) and suggests that the elevated gene expression values were due to the larger number of hypertrophic chondrocytes. Despite having a larger number of hypertrophic chondrocytes, the amount of mineral deposited within each construct was not significantly different amongst the groups. The deposition pattern was different, as demonstrated by the bone surface to volume ratio, with the prolonged durations producing small clustered groups throughout the construct and the 1 wk group producing continuous, large sheets. Hypertrophic chondrocytes release a number of cell signaling molecules, some of which are responsible for controlling the chondrogenic state of nearby cells (i.e. growth plate) (19, 24, 133). The continuous nature of the 1 wk depositions suggests an alignment in production, possibly orchestrated by the hypertrophic maturation of a centralized location that prompted the subsequent advanced chondrogenesis and maturation of the surrounding cells. Quantitation showed a significant increase in the deposited amount of GAG between the end of chondrogenic culture and hypertrophic culture, indicating differentiation to a

cartilage-producing chondrogenic state occurred even after the removal of TGFß. In addition, recent work within our laboratory has shown that localized hypertrophic chondrocyte differentiation can stimulate chondrogenesis and spatial alignment in the surrounding tissue. In contrast, that widespread advanced chondrogenic state found in the prolonged duration constructs possibly impeded the ability of a localized group to control widespread deposition. It appears that hypertrophic chondrocytes differentiated within multiple, separate scaffold pores organizing mineralization within their local environment.

Interestingly, despite significant difference in the original chondrocyte state and expression of hypertrophic markers, bone gene expression and protein/ mineral deposition was not different between the 2.5 wk and 4 wk groups. The only noticeable difference between the two groups was the stiffness of the constructs, which can be attributed to the significant difference in GAG content (151) between the two groups, and not necessarily the hypertrophic differentiation and matrix deposition. The similarity in hypertrophic chondrocyte performance suggests that there is a chondrocyte state threshold, that once reached allows the widespread differentiation of hypertrophic chondrocytes and subsequent bone template deposition.

5.6 CONCLUSION

Varying chondrogenic states were derived in MSC constructs by prolonging the duration of chondrogenic culture. Prolonged culture produced enhanced chondrocyte gene expression and cartilage deposition, as well as increased expression and deposition of hypertrophic markers. Upon induced hypertrophic maturation, the advanced chondrocyte state constructs had more and broader hypertrophic chondrocyte differentiation. Whereas the early chondrocyte state created by 1 wk of chondrogenic culture prompted minimal bone template deposition from the localized

hypertrophic chondrocytes, the 2.5 wk and 4 wk groups had similar levels of bone template deposition and mineralization. The results demonstrate the partial truth of our hypothesis that advanced chondrocyte states do enhance hypertrophic chondrocyte differentiation, but that a threshold exists in the chondrocyte state between 1 wk and 2.5 wks. The attainment of the threshold allows the widespread hypertrophic chondrocyte differentiation and bone template deposition needed for bone tissue engineering.

PART IV

EVALUATE THE ABILITY OF HYPERTROPHIC CHONDROCYTES TO MEDIATE FAST, VASCULARIZED BONE DEPOSITION THAT INTEGRATES WITH HOST BONE

6 Mimicked Ossification Pathway influences Differentiated Stem Cell Bone Matrix Deposition and Remodeling

6.1 ABSTRACT

In the native skeleton, bone formation occurs through two ossification pathways, intramembranous and endochondral. Advancements in tissue engineering have demonstrated the ability to mimic these pathways by differentiating mesenchymal stem cells into osteoblasts for intramembranous and hypertrophic chondrocytes for endochondral. In this study, we created and implanted constructs derived from both differentiated cell types with the aim to analyze and compare the characteristics and regenerative capabilities of each mimicked pathway. After cultivation, the differentiated osteoblasts were uniquely present along the scaffold walls, where all deposited bone matrix was located. In contrast, the differentiated hypertrophic chondrocytes formed within the scaffold pore space, and produced a greater amount of mineral, but of immature composition, compared to the osteoblasts. Upon implantation, differentiated osteoblasts facilitated enhanced deposition of mineral onto the scaffold, but moderate overall construct regeneration. The differentiated hypertrophic chondrocytes stimulated turnover of the construct, with remodeling of the deposited bone matrix into cortical-like bone and extensive construct vascular infiltration. This study reveals the suitability of differentiated hypertrophic chondrocytes for use in bone repair situations that require fast bone formation and vascularization, whereas differentiated osteoblasts should be paired with advanced bone scaffolds to orchestrate remodeling and incorporation.

6.2 SIGNIFICANCE

Bone tissue engineering has yet to deliver on its promise for improved long bone repair due to inconsistencies in integration, remodeling, and mechanical maintenance. The ability to mimic the natural ossification pathways through stem cell differentiation provides another variable that tissue engineers can use to address these problems. In the proposed study, we investigated the characteristics and performance of each mimicked pathway, elucidating key attributes that dictate each pathway's suitability for tissue engineering. With the presented data, tissue engineers can make informed decisions and develop complex strategies to finally deliver on bone tissue engineering's promise.

6.3 INTRODUCTION

In humans, bone formation occurs through two ossification pathways, intramembranous and endochondral (132). Intramembranous ossification is characterized by direct differentiation of stem cells into osteoblasts, is utilized in the repair of small, stabilized fractures and is responsible for bone formation during turnover and remodeling (41, 133, 152). In contrast, endochondral ossification is characterized by an initial deposition of a cartilage anlage, formed by stem cell derived chondrocytes (19, 41, 51). After cartilage deposition, these chondrocytes mature into hypertrophic chondrocytes, and initiate the formation of bone from the cartilage template (19, 24, 132). Endochondral ossification is the process by which the growth plate stimulates bone lengthening and is the primary method for bone regeneration after long bone fracture (24, 51). As noted, each ossification process has specific situations in which it contributes to the generation and maintenance of the skeletal system.

Tissue engineering has mimicked each ossification pathway by differentiating the key cell type of each process from stem cell sources. For intramembranous ossification, osteoblasts are directly differentiated, with bone production confirmed both in vitro, and in a number of in vivo applications (59, 153-155). Endochondral ossification is mimicked through the initial differentiation of chondrocytes and deposition of a cartilage-like matrix. After a set cultivation period, the chondrocytes are matured, through the addition of hormones, into hypertrophic chondrocytes (61, 62, 143, 156). The derived hypertrophic chondrocytes deposit mineral in vitro and have produced a bone marrow containing bone model upon in vivo implantation (93). Though successful bone production has occurred through both processes, implantation of tissue engineered constructs into orthotopic models has produced inconsistent results, largely because of failure attributed to one of three reasons: failure to integrate, inability to stimulate native bone generation, or mechanical property insufficiency (3, 157). It is possible that these failures occur due to a poor understanding of the capabilities of the chosen tissue engineered ossification pathway, as even natively, the followed ossification pathway is based on the fracture environment (41).

The aim of this study was to characterize the bone produced using each key cell type in an attempt to elucidate the attributes and abilities of each mimicked ossification pathway. A better understanding of the pathways would allow tissue engineers to promote better bone regeneration and design the next generation of clinically-feasible grafts. We created representative tissue engineered constructs from the key cell type in each mimicked ossification pathway, osteoblasts and hypertrophic chondrocytes, by differentiating each from human mesenchymal stem cells according to the existing literature (59, 61, 62). Upon differentiation, constructs were analyzed for cellular behavior with regards to bone formation and matrix

deposition. Constructs were then implanted subcutaneously in nude mice and harvested regularly to understand the differing bone regeneration events instigated by the cell types.

6.4 MATERIALS AND METHODS

All materials were purchased from Sigma Aldrich (St. Louis, MO) unless otherwise noted.

Scaffold Fabrication:

Bombyx mori silk fibroin solution at 16 wt% in HFIP was prepared following published methods (135). Porous scaffolds were formed using NaCl salt, 400-600 μm in diameter, as a porogen. The HFIP silk solution was poured over the salt and allowed to solidify. After solidification, ß-sheet formation was induced by submerging the silk-NaCl scaffolds in methanol for 1-2 days. NaCl was removed from the scaffolds by washing in diH_2O for 2 days, and then the scaffolds were sized into cylinders of 4 mm in dimeter and 2 mm in height. Scaffolds were disinfected in sterile-filtered 70% ethanol before use.

Cell Expansion, Seeding, Differentiation and Cultivation:

Human bone marrow stem cells (hBMSCs, Lonza, Basel, CH) were expanded in expansion medium consisting of high glucose medium with L-glutamine, 10% fetal bovine serum, and 1% penicillin/ streptomycin. After disinfection in 70% ethanol, scaffolds were incubated in expansion medium for one day. Passage 5 hBMSCs were trypsinized, resuspended in culture medium at 30M cells/ mL, and the cells were seeded into the scaffolds using the drip method. Seeded scaffolds were incubated in expansion medium for an additional day and then switched to the appropriate cultivation regime. Intramembranous-mimicking constructs (termed

Osteo) were generated by differentiating hBMSCs into osteoblasts over five weeks in osteogenic medium, low glucose DMEM (ThermoFisher, Waltham, MA), 100 nM dexamethasone, 50 ug/mL ascorbic acid, 10 mM HEPES buffer, 10% fetal bovine serum, 1% P/S, and 5mM β-glycerophosphate. Endochondral-mimicking constructs (termed Hyper) were generated by first differentiating the hBMSCs into chondrocytes for two weeks in chondrogenic medium, high glucose DMEM (ThermoFisher, Waltham, MA) supplemented with 100 nM dexamethasone, 50 µg/mL ascorbic acid, 50 µg/ mL proline, 100 µg/mL sodium pyruvate, 1% ITS+, 1% P/S, 10 ng/mL BMP6 and 10 ng/mL TGF-β3. After the successful differentiation and cartilage matrix deposition, the chondrocytes were induced to hypertrophic chondrocytes for three weeks by the change in medium composition. Hypertrophic chondrocyte maturation medium had the same composition as chondrogenic medium but without TGF-β3, a dexamethasone concentration of 1 nM, 50 ng/mL of L-thyroxine, and 5mM of β-glycerophosphate.

Real time PCR:

Construct RNA was extracted using TRIzol (ThermoFisher, Waltham, MA), with total RNA content measured using NanoDrop spectrophotometric quantitation (ThermoFisher, Waltham, MA). Contaminating DNA was removed through treatment with DNase, and cDNA was transcribed using the High Capacity cDNA Reverse Transcription kit (ThermoFisher, Waltham, MA) according to the manufacturer's instructions. Once cDNA was obtained, quantitative RT-PCR was performed using Fast Sybr Green mix (ThermoFisher, Waltham, MA). Quantitation was normalized using the ΔC_t, the C_t of GAPDH subtracted from the C_t of the gene of interest. Forward and reverse primers for each gene are present in Table 6.1. Samples were run in duplicate, with n=4 for each experimental group.

Table 6.1: Primers used in RT-PCR

Gene	Forward	Reverse
GAPDH	AAGGTGAAGGTCGGAGTCAAC	GGGGTCATTGATGGCAACAATA
RUNX2	CCGTCTTCACAAATCCTCCCC	CCCGAGGTCCATCTACTGTAAC
COL1A1	GATCTGCGTCTGCGACAAC	GGCAGTTCTTGGTCTCGTCA
IBSP	GAACCTCGTGGGGACAATTAC	CATCATAGCCATCGTAGCCTTG
ALPL	GGGACTGGTACTCAGACAACG	GTAGGCGATGTCCTTACAGCC
BGLAP	GGCGCTACCTGTATCAATGG	GTGGTCAGCCAACTCGTCA
SPARC	CCCAACCACGGCAATTTCCTA	CGTCTCGAAAGCGGTTCC
SPP1	GTTTCGCAGACCTGACATCCA	GCTTTCCATGTGTGAGGTGAT

DNA and Matrix Quantitation:

Constructs were weighed and then digested with papain (40 units/ mg) in digest buffer (0.1M sodium acetate, 10 mM cysteine HCl and 50 mM EDTA, pH 6.0) at 60 ^{o}C overnight. DNA content per wet weight was measured from the digest using the Quant-iT PicoGreen assay kit (ThermoFisher, Waltham, MA) following the manufacturer's instructions and with the supplied lambda DNA as the standard.

Construct collagen content was determined through a modified protocol from Reddy and Enwemeka (137), where papain digest solution was incubated in 6M HCl at 110 ^{o}C overnight, then reacted with Chloramine T and Elrich's reagent to visualize the amount of hydroxyproline present within the samples, as determined by spectrophotometry and the hydroxyproline standard.

After harvest, constructs were snap frozen in liquid nitrogen and stored at -20 ^{o}C. Calcium was extracted from the samples through incubation with 5% trichloroacetic acid solution and quantified using the Calcium (CPC) Liquicolor kit (Stanbio Laboratory, Boerne, TX).

Histology and Immunohistochemistry (Pre-implantation):

Samples were preserved in 10% formalin for 24 hours, then rinsed excessively in PBS, and dehydrated in solutions of ascending ethanol concentrations. After dehydration, constructs were embedded in paraffin and sectioned at 6 µm per slice. Constructs were stained with hematoxylin and eosin for construct morphology and von Kossa for phosphate presence in deposited mineral following easily accessible and established protocols. Collagen type I and bone sialoprotein (BSP) presence were visualized through immunohistochemistry. For collagen type I, the protein was exposed by first incubating samples in 0.01% trypsin for 15 minutes at 37^{o}C. In contrast, BSP underwent antigen retrieval, with slides placed in a container filled with citrate buffer and that container submerged in boiling water for 20 minutes. After these preparation steps, both sets of stains were blocked through incubation of samples in 0.3% hydrogen peroxide for 30 minutes and then Vectastain Elite Universal staining kit (PK-6200, Vector Laboratories, Burlingame, CA) was utilized to prepare and detect the primary antibody (Vector Laboratories, Burlingame, CA). Primary antibodies for collagen type I (AbCam, 1/200 dilution, AB6308, San Francisco, CA) and BSP (EMD Millipore, 1/500 dilution, AB1854, Bilerica, MA) were incubated on the slides overnight at 4 ^{o}C. Samples were counterstained with Hematoxylin QS (Vector Laboratories, Burlingame, CA).

Micro-Computed Tomography (µCT) and Quantitation (Pre-Implantation)

Pre-implantation, constructs were scanned on a vivaCT 40 (Scanco Medical, Bruttisellen, Switzerland) system using a modified protocol by Liu, X.S. et al (138). Scanner settings were as follows: voltage 55 kV, current 0.109 mA, slice thickness 21 µm. Scans had a 21 µm isotropic resolution. Three dimensional reconstructions and quantitation was performed by using

thresholding set at 220. Bone Volume, bone mineral density (BMD), and bone surface to bone volume ratio (BS/BV) were calculated for the scanned samples.

Fourier Transform Infrared Spectroscopy (FTIR):

FTIR spectra were recorded using a Nicolet iS5 (ThermoFisher, Waltham, MA) with an iD5 ATR accessory containing a diamond window. 6 μm thick, paraffin-embedded sections, 15 for each sample, were measured from a specimen for each group. The spectra were acquired using scans with a resolution of 4 cm^{-1} thick ranging from 400-4000 cm^{-1}. After acquisition, the regions of interest (900-1200 cm^{-1} & 1590-1720 cm^{-1}) were isolated, baselined and normalized for further post-processing using the Omnic software (ThermoFisher, Waltham, MA). The normalized data was de-convoluted, using a genetic algorithm, utilizing Matlab software (Mathworks, Natick, MA) that fit up to 12 Gaussian distributions. The peak intensity of the subpeaks of interest was recorded for each measurement.

Mechanical Compression Testing:

The equilibrium and Young's modulus were determined for each construct (n=6) following previously published methods (102). An initial compressive load of 0.2N was applied to all samples, followed by a stress-relaxation step with compression occurring at a ramp velocity of 1% per second to 10% total strain, which was then held at 10% strain for 1800 s. The Young's and equilibrium modulus were calculated based on the forces measured during this step.

Construct Subcutaneous Implantation

After five weeks of cultivation, constructs from both experimental groups, Hyper and Osteo, were placed in nude mouse subcutaneous pouches. Constructs were implanted for 3, 6, and 12 weeks, with sample harvest occurring at each designated time point.

Micro-Computed Tomography (µCT) and Quantitation (Post-Implantation)

After explant of the constructs following 3 weeks (n=4), 6 weeks (n=6), and 12 weeks (n=4) *in vivo*, constructs were scanned on a µCT 50 (Scanco Medical, Bruttisellen, Switzerland) using scanner settings as follows: voltage 70 kV, current 0.200 mA, slice thickness 10 µm. Scans had a 10 µm isotropic resolution. Three dimensional reconstructions and quantitation was performed by using a global thresholding technique set at 282.9 mg HA/ cm^3. Bone Volume, bone mineral density (BMD), and bone surface to bone volume ratio (BS/BV) were calculated for the scanned samples.

Hard Bone Histology:

Subcutaneous implants were immersed in 4% neutral-buffered formaldehyde solution for 24 hours, split in half, then dehydrated in ascending grades of ethanol and imbedded in light curing resin (Technovit 7200 VLC; Kulzer & Co., Wehrheim, Germany). Undecalcified thin ground sections along the longitudinal axis of the constructs were produced according to Donath (158) and stained with Levai-Laczko (159) dye. Histological specimens were digitized with the Olympus dotSlide 2.4, digital virtual microscopy system (Olympus, Japan, Tokyo) at a resolution of 0.32 µm per pixel. Sample number for 3 weeks (n=4), 6 weeks (n=6), and 12 weeks (n=4)

Immunohistochemistry (Post-implantation)

The remaining half of the harvested subcutaneous implants were extensively washed in PBS post 4% formaldehyde submersion, then decalcified using a formic acid based solution (Immunocal Decalcifier, StatLab, McKinney, TX). After decalcifying, grafts were washed multiple times with PBS, dehydrated, embedded in paraffin, and sectioned at 6 µm. Antigen retrieval and subsequent staining was conducted as described previously, but this time with the Vectastain ABC Kit for Rabbit IgG (PK-4001, Vector Laboratories, Burlingame, CA). Primary antibody for CD31 (AbCam, AB28364, San Francisco, CA) was incubated on the slides overnight at 4 ^{o}C. Samples were counterstained with Hematoxylin QS (Vector Laboratories, Burlingame, CA). Utilizing ImageJ, semi-quantitative values for the number of blood vessels, the area of the construct and blood vessels, and the distance of blood vessels were determined by two independent, blinded researchers on the 6 week (n=6) harvested constructs.

Statistics:

All data is presented as mean ± standard deviation. Statistical significance of pre-implantation analyses and the post-implantation semi-quantitative histology images was determined using a Student's T-Test, $\alpha = 0.05$, with significance determined by $p<0.05$ (Prism Software, GraphPad, La Jolla, CA, USA). Statistical significance of µCT quantitation post-implantation was determined by using a one-way analysis of variance (ANOVA) followed by Tukey's post-test, $\alpha=0.05$, with significance determined by $p<0.05$ for each construct type.

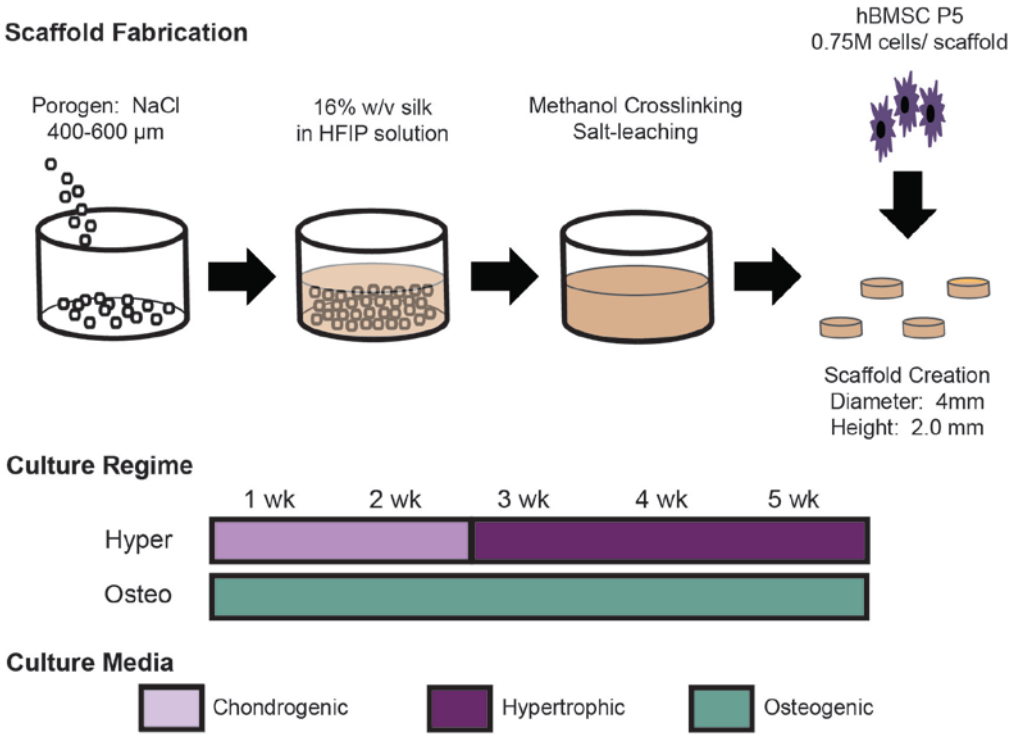

Figure 6.1: Methodology of mimicked ossification pathways*. Silk fibroin scaffolds were created by pouring 16% w/v silk dissolved in HFIP over NaCl particles 400-600 microns in size. Methanol was used to induce ß-sheet formation within the silk and the salt porogen was removed through multiple washes in deionized water. Scaffolds were sized, disinfected, and seeded with human bone marrow stem cells (hBMSC). Seeded constructs were cultured over five weeks corresponding to their designated experimental group. Hypertrophic chondrocyte-based constructs (Hyper) were derived by first inducing chondrogenesis in chondrogenic medium for two weeks, followed by hypertrophic maturation in hypertrophic medium for three weeks. Osteoblast-based constructs (Osteo) were formed by differentiating the stem cells in osteogenic medium for the entire five weeks.*

6.5 RESULTS

Cell behavior and matrix deposition:

After 5 weeks of their respective, designated culture regimes (Figure 6.1), the expression profiles of bone forming genes of the Hyper and Osteo constructs were explored (Figure 6.2A). RUNX2, a master regulator of bone formation (160), had significantly higher expression in the Hyper constructs, as was the main bone protein collagen type I (COL1A1). Important proteins related to matrix deposition and mineralization (IBSP, ALPL, BGLAP, SPARC, and SPP1) were all enhanced in the hypertrophic chondrocyte-based constructs. The DNA content was not significantly different between the constructs (Figure 6.2B), but H&E staining showed cellularity of the Hyper spread throughout the scaffold's pore space, whereas the Osteo cells were group together in close proximity to the scaffold walls (Figure 6.2D). Quantitation of the collagen content within the constructs was also not significantly different, but immunohistochemical staining of collagen type I showed differences, with Hyper constructs depositing collagen type I within the pore space and Osteo deposition largely confined to the construct walls on the periphery of the construct. Additional staining for the bone matrix protein bone sialoprotein showed deposition within the pore space of the Hyper constructs, but was again confined to the construct boundaries within the Osteo group.

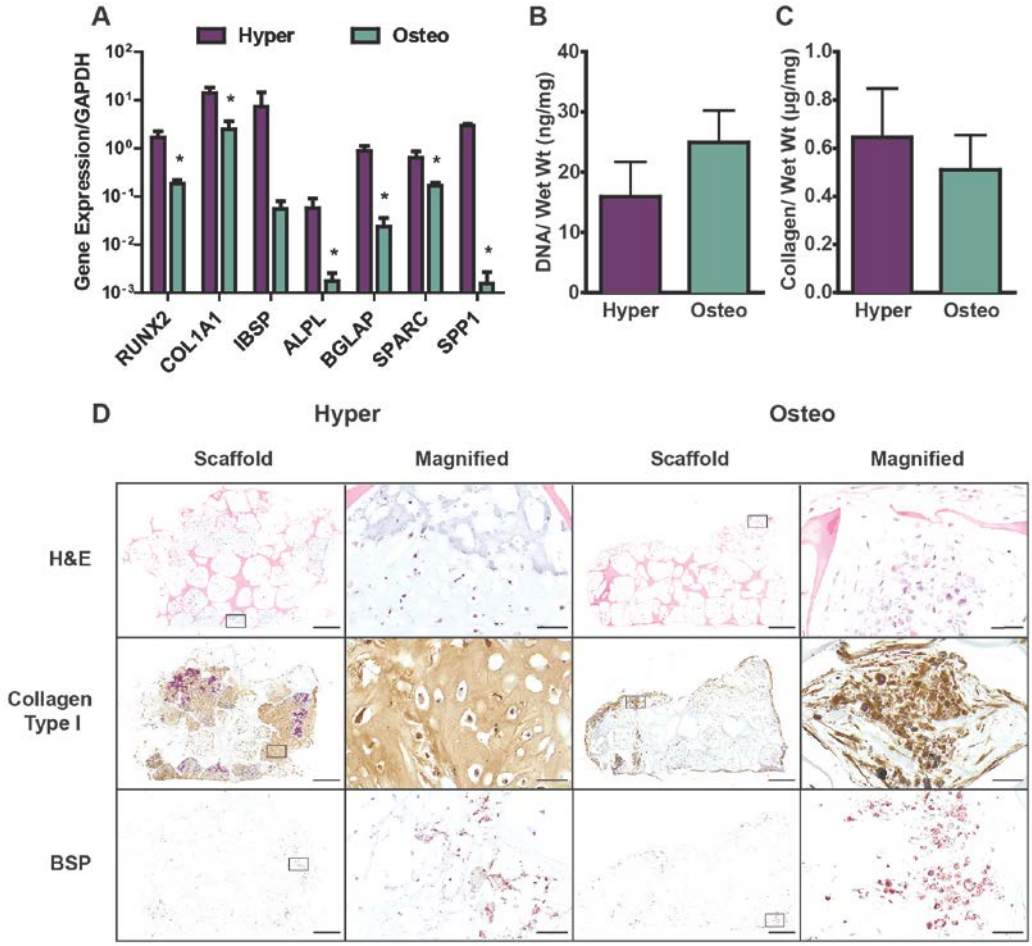

Figure 6.2: Gene expression and matrix deposition for the differentiated key cells. *Expression of key genes related to the deposition of bone was significantly upregulated in the Hyper constructs (Figure 6.2A). The cellularity of each construct at the end of cultivation demonstrated increased DNA content within the Osteo constructs, though it was not significant (Figure 6.2B). The amount of collagen, determined through hydroxyproline quantitation, was also not significantly different with a slight increase seen in the Hyper constructs (Figure 6.2C). The disparity in DNA content wasn't noticeable upon histological analysis, as H&E staining showed widespread cell content in both constructs (Figure 6.2D, H&E). Though not significantly different, immunohistochemistry staining of collagen type I showed very different deposition patterns between the two groups (Figure 6.2D, collagen type I). The deposition of BSP was localized to locations of collagen type I, indicating a difference in the deposition pattern of important bone matrix proteins. [RT-PCR primers are provided in Table 6.1, expression values displayed in logarithmic scale, n=4, Student's T-test with *= $p<0.05$ (6.2A), n=4, Student's T-test with *= $p<0.05$ (6.2B-C), Scale bar = 50 µm, with inset Scale Bar = 500 µm]*

Mineralization:

The mineralization of the bone matrix is essential for its structural competency, and was extensively analyzed in these constructs. Three dimensional reconstructions of the μCT scans revealed a noticeable difference in deposition pattern (Figure 6.3A). Mineral deposition in the hypertrophic chondrocyte-based constructs was clumped at a set distance from the scaffold edge (white circle depicts the scaffolds dimensions). Viewed from an angle, the mineral was also confined in the vertical direction, with the mineral deposited all in close proximity in a hollow cylindrical shape. In contrast, the osteoblast-based constructs produced mineral in spindles along the periphery of the scaffold. The mineral depositions were well spaced, but tended to form a shell defined by the exterior of the scaffold, as seen in the angled view. Quantitation of the mineral detected in the scans matched observations (Figure 6.3B), with the Hyper constructs containing significantly more and significantly denser mineral than the Osteo constructs. The bone surface to bone volume (BS/BV) was approximated for each group of constructs, and mirrored the deposition patterns prevalent from the 3D reconstructions. The BS/BV of the Hyper constructs was significantly lower than the Osteo construct, demonstrating a more compact mineral pattern in the Hypers compared to the spread, spindle shape suggested by the higher Osteo BS/BV. Using biochemical quantitation methods, the amount of calcium was significantly increased in the Hyper constructs compared to the Osteo, agreeing with the scans.

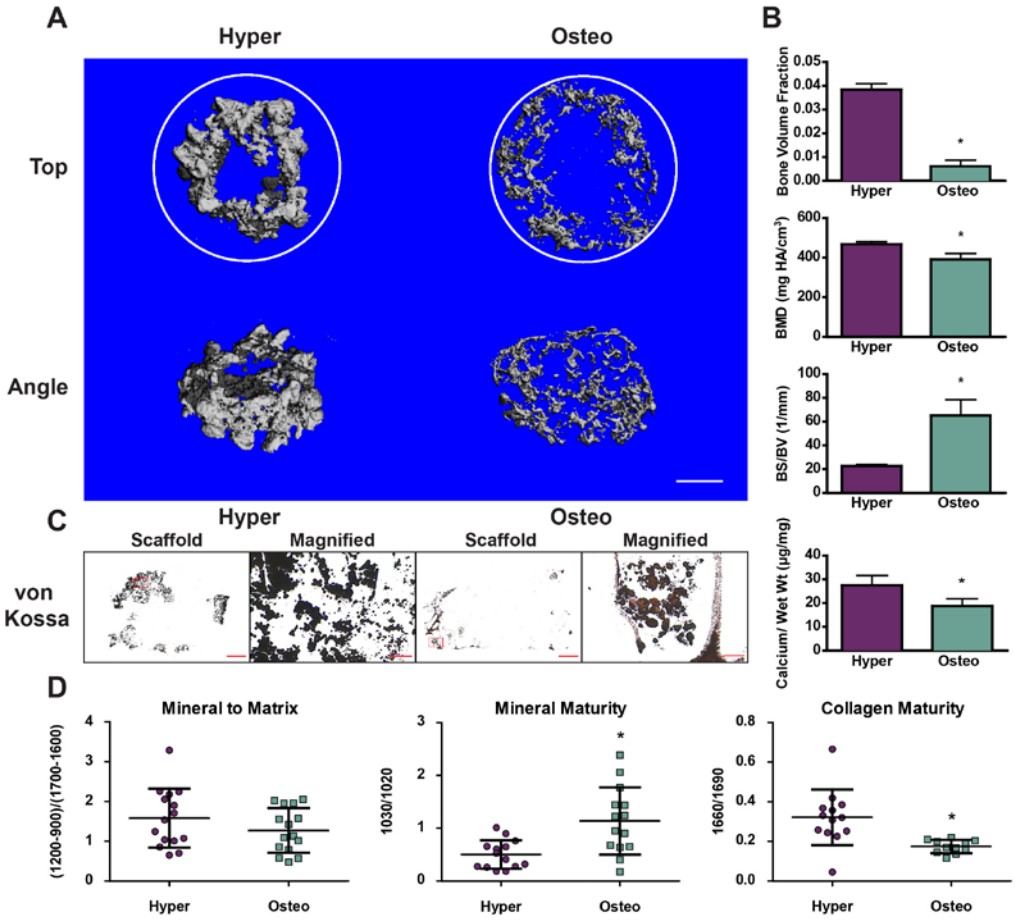
A
Hyper
Osteo
Top
Angle
B
Bone Volume Fraction
0.05
0.04
0.03
0.02
0.01
0.00
Hyper
Osteo
BMD (mg HA/cm³)
600
400
200
0
BS/BV (1/mm)
100
80
60
40
20
0
Calcium/ Wet Wt (µg/mg)
40
30
20
10
0
C
Hyper
Osteo
Scaffold
Magnified
von Kossa
D
Mineral to Matrix
(1200-900)/(1700-1600)
Mineral Maturity
1030/1020
Collagen Maturity
1660/1690

Figure 6.3: Mineralization of tissue engineered constructs (previous page). *Representative three-dimensional μCT reconstructions are presented demonstrating the differences in deposition between the constructs (Figure 6.3A). The associated scans were quantified to determine the volume (Bone Volume Fraction), density (BMD), and the ratio of surface area to volume (BS/BV). Hyper constructs contained significantly more volume, denser mineral, and a less surface area per volume than Osteo constructs (Figure 6.3B). Quantitation of the amount of calcium within the constructs showed significantly more calcium in the Hyper groups (Figure 6.3B). Histological sections were sliced and stained with von Kossa to reveal the presence of mineral within the constructs. Hypertrophic chondrocytes deposited mineral within the pore space, in areas surrounding the cells, whereas the osteoblasts contained mineral within the cell and externally deposited into the scaffold (Figure 6.3C). FTIR analysis of the mineral within the constructs was conducted to elucidate the mineral to matrix ratio, the deposited mineral maturity, and the collagen matrix maturity (Figure 6.3D). The mineral to matrix ratio was similar between the two constructs, less than native bone. The Hyper constructs contained significantly less mature mineral but significantly more mature collagen. [Scale Bar = 1 cm (6.3A), n=5, Student's T-test with *= p<0.05 (6.3B), Scaffold Scale Bar = 500 μm, Magnified Scale Bar = 50 μm (6.3C), n=15, Student's T-test with *= p<0.05 (6.3D)]*

To better understand the spatial aspect of the mineral deposition within the scaffolds' interior architecture, histological slices were stained with von Kossa for mineral presence (Figure 6.3C). In the Hyper constructs, mineral was deposited in the area immediately surrounding the hypertrophic chondrocytes, confined to the pore space of the scaffolds. Osteo staining showed that considerable mineral was present within the cells, but that deposited mineral was localized to the scaffold surface. With the deposition profiles being so drastically different, we analyzed the chemical composition of each construct's deposited matrix through FTIR (Figure 6.3D). Interestingly, the mineral to matrix ratio was not significantly different between the groups, showing that the mineral content per deposited matrix is not significantly different between the groups even though the total amount of mineral was quantifiably different. However, differences were present when investigating the maturity of the mineral and collagen content present within the constructs. The Hyper had significantly less mature mineral, but significantly more mature collagen. From the FTIR, it became apparent that not only was the deposition pattern different

between the two groups, but the composition of the deposited mineral was different as well. The increased mineral content and the widespread glycosaminoglycan content of the Hyper constructs contributed to its increased mechanical properties, as the hypertrophic chondrocyte-based constructs had a significantly higher elastic and equilibrium moduli compared to just the silk scaffold and the osteoblast-based construct (Figure 6.4).

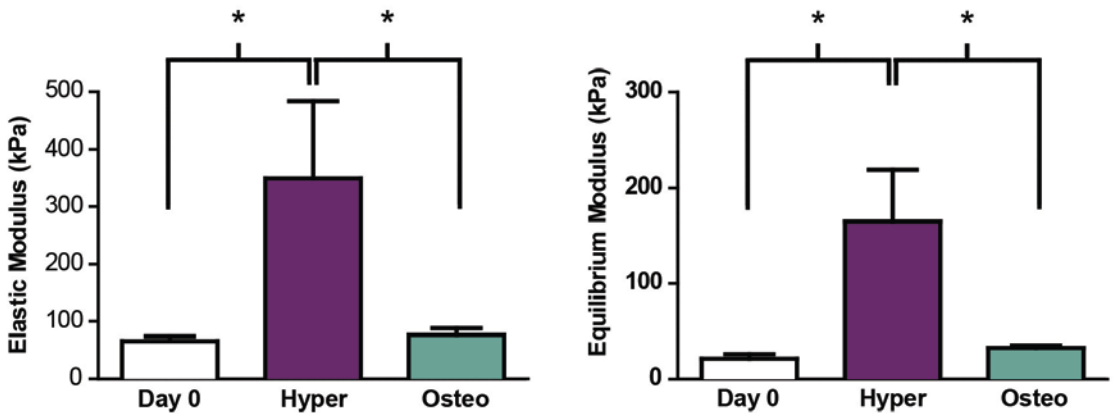

Figure 6.4: Mechanical properties of the differentiated constructs. *Constructs were compressed at a strain of 1% per second for 10 seconds, with the strain than held for the next 1800 s. From this compression, elastic and equilibrium moduli were calculated for the two experimental constructs, and scaffolds on the day of seeding. Hyper constructs had significantly higher moduli, with the Day 0 and Osteo constructs not being significantly different from each other. [n=4, One-way ANOVA with Tukey post-test, significant *=p<0.05]*

Subcutaneous Implantation Bone Turnover and Regeneration:

The unique matrix deposition pattern and composition by each key cell type prompted investigation as to whether these differences would influence bone regeneration *in vivo*. Constructs from each group were placed subcutaneously in nude mice, with samples being harvested at 3, 6, and 12 weeks post implantation. 3D reconstructions of μCT scans demonstrated the progression of bone formation within the constructs (Figure 6.5A,C). In the

Hyper constructs, no noticeable increase in the amount of deposited mineral was noticeable, but the constructs appeared to refine the existing mineral, removing mineral particulates and creating a dense, smooth composition. The Osteo constructs saw a drastic increase in the amount of designated mineral with the deposition pattern closely matching, in appearance, the original silk scaffolds. Quantitation of the computed scans demonstrate unique trends for each construct (Figure 6.5E). In agreement with the visual evidence, the Hyper constructs didn't significantly increase the amount of mineral present within the constructs. However, the mineral density did significantly increase, with the mineral density at 12 weeks approaching native values of cortical bone (1050 vs 1200 mm HA/cm^3) (161). The Osteo constructs were almost opposite in behavior, as there was a significant increase in the deposited mineral within the construct, but not a significant change in the mineral density. The pattern of mineral deposition was altered in the Osteo constructs, as an increase in bone volume corresponded to a significant decrease in the bone surface to volume ratio. Hard bone histology was performed on the samples with Levai-Laczko staining utilized to demonstrate bone regeneration (Figure 6.5B,D). Overtime, the turnover of the Hyper constructs was evident, as the calcified cartilage nodules (dark blue/ purple) seen at 3 weeks were remodeled into mature, compact bone with embedded cells at 12 weeks (Figure 6.5B). New bone deposition seams are clearly present at the borders between the different stages of bone formation. For Osteo samples, the increase in bone volume is clearly visible, as the progression from 3 weeks to 12 weeks demonstrates a clear change in the quantity and spread of deposited mineral within the constructs (dark blue/ purple) (Figure 6.5D). Osteoid deposition can be visualized by the light purple forming on the scaffold at 3 weeks, which becomes heavily mineralized (dark purple) at 12 weeks.

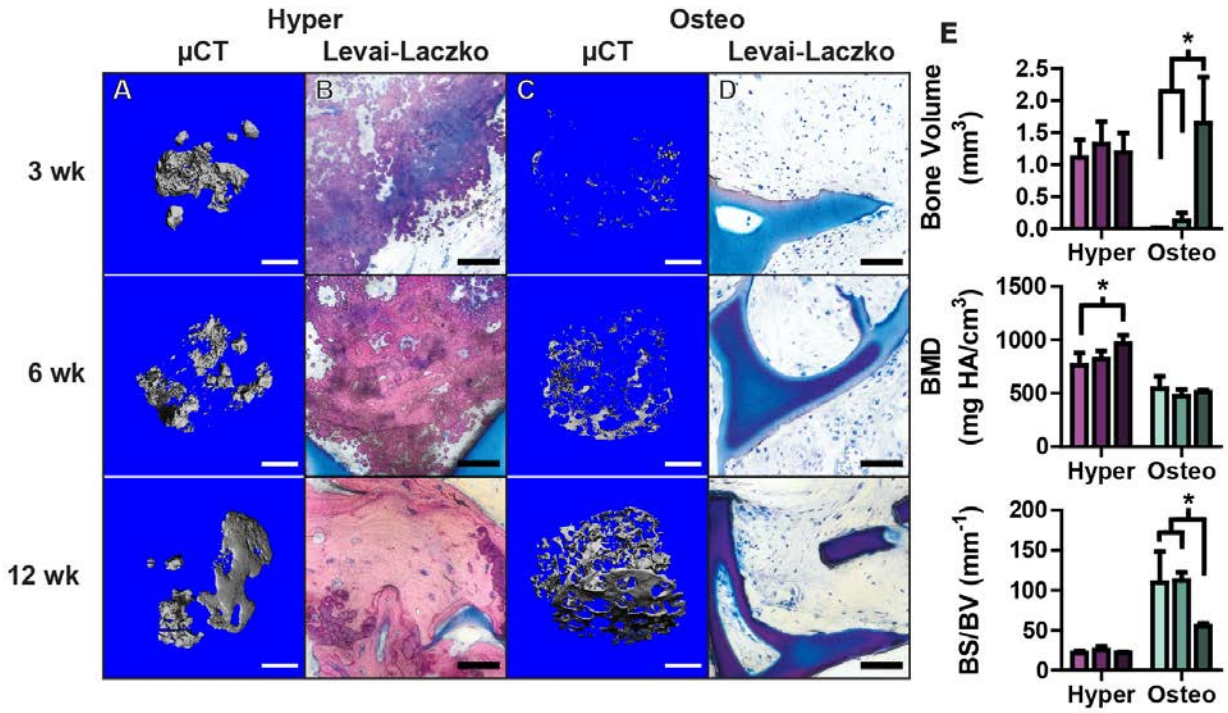

Figure 6.5: Bone regeneration upon subcutaneous implantation. *Scaffolds were evaluated 3, 6, and 12 weeks after subcutaneous implantation. Representative three-dimensional µCT reconstruction are presented to demonstrate the progression in bone regeneration during in vivo cultivation of each construct (6.5A,C). Hyper constructs didn't change substantially, with slight refinement in the grouping of the mineral. In contrast, the Osteo constructs dramatically increased in the volume of mineral deposited, resembling the scaffold at 12 weeks. Hard bone histology was performed on harvested constructs, with Levai-Laczko staining utilized to elucidate the different aspects of the bone regeneration (6.5B,D). Hyper constructs underwent extensive remodeling, with calcified cartilage (dark blue/ purple) refined into dense, mature bone (pink), complete with remodeling seams and entrapped cells. Osteo constructs continued to deposit mineral within the scaffold walls, and the increase in amount of mineral was evident in the progressive accumulation of dark purple mineral within the scaffold. The µCT scans were quantified at each time point to determine the progression in volume (Bone Volume Fraction), density (BMD), and the ratio of surface area to volume (BS/BV) (6.5E). Hyper constructs contained the same approximate amount of bone, but saw a significant increase in the density, approaching values measured in cortical bone. The mineral density of Osteo constructs stayed at cancellous-like levels, but underwent a significant increase in the bone volume and subsequent decrease in surface to volume ratio. [µCT Scale Bars = 1 cm (6.5A,C), Levai-Laczko Scale Bars = 50 µm (6.5B,D), One-way ANOVA within each construct type with Tukey post-test, significant *=$p<0.05$, 3 wk n = 4, 6 wk n =5, 12 wk n = 3 (6.5E)]*

Subcutaneous Implantation Vascularization:

As the mimicked ossification pathway strongly influenced the bone formation, their effect on overall regeneration, as determined by construct vascularization, was studied. Immunohistochemical staining of CD31 elucidated blood vessels in both constructs (Figure 6.6A), and semi-quantitation was utilized to confirm the visual differences seen within the constructs. The hypertrophic chondrocyte-derived constructs had a greater presence of blood vessels, as the number of vessels per construct area and the total blood vessel area was significantly higher than the osteoblast-derived constructs (Figure 6.6B,C). The Hyper constructs had a significantly deeper average vessel location, as measured from the nearest construct edge, and a greater maximum distance into the construct, also measured from the nearest construct edge (Figure 6.6E,F). A histogram created of the distances of vessels from the closest scaffold edge clearly indicated the differences in regeneration (Figure 6.6D). Whereas the Osteo constructs had a large majority of vessels located within 200 microns of the scaffold edge, the Hyper constructs had a more even distribution of vessels throughout the construct.

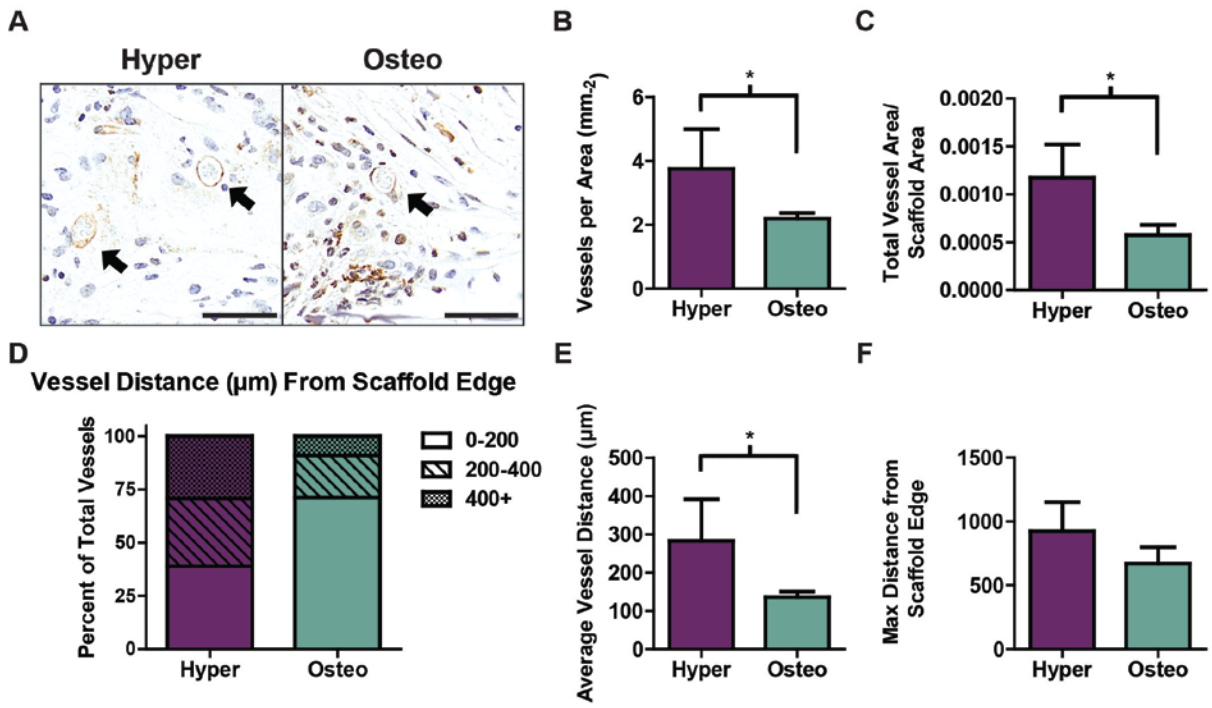

Figure 6.6: Vascularization of subcutaneously implanted constructs. *Immunohistochemistry staining for CD31+ vessels of constructs that were implanted for six weeks (Figure 6.6A). From images of each construct, the construct area, vessel area, distance of vessel to the closest construct boundary were calculated. Hyper constructs had a significantly higher number of vessels per construct area (Figure 6.6B) as well as a significantly greater total vessel area normalized to the construct area compared to the Osteo constructs (Figure 6.6C). Categorizing the blood vessels based on their distance from the construct periphery demonstrated a more even distribution of vessels throughout the Hyper constructs, with Osteo vessels primarily localized to the periphery (Figure 6.6D). This distribution was reflected in the average vessel distance and the maximum vessel distance from the scaffold edge, as Hyper constructs had larger distances in both measurements.[Scale Bars = 50 µm (6.6A), n=5, Student's T-test with *= $p<0.05$ (6.6B,C,E,F)]*

6.6 DISCUSSION

Autologous mesenchymal stem cells provide the ideal cell source for bone tissue engineering, due to their ease of harvest and multipotent nature (162). Traditionally, bone tissue engineering strategies focused on the direct differentiation of osteoblasts (59), but researchers have recently discovered a way to mimic endochondral ossification utilizing mesenchymal stem

cells by deriving hypertrophic chondrocytes (61, 62, 69, 143). This ability to now mimic both ossification processes provides tissue engineers a unique tool to dictate bone graft performance. Despite this ability, there is little published literature to aid in deciding which pathway is best for a given application. In this study, we differentiated human mesenchymal stem cells along the two mimicked ossification processes, documenting the differences in cell behavior, matrix production, bone formation, and graft regeneration.

Upon the successful differentiation of each cell type, the gene expression profiles were compared with regards to bone formation. Interestingly, the differentiated hypertrophic chondrocytes had higher expression in every bone gene studied. The initial belief about hypertrophic chondrocytes would refute this data, as it was thought that hypertrophic chondrocytes recruited osteoblasts to facilitate bone deposition, not deposit themselves (163). However, recent studies have demonstrated that this process is more of a continuum, with hypertrophic chondrocytes depositing preliminary bone, with some studies suggesting that these hypertrophic chondrocytes even transdifferentiate into osteoblasts (22, 164, 165). The differentiated hypertrophic chondrocytes' protein and mineral deposition would also agree with these recent studies, as the presence and distribution of the bone-related proteins collagen type I and BSP were present throughout the endochondral mimicking constructs and heavily localized to the area surrounding hypertrophic chondrocytes.

The localization of the matrix depositions and mineral suggests the first major difference between the differentiated hypertrophic chondrocytes and osteoblasts. Whereas the differentiated osteoblasts deposited mineral along the scaffold walls, the differentiated hypertrophic chondrocytes deposited within the pore space. This behavior by differentiated osteoblasts has been seen in our other work, with mineral deposition only occurring along an established surface

(110), and agrees with the known polarized deposition nature of native osteoblasts (166, 167). The differentiated hypertrophic chondrocyte deposition also aligns with native behavior, as bone deposition in endochondral ossification occurs within the cartilage anlage produced by condensed chondrocytes (19, 51). Very little of the hypertrophic chondrocyte deposition occurred along the scaffold, indicating that hypertrophic chondrocytes deposit within their condensation. Investigation within our lab has shown that this deposition tendency is maintained by the hypertrophic chondrocytes regardless of the scaffold, depositing heavily wherever cells have enough space (usually within the pores) to condense. In contrast, we have shown that osteoblast deposition is dramatically influenced by the scaffold composition (102).

The amount of mineral between the two types of constructs was significantly different, with differentiated hypertrophic chondrocytes consistently depositing more mineral, faster than the differentiated osteoblasts. The speed and volume of mineral deposition alludes to the instances in which each process is used in vivo. Endochondral ossification is utilized in situations where a lot of new bone is needed, such as in native skeletal development and long bone fracture repair (19, 41, 132). In contrast, intramembranous ossification is found in remodeling situations, where a methodical, coordinated process is utilized to deposit bone (41, 132). Analyzing the deposited mineral maturity using FTIR, the hypertrophic chondrocytes deposited a significantly less mature mineral than the osteoblasts. Natively, calcified cartilage's mineral is immature due to interactions with the localized GAG and poor organization of the apatite concurrently with an abundance of non-apatite phosphate ions (100, 101), a situation that appears consistent with the hypertrophic chondrocyte-based grafts (Figure 6.3). The osteoblast value was consistent with trabecular bone maturities, and suggests the advanced state of the differentiated osteoblasts (168). The maturity of the mineral appeared to also relate to its

turnover after implantation. The immature mineral deposited within the hypertrophic chondrocyte-based grafts underwent extensive remodeling by mouse cells, increasing greatly in bone density until it was cortical-like in density and appearance (161). Osteoblast deposited mineral didn't undergo noticeable remodeling, but rather the constructs saw increased bone volume deposition within the scaffolds, transforming the scaffold into trabecular-like bone.

Bone tissue engineering has been plagued by poor vascularization, experiencing construct necrosis before sufficient integration into the native skeleton (3, 157). Though numerous strategies have been investigated to address this problem, previous work has suggested that hypertrophic chondrocyte-based constructs might sufficiently address this issue, with the demonstration of vascularization and mature vessel formation (62, 69, 93). The results of the current study agree with their results, with substantial vascularization penetrating the hypertrophic chondrocyte-based construct. The osteoblast-based constructs had minimal vascularization, confined to the exterior of the construct, demonstrating the limited potential of osteoblasts to promote vascularization. The superior ability of hypertrophic chondrocytes agrees with native development, as hypertrophic chondrocyte knock-out has shown to halt vascular invasion into the cartilage anlage (169, 170).

6.7 Conclusion

To summarize, the differentiated hypertrophic chondrocytes quickly deposited dense, immature bone that facilitated extensive turnover and vascularization when implanted. In contrast, differentiated osteoblasts slowly produced mature bone confined to the scaffold walls that facilitated further deposition on just the existing scaffold when implanted. These results present clear evidence to dictate the situations in which each mimicked pathway should be

utilized. In strategies containing no or an insufficient scaffold and that require fast mineral production or the presence of extensive vascularization, hypertrophic chondrocytes should be utilized. In situations with an advanced scaffold ready for biological incorporation that will be implanted in a nutrient dense environment, osteoblasts should be utilized. This information also allows the future design of more complex systems, with the localization of select cell types to elicit specific repair events.

7 Derived hypertrophic chondrocyte grafts boost critical-sized long bone defect regeneration

7.1 Abstract

Bone tissue engineering provides a tantalizing treatment option for critical long bone fractures, but hasn't delivered on this promise due to the difficulties in creating large grafts and the inconsistencies these grafts have in regeneration. In the current study, we created novel, large tissue engineered constructs replicating natural endochondral ossification through hypertrophic chondrocyte differentiation, and compared these constructs to tissue engineering-established, intramembranous ossification-mimicked constructs fabricated with differentiated osteoblasts. The constructs were implanted into orthotopic, femoral critical-sized defects to evaluate the ability of each construct to stimulate healing and promote bone regeneration. With long bone fractures naturally healing through endochondral ossification, we hypothesized that the hypertrophic chondrocyte-based constructs would enhance bone regeneration. After 12 weeks *in vivo*, the hypertrophic chondrocyte-based grafts demonstrated enhanced bone regeneration by facilitating increased bone deposition, superior integration into the native skeleton, and widespread bone marrow formation. This enhanced bone regeneration corresponded to 7/8 hypertrophic chondrocyte-based constructs successfully bridging the defect, compared to only 1/8 defects bridged with osteoblast-based constructs. Despite replicating the intramembranous process, the osteoblast-based constructs still formed new bone through endochondral ossification, but to a significantly lesser degree than the derived hypertrophic chondrocytes. Further investigation of the defect space indicated that the derived hypertrophic chondrocytes

established a superior bone-forming environment, with reduced numbers of osteoclasts and an increased presence of M2-polarized macrophages. The success of hypertrophic chondrocyte-based constructs indicates an importance in matching the tissue engineered development to the natural process, and beckons a more detailed investigation of hypertrophic chondrocyte-based constructs for clinical translation.

7.2 SIGNIFICANCE

Bone tissue engineering promises to revolutionize clinical treatment of fractures and bone defects by providing the benefits of the best treatment option, autografts, without the difficulties associated with harvesting. In this study, we mimicked the two natural bone forming processes in the body, endochondral and intramembranous ossification, by differentiating mesenchymal stem cells into the key cell type of each process, hypertrophic chondrocytes and osteoblasts. We evaluated each process's ability to regenerate a critically-sized rat femur defect. The hypertrophic chondrocyte-based constructs promoted better regeneration, bridging the critical-sized defect and depositing a more complete bone. Hypertrophic chondrocyte-based grafts provide an exciting possibility to deliver on the promise of bone tissue engineering.

7.3 INTRODUCTION

Bone repair after fracture occurs through two distinct ossification processes, intramembranous and endochondral (152). In intramembranous ossification, repair occurs through the direct differentiation of mesenchymal sources into osteoblasts that mend the break and fabricate new bone (152). In contrast, endochondral ossification heals by the initial deposition of a cartilage anlage before new bone formation is orchestrated by the matured hypertrophic chondrocytes (19, 28). Though these repair processes successfully reconstruct a

high percentage of fractures, estimates suggest >100,000 fractures fail in their repair efforts, clinically diagnosed as nonunions (171). Though a number of factors contribute (172), many nonunions occur due to complex fractures of the long bones (e.g. femur, humerus, tibia). Once the bone has failed to regenerate, external intervention is required to return functionality (171). Though numerous fabricated prosthetics exist, the gold standard for bone regeneration remains autologous grafts (57).

Despite their clinical success, autografts present a number of disadvantages, principally the scarcity of suitable bone and donor site morbidity (173). An attractive alternative, tissue engineering promises to provide the benefits of autologous bone without these troublesome disadvantages by utilizing autologous cells, prepared scaffolds, and external stimuli to create curative grafts (174). Due to their multipotent nature and ease of harvest, mesenchymal stem cells are a clinically-ideal cell source for tissue engineered grafts (175). Advances within the mesenchymal stem cell field have demonstrated the ability to derive osteoblasts (59) and, recently, hypertrophic chondrocytes (61, 62), the key cells in intramembranous and endochondral ossification. Utilizing these derived cells, a developmental engineering approach can be taken to mimic the native bone repair processes (4, 59, 62, 176). Therefore, creating large grafts with the differentiated, key cells already incorporated should accelerate the native repair processes and facilitate enhanced bone regeneration. As both processes are integral in the repair of certain bone fractures, our aim was to create viable tissue engineered grafts and investigate the regenerative capability of each key cell type for long bone repair.

The present study created intramembranous- (117) and novel endochondral-like grafts by deriving osteoblasts and hypertrophic chondrocytes from adipose derived stem cells within decellularized bone cores. Following nature's template for long bone repair, we hypothesized

that the hypertrophic chondrocyte-based grafts would facilitate enhanced regeneration of the orthotopic, femoral critical-sized defect. Our results demonstrate that the engineered hypertrophic chondrocyte grafts mediated fast integration and thorough remodeling continuous with the native bone, whereas the osteoblast constructs produced minimal bone and failed to bridge the defect. This study demonstrates the ability of hypertrophic chondrocyte tissue engineered grafts to facilitate bone regeneration in critical-sized orthotopic defects, and advocates for the further investigation and utilization of hypertrophic chondrocytes to alleviate nonunions.

7.4 METHODS

Human adipose tissue collection and rat experimentation were performed following all relevant guidelines and procedural approval from the appropriate Austrian authorities. Adipose derived stem cells (ADSCs) were expanded to p4 and seeded in decellularized juvenile bovine wrist bone cores. Based on our previous studies that optimized the creation of osteoblast-based tissue engineered bone grafts (177), osteoblast-based grafts were cultured in a perfusion bioreactor in osteogenic medium for 5 weeks at a perfusion rate of 400 µm/s. Novel hypertrophic chondrocyte-based grafts were cultured based on literature-defined conditions and our yet unpublished optimization work (61, 62), with the constructs cultured statically first in in chondrogenic medium for 2 weeks, followed by hypertrophic medium for 3 weeks. Upon culture completion, grafts were analyzed biochemically, histologically, immunohistochemically, and by real time RT-PCR (Primers Table S1). Critical-sized defects were created by extracting a 5 mm portion of the right femur in male RNU nude rats. Osteoblast-based constructs, hypertrophic chondrocyte-based constructs, and empty decellularized bone cores were implanted into the defects. The femur, not the graft directly, was stabilized by a four-pin, POM-based internal

fixator. In vivo micro-computed tomography (μCT) scans were performed the day after implantation and at 3, 6, and 9 weeks post implantation. Grafts were harvested at 12 weeks and bone formation and graft regeneration were analyzed by high resolution μCT, hard bone histology, histology, and immunohistochemistry. A complete and detailed account of the methods is included in the SI Text.

7.5 RESULTS

In vitro cultivation and characterization

Endochondral and intramembranous-like tissue engineered constructs were created utilizing decellularized bone (DCB) scaffolds seeded with clinically-relevant adipose derived stem cells. The constructs were cultured in conditions to optimize their differentiation of the key cell types (hypertrophic chondrocytes and osteoblasts) in the mimicked ossification pathways (Figure 7S.1). Hypertrophic chondrocyte-based constructs (SH) were differentiated in static conditions by first prompting chondrogenesis and cartilage tissue formation for two weeks and then inducing chondrocyte hypertrophy over the subsequent three weeks (Figure 7S.1). After five weeks of total culture, the hypertrophic chondrocyte-based constructs demonstrated endochondral-like characteristics, with upregulated gene expression of chondrocyte and hypertrophic chondrocyte markers and collagen X and glycosaminoglycan deposition surrounding enlarged chondrocyte lacunae (Figure 7S.2). Osteoblast-based constructs (PO) were formed through osteogenic differentiation in a perfusion flow bioreactor for the entire five week culture period (Figure 7S.1). Osteoblast-based constructs had increased cellularity and had deposited bone matrix during cultivation.

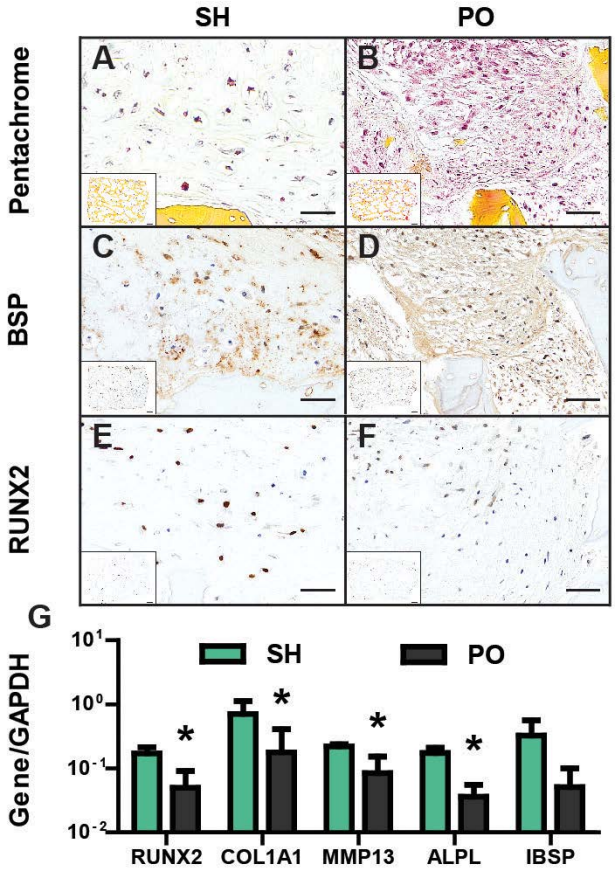

Figure 7.1: State of ossification mimicking bone constructs pre-implantation*: Histology and immunohistochemistry revealed the differences in morphometry and bone template deposition between the construct groups. The static hypertrophic chondrocyte-based (SH) constructs contained hypertrophic chondrocytes with an increased lacunae size surrounded by a cartilaginous matrix defined by the greenish staining of glycosaminoglycans (GAG) (7.1A). Bone sialoprotein (BSP) (7.1C) was present on the exterior co-localized with heavy GAG deposition, whereas nuclear RUNX2 staining (7.1E), a key protein to prompt skeletal formation, was present in cells throughout the entirety of the construct. The osteoblast-based (PO) constructs contained high cellularity throughout the graft, accompanied by widespread fibrous deposition, most strongly present on the outer parts of the construct (7.1B). BSP (7.1D) was present on this fibrous tissue throughout the construct, with nuclear RUNX2 staining in osteoblasts (7.1F) confined to the exterior of the construct. After five weeks of cultivation, SH constructs had a significantly enhanced expression of important bone production genes compared to PO constructs (7.1G). [n=5, Student's T-test with* = $p<0.05$ (7.1A), Scale Bar = 50 µm, with inset Scale Bar = 500 µm (7.1B-G)].*

The different state of the two constructs at the culmination of culture was clearly evident through histology and immunohistochemistry. Movat's pentachrome (Figure 7.1A,B) staining revealed that SH constructs had high cellularity and heavy cartilage-like deposition around the periphery of the construct, but minimal of either within the interior (Figure 7.1A). In contrast, PO constructs had high cellularity throughout the construct, significantly higher than the SH constructs (Figure 7S.2), with widespread dense collagenous matrix deposits (Figure 7.1B). With regards to bone production, deposition of bone sialoprotein (BSP), a key nucleating protein for bone mineral formation, correlated with the general matrix characteristics. SH BSP was located near hypertrophic chondrocytes within the dense cartilage matrix on the periphery of the construct (Figure 7.1C). PO BSP was present on fibers throughout the construct but concentrated at the locations of the most dense tissue (Figure 7.1D). In addition, new osteoid formation was more prevalent in the PO constructs (Figure 7S.3). Interestingly, despite the enhanced matrix production of the PO constructs, gene expression of key bone-related genes was significantly greater for the SH constructs (Figure 7.1G). A master regulator for bone formation (RUNX2), matrix deposition (COL1A1 and MMP13) and mineral formation (ALPL and IBSP) were all enhanced in the SH group. Nuclear staining of RUNX2 showed widespread presence throughout the SH construct but was only minimally present in PO, localized to the exterior segments of the construct (Figure 7.1E,F). Pre-implantation, PO constructs had an enhanced matrix composition for bone deposition but the SH constructs had superior gene expression.

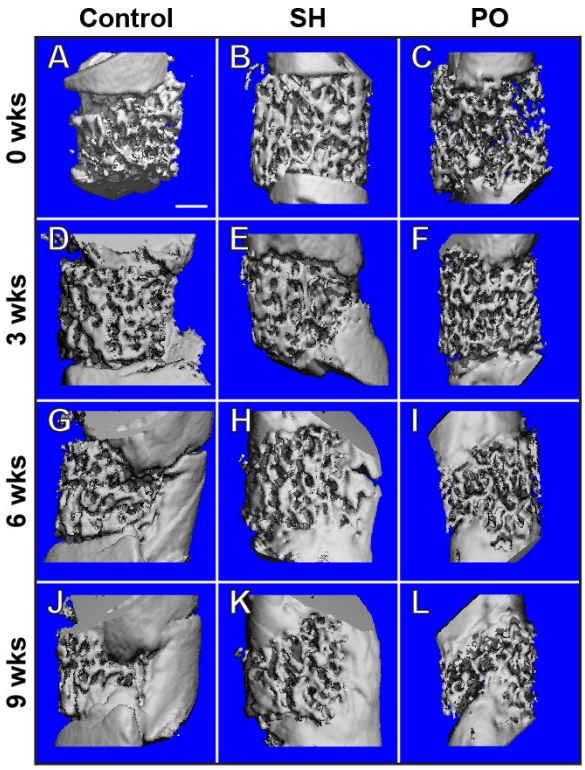

Figure 7.2: Temporal progression of the femoral, critical-sized defect regeneration*: Representative in vivo three-dimensional µCT reconstructions of the rat femur are presented at 0 (day 1) [7.2A-C], 3 [7.2D-F], 6 [7.2G-I], and 9 weeks [7.2J-L] post-implantation from the ventral view. Week 0 reconstructions depict the defect size and shape, and the initial state of the implanted constructs [7.2A-C]. At 3 weeks post-implantation, control [7.2D] and SH [7.2E] demonstrated some construct integration and initial mineral deposition along the medial side of the graft. At 6 weeks, the control [7.2G] showed external deposition, the SH [7.2H] demonstrates substantial reconstruction and graft remodeling, and the PO [7.2I] construct has integrated with the native skeleton and undergone some remodeling. At 9 weeks, the control [7.2J] had almost formed a bridge and experienced extensive mineral deposition external to the graft, SH [7.2K] had bridged the union with broad construct remodeling, and the PO [7.2L] developed a fissure diagonally through the graft, between the integration sites. [Scale bar: 1 cm]*

In vivo graft integration, deposition, and bridging

To evaluate the constructs capabilities to facilitate bone regeneration, SH, PO and DCB control constructs were implanted into a critically-sized, 5mm defect in the right femur of nude

rats, an orthotopic model for long bone fracture repair (Figure 7S.1). Live μCT scans were taken routinely to monitor construct integration and turnover, presented as representative 3D reconstructions (Figure 7.2). At 3 weeks post-implantation, SH constructs had already begun integration into the native skeleton, and had large mineral deposition along the medial exterior of the graft (Figure 7.2E). The PO group had very little noticeable change, with minimal integration and no apparent mineral deposition (Figure 7.2F). The DCB scaffold control resembled the SH group, with external mineral deposition apparent (Figure 7.2D). At 6 weeks, a difference in regeneration was noticeable between the groups, as the SH construct had extensive integration along both ends, and a bridge had almost occurred along the medial side (Figure 7.2H). The PO constructs had partial integration along both ends and very little new mineral deposition (Figure 7.2I). The DCB control had extensive new deposition along the medial side of the scaffold, but very little remodeling of the actual scaffold. At 9 weeks, both the SH and control groups had bridged the defect, but the PO construct had failed, developing a large fissure through the construct. The SH construct had extensive remodeling, with new deposition occurring throughout the construct and the formation of a solid bridge along the medial side of the construct (Figure 7.2K). The PO construct advanced the integration into the defect space; however, the construct, still very similar in appearance to the Day 0 status, had broken apart (Figure 7.2L). The DCB control appeared very similar to 6 weeks, but with a more refined medial-side bridge and a slight progression in integration (Figure 7.2J).

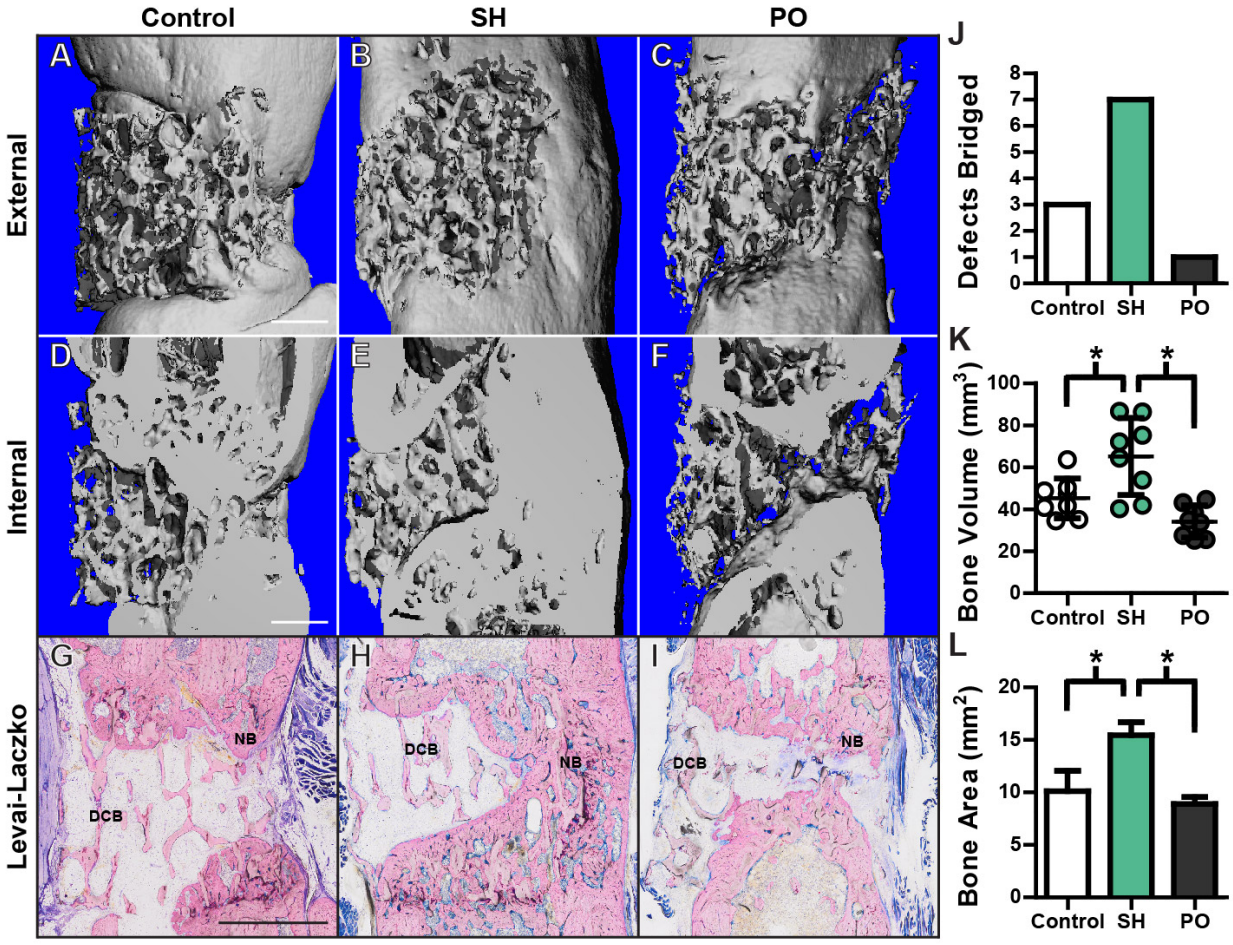
Control
SH
PO
External
Internal
Levai-Laczko
A
B
C
D
E
F
G
H
I
NB
DCB
J
Defects Bridged
K
Bone Volume (mm3)
L
Bone Area (mm2)
Control
SH
PO

Figure 7.3: Bone deposition and critical-sized defect bridging (previous page)*: Representative high resolution, three dimensional reconstructions of the critical-sized femoral defects after harvest at 12 weeks (external: 7.3A-C, internal: 7.3D-F). The control group shows integration into the native skeleton, but only minimal mineral deposition at the integration sites (7.3A-D). The SH group demonstrated bridging and extensive deposition along the medial side, with trabeculae of the implanted scaffold still present on the lateral side (7.3B,E). The PO group had progression of the native skeleton into the defect space with a degradation of the implanted construct resulting in a noticeable fissure (7.3C,F). Hard bone histology using the Levai-Laczko stain demonstrated the overall morphology of the defect region and denoted the difference between implanted construct (DCB) and newly deposited bone (NB) (7.3G-I). In the control, new bone deposition was largely constrained to the medial side at the integration sites (7.3G). New bone deposition was widespread throughout the SH defect, with some implanted scaffold present on the lateral side (7.3H). In the PO, new bone was located at the leading edge of the native skeleton, with minimal amounts of implanted scaffold scattered throughout the defect (7.3I). Successful bridging of the defects as determined by µCT analysis demonstrated 3/8 control, 7/8 SH, and 1/8 PO bridged (7.3J). Quantitation of the µCT scans within the defect site showed significantly more bone volume in the SH group compared to the other two groups (7.3K). Semi-quantitative analysis of the histological stains showed a similar pattern, with significantly more bone (both DCB and NB) in the SH group compared to the other two (7.3L). [Scale bars: 1 cm (73A-F), 2 cm (7.3G-I), Statistics: One-way ANOVA with Tukey post-test, significant *=$p<0.05$ (7.3K, L), n=8 (7.3K), n=4 (7.3L)]*

At 12 weeks, the femurs were harvested and scanned with a high-resolution µCT. The exterior of the SH construct had undergone extensive remodeling, with seamless integration into the femur and large portions of the graft resembling native bone (Figure 7.3B). Interior reconstructions demonstrated a thick, cortical-like bridge had formed along the medial interior of the construct (Figure 7.3E). The PO construct lacked remodeling and showcased the severe lack of bone present within the fissure (Figure 7.3C). Interior reconstructions showed that minimal integration had occurred and that the construct failed to facilitate bridging or regeneration (Figure 7.3F). Demonstrating the negative impact the PO constructs had on healing, the DCB scaffold experienced bridging of the defect, and partial integration of the scaffold (Figure 7.3A,D). Based on µCT reconstruction, 3/8 DCB, 7/8 SH, and only 1/8 PO constructs successfully bridged the defect (Figure 7.3J). The SH constructs' increased incidence of bridging

correlated with enhanced mineral deposition within the defect space, as the SH constructs had significantly greater bone volume than the other two groups (Figure 7.3K). Hard bone histology of the defects, stained with Levai-Laczko, visualized the difference between newly deposited bone (fuchsia) and the implanted DCB scaffold (light pink). The new bone deposition matched the mineral depositions visualized in the μCT, with SH constructs containing substantial new bone deposition (Figure 7.3H). In the PO constructs, new bone was localized to the integration sites and the advancement into the defect space. Much of the DCB scaffold was intact in the control group, with new bone deposition localized to the integration sites and the medial side of the construct. Semi-quantitation demonstrated significantly more bone in the SH compared to the DCB control and PO groups, confirming the enhanced bone production seen within the SH histology (Figure 7.3L).

Bone formation:

Magnified views of the Levai-Laczko highlighted the formation of bone within the defect. Large sections of the DCB scaffold were present in all three groups, with new bone forming around the DCB (Figure 7.4A,D,G). In the SH group, numerous sections of calcified cartilage were present, a precursor to bone formation through endochondral ossification (Figure 7.4D). Movat's pentachrome revealed that all groups underwent endochondral ossification to form new bone, as shown by the transition of hypertrophic chondrocytes in a cartilage matrix (black arrows) transitioning into newly formed bone (black stars) (Figure 7.4B,E,H). This endochondral ossification was located at the edge of new bone formation within the control and PO groups, and found in areas throughout the SH constructs. This widespread endochondral ossification correlated with the amount of new bone formed, as SH had a significantly higher amount than the control and PO groups (Figure 7S.4A). An increase in new bone production

resulted in a significant reduction in the amount of fibrous tissue within the SH defects compared to the other two groups (Figure 7S.4D). Besides producing bone, endochondral ossification has been shown to be essential for the formation of hematopoietic stem cells in bone marrow (178). Though all constructs prompted bone marrow formation within areas of newly formed bone, the SH constructs had significantly greater bone marrow area than the control and PO constructs (Figure 7S.4B). Previous work has shown that implanted hypertrophic chondrocytes serve as the driving force for, and remain within, new bone deposition by endochondral ossification (95). However, in the current experiment, all constructs, not just the implanted hypertrophic chondrocytes, underwent endochondral ossification. Therefore, human anti-mitochondria antibody staining was used to determine the source of new bone formation, and to determine if it was related to the implanted cell type. All cells present within the defect space, of all samples, were rat in origin (Figure 7.4C,F,I). However, the new bone did demonstrate abundant bone formation seams, indicating bone and cell turnover had already occurred in this newly deposited bone.

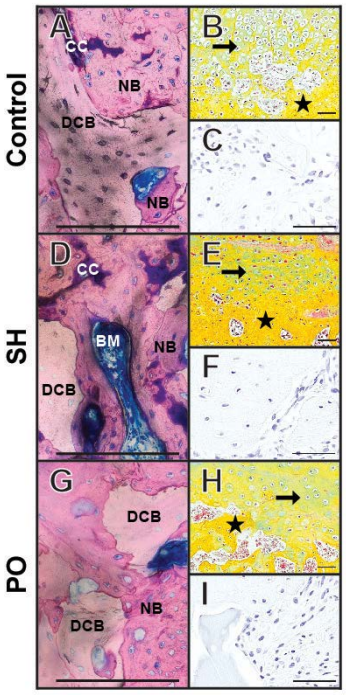

Figure 7.4: Bone formation*: Representative images of the bone formation process within the defect space utilizing Levai-Laczko (7.4A,D,G), Movat's pentachrome (7.4B,E,H) and human mitochondrial antibody (7.4C,F,I). Magnified views of the Levai-Laczko staining demonstrate the formation of new bone (NB) enveloping the implanted decellularized scaffold (DCB) in all three groups (7.4A,D,G). Calcified cartilage (CC) was seen most evidently in the SH group, which also contained extensive bone marrow (BM) formations. At the location of new bone formation, a cartilage anlage characteristic of endochondral ossification was present for all three groups, as shown by the green staining in Movat's pentachrome sections (7.4B,E,H). The included images demonstrate the turnover of this cartilage (black arrow) into newly deposited bone (black star). Human mitochondrial antibody (113-1), utilized to determine if any implanted human cells remained to aid bone regeneration, stained negative for the presence of human cells (7.4C,E,I). Semi-quantitation and statistical evaluation of the histological staining are included in the supplementary information. [Scale Bars: 200 µm (7.4A,D,G), 50 µm (7.4B,E,H), 50 µm (7.4C,F,I)]*

Graft Regeneration:

As a more direct measurement of the degree of bone turnover, osteoclasts, identified by their multinucleation and Howship's lacunae, were counted within the defect space of each construct (Figure 7.5A-C). The number of osteoclasts present within the SH constructs was

significantly lower than the number of osteoclasts present in the other two groups (Figure 7S.5). As can be seen in Figure 5A-C, there was a tendency for osteoclasts to appear on DCB scaffolds located within the fibrous tissue portions of the defect. The number of osteoclasts digesting DCB, normalized to the DCB area, was calculated, and overall osteoclast number trends held, as SH constructs had significantly less osteoclasts digesting DCB scaffolds (Figure 7S.5). In addition, the proportion of DCB osteoclasts to overall osteoclasts was significantly lower for the SH constructs (Figure 7S.5), thereby containing a higher portion of osteoclasts localized to areas undergoing remodeling. M2-macrophages have been shown to be integral in long bone regeneration, providing key molecules and generating a pro-repair environment (104). Immunohistochemistry staining of CD206, a key M2 marker, demonstrated increased presence within the SH construct defect space, with minimal presence in the PO constructs (Figure 7.5D-F). Staining of CD163, another M2 marker, matched the CD206 staining patterns (Figure 7S.6).

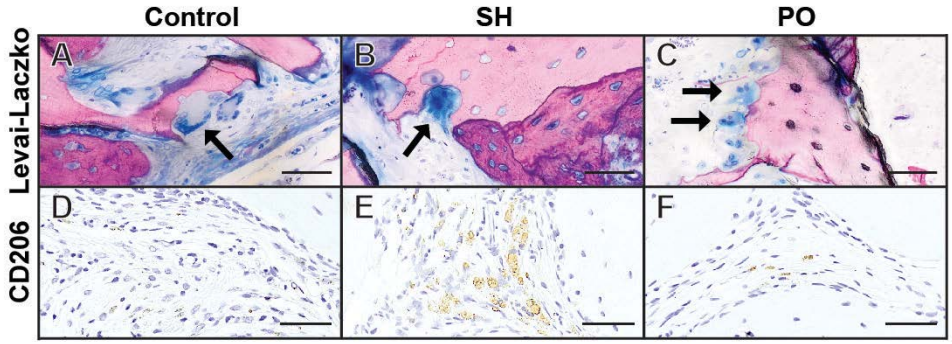

Figure 7.5: Implant Turnover and Regeneration: *Representative images of the degradative and regenerative environment of the critical-sized defect through the histological evaluation of osteoclasts (7.5A-C) and M2-polarized macrophages (7.5D-F). Osteoclasts, identified by the presence of multinucleated cells within a Howship's lacunae, demonstrated increased bone turnover, of both the implanted DCB and newly formed bone, within the control and PO constructs (7.5A-C). M2-polarized macrophages were identified by CD206 staining and were most present within the SH defect space (7.5D-F). [Scale Bars: 50 µm (7.5A-F)]*

7.6 DISCUSSION

Autologous bone tissue engineering has promised to provide customized, superior repair options for bone defects, but has had difficulty fulfilling this promise due to incomplete integration, stunted regeneration, and poor mechanical maintenance (3, 157). In this study, we evaluated the ability of current bone tissue engineering options, our novel hypertrophic chondrocyte-based and osteoblast-based constructs, to facilitate bone regeneration within an orthotopic bone defect model. We demonstrated the superiority of hypertrophic chondrocyte-based constructs to promote regeneration by (i) integrating faster with the native skeleton, (ii) depositing more bone, (iii) bridging the critical-sized defect, and (iv) promoting a more regenerative environment within the defect space.

The long bone critical sized-defect model creates a unique bone regeneration situation that occurs in a mechanically complex, bone marrow rich environment (109). Despite direct cultivation of osteoblasts for PO constructs, all experimental groups demonstrated instances of endochondral ossification. Naturally, long bone fracture repair undergoes endochondral ossification, and the relatively large pore size of the DCB scaffolds and the supply of a large number of stem cells from the bone marrow and surrounding tissues contributed to conditions that would support endochondral ossification (27). In the differentiation of the SH constructs pre-implantation, the seeded stem cells replicated condensation and cartilage formation within the DCB pore space, and the pentachrome staining of the PO and DCB constructs suggests a similar effect happened *in vivo*. Therefore, it was apparent that the conditions for bone regeneration within the defect favored endochondral ossification (179), and SH constructs thrived, showing integration and new bone deposition as early as 3 weeks, well before any noticeable regeneration had occurred in the osteoblast-derived constructs. Hypertrophic chondrocytes are the key

orchestrator of endochondral ossification, and previous studies have showcased their importance at facilitating new bone formation and defect regeneration (69, 95). The *in vitro* cultivation successfully resulted in hypertrophic chondrocytes within a cartilage matrix, accelerating the natural endochondral ossification process *in vivo* and producing fast integration and remodeling. Consistent with the results seen in literature (62), differentiating hypertrophic chondrocytes pre-implantation boosted bone regeneration, as highlighted by the more complete and advanced defect repair seen in the SH group compared to the DCB scaffold (natural endochondral ossification) and the PO constructs (primed intramembranous ossification).

The specific role of hypertrophic chondrocytes in bone formation is a popular topic, as recent publications have shown the ability of hypertrophic chondrocytes to transdifferentiate into osteoblasts and remain within the newly formed bone space (22, 164, 165). In the current study, only host rat cells were present in the SH constructs at the 12 week harvest. Though contradictory in appearance, there are a number of suitable possibilities as to why no implanted human cells remained in the defect space. In the published studies ((22, 95), the transdifferentiated hypertrophic chondrocytes were localized to the spongy bone layers; however, in the present study, much of the new bone more closely resembled the bony collar formed by invading cells (180). In addition, the newly deposited bone had already undergone turnover, as seen by the intersection of bone seams. Therefore, it is not clear if implanted hypertrophic chondrocytes underwent transdifferentiation, but they did orchestrate enhanced bone production by invading host cells.

In contrast, the role of differentiated osteoblasts appears to act in an adverse way to hypertrophic chondrocytes. The PO constructs had methodical integration with localized bone deposition during the 12 weeks *in* vivo. This behavior matched recent results in our laboratory

that suggest that osteoblasts controlled turnover within the defect space by localizing bone deposition and moderating the implant resorption. Unfortunately, the mechanical environment of the long bone defect resulted in its eventual failure, as the osteoblast-controlled regeneration slowed new bone deposition, opposite to the hypertrophic chondrocytes, which prevented successfully bridging of the defect and adequate construct mechanical stiffness.

The enhanced bone regeneration of the hypertrophic chondrocytes correlated with an increased presence of M2 polarized macrophages, which have shown to be integral in successful bone fracture healing (104). The increased presence of M2 macrophages, known as the tissue repair macrophages, has been shown to accelerate endochondral ossification and improve bone regeneration (103). In the current study, staining for M2 macrophages showed a greater number present within the SH constructs. Coupled with the reduced number of osteoclasts present within the defect, the implanted hypertrophic chondrocytes promoted a more conducive environment for tissue repair, possibly promoting the increased prevalence of deposited bone and defect bridging.

In total, this study demonstrates the superiority of hypertrophic chondrocyte-based constructs to stimulate enhanced bone production and successful defect bridging. Though osteoblast-based constructs have been successful in other situations of bone regeneration, they failed in this long bone critical-sized defect study. The results suggest an importance in matching the mimicked ossification pathway with the native ossification repair pathway. The results also prompt for further investigation into hypertrophic chondrocyte-based grafts to finally provide a tissue engineered solution for nonunion bone fractures.

7.7 SUPPLEMENTAL INFORMATION

Materials and Methods:

All materials were obtained from Sigma-Aldrich (St. Louis, MO, USA) unless otherwise noted.

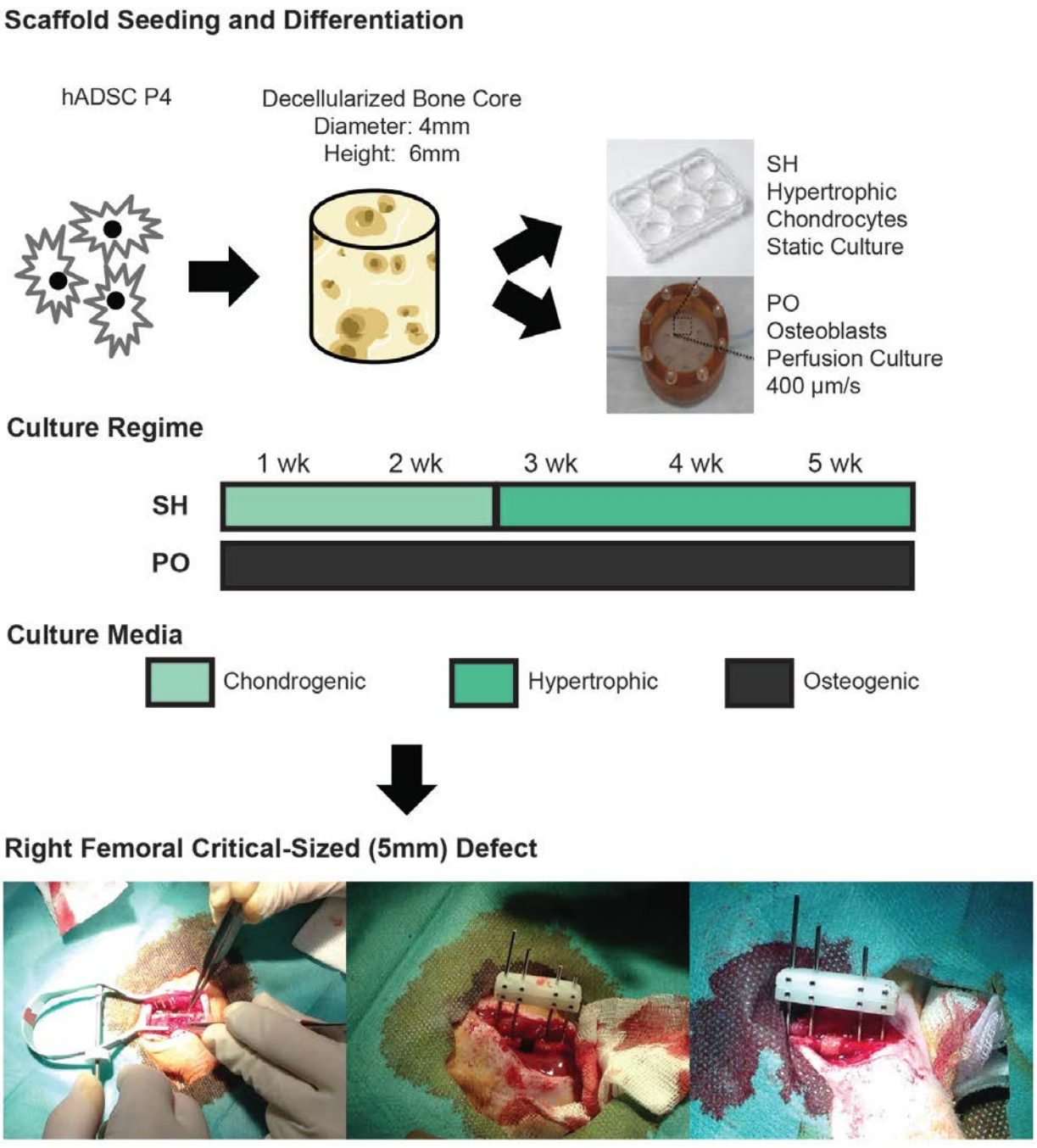

Figure 7S.1: Graphical illustration of the project methodology and femoral defect creation

Bone Core Harvest and Decellularization:

Bone cores were harvested from bovine juvenile wrists as previously denoted, (117). Cores were cut and measured to a height of 6 mm, diameter of 4 mm, and a density between 0.35 – 0.50 g/mL. Cores were decellularized following published protocols. Briefly, cores were washed in a series of detergent and enzymatic solutions: 1) 0.1% EDTA in PBS for 1 hour, 2) hypotonic buffer consisting of 10mM Tris and 0.1%EDTA in PBS for 12 hours at 4 degrees Celsius, 3) detergent consisting of 10mM Tris and 0.5% SDS in PBS for 24 hours at room temperature on an orbital shaker at 300 revolutions per minute, 4) enzymatic solution of 100 units/ mL DNase and 1 unit/ mL of RNase with 10 mM Tris in PBS at 37 degrees Celsius for 6 hours. After multiple washes in PBS to remove all solutions, cores were frozen and lyophilized.

Stem Cell Isolation, Expansion, and Graft Seeding:

Adipose tissue was obtained with the informed consent of the patient at the Rotes Kreuz facility in Linz, Austria, with adipose derived stem cells were extracted. The stem nature of the cells was verified by tri-differentiation testing. Cells were expanded until passage 4 in expansion medium consisting of high glucose medium with L-glutamine, 10% fetal bovine serum, and 1% penicillin/ streptomycin. In preparation for seeding, bone cores were disinfected in sterile-filtered 70% ethanol for 2 days, and then incubated in culture medium for 1 day. P4 adipose derived stem cells were trypsinized, resuspended in culture medium, and then applied to dried scaffolds in a drip method to seed the cores at 30M cells/ mL. The seeded cores were incubated in expansion medium for 2 days to promote cell attachment and expansion.

Graft Seeding and Cultivation:

After 2 days of expansion medium incubation, the culture conditions were modified to produce optimized grafts for each experimental group. Extensive work in our laboratory has shown that perfusion culture at a flow rate between 400-800 µm/s is optimal for osteoblast differentiation and bone graft culture (177). Therefore, osteoblast-based constructs were placed into a previously designed perfusion bioreactor (177) and cultured in osteogenic medium (low glucose DMEM (ThermoFisher, Waltham, MA), 100 nM dexamethasone, 50 ug/mL ascorbic acid, 10 mM HEPES buffer, 10% fetal bovine serum, 1% P/S, and 5mM β-glycerophosphate) at a perfusion rate of 400 µm/s for 5 weeks. With reference to published articles detailing the differentiation of hypertrophic chondrocytes (61, 62) and our own unpublished works, hypertrophic chondrocyte-based constructs were incubated statically first in chondrogenic medium (high glucose DMEM (ThermoFisher, Waltham, MA) supplemented with 100 nM dexamethasone, 50 µg/mL ascorbic acid, 50 µg/ mL proline, 100 µg/mL sodium pyruvate, 1% ITS+, 1% P/S, 10 ng/mL BMP6 and 10 ng/mL TGF-β3) for 2 weeks, followed by 3 weeks of hypertrophic medium (the same as chondrogenic medium, but without BMP6 and TGF-β3, a dexamethasone concentration of 1 nM, 50 ng/mL of L-thyroxine, and 5mM of β-glycerophosphate). At the culmination of cultivation, grafts were either implanted into orthotopic, critical-sized defects, or harvested for pre-implantation analysis. For pre-implantation analysis, grafts were cut in half and the corresponding wet weight was recorded.

Quantitative biochemical analysis:

Graft halves were digested with papain (40 Units/ mg) in digest buffer (0.1M sodium acetate, 10 mM cysteine HCl and 50 mM EDTA, pH 6.0) at 60 ^{o}C overnight. DNA content per

wet weight was measured from the digest solution using Quant-iT PicoGreen assay kit and the supplied lambda DNA standard (ThermoFisher, Waltham, MA). Sulfated glycosaminoglycan (GAG) content was measured using the dimethylmethylene blue assay with chondroitin 6 sulfate as a control. Each sample was run in duplicate, with n=4 for each experimental group.

Real time RT-PCR quantitation:

Total RNA was extracted from graft halves using the TRIzol-based method (ThermoFisher, Waltham, MA). DNase I treatment was utilized for ten minutes at 37 ^{o}C to remove any contaminating DNA. cDNA was transcribed using the High Capacity cDNA Reverse Transcription kit (ThermoFisher, Waltham, MA) according to the manufacturer's instructions. Quantitative RT-PCR was performed using Fast Sybr Green mix (ThermoFisher, Waltham, MA). Expression levels were quantified applying the ΔC_t method, with the C_t of GAPDH subtracted from the C_t of the gene of interest. Forward and reverse primers for each gene of interest are presented [Table 7S.1]. Samples were run in duplicate, with n=5 for each experimental group and time point.

Histology and Immunohistochemistry:

Grafts from each experimental group were fixed in 10% formalin, rinsed to PBS, and decalcified using a formic acid based solution (Immunocal Decalcifier, StatLab, McKinney, TX). After decalcifying, grafts were washed multiple times with PBS, dehydrated, embedded in paraffin, and sectioned at 6 µm. Grafts were stained with alcian blue for GAG content following publicly available protocols and Movat's Pentachrome for construct morphology following the manufacturer's instructions. Antigen retrieval was required for immunohistochemistry. Slides were placed in a container filled with citrate buffer (1.8 mM citric acid, 8.2 mM sodium citrate,

pH 6.0), and the container was submerged in boiling water for 20 min. Slides were blocked with 0.3% hydrogen peroxide in absolute methanol for 30 minutes before following the Vectastain Elite Universal staining kit (Vector Laboratories, Burlingame, CA). The primary antibodies for BSP (EMD Millipore, 1/500 dilution, AB1854, Bilerica, MA) and RUNX2 (Abcam, 1/1000 dilution, AB192256, San Francisco, CA) were incubated on the samples overnight at 4 ^{o}C. The slides were counterstained with Hematoxylin QS (Vector Laboratories, Burlingame, CA). Slides for collagen type X immunohistochemistry followed the previously described protocol (118). The primary antibody was obtained from Abcam (1/1000 dilution, AB49945, San Francisco, CA), and Hematoxylin QS was used as a counterstain.

Critical-sized Defect Creation and Graft Implantation:

An animal experiment permit was issued by the municipal government of Vienna, Austria and all experiments were consistent with the Guide for the Care and Use of Laboratory Animals of the National Institute of Health (revised 2011). Twenty-eight male, RNU nude rats were used in this study. Animals were kept in conventional housing in cages with filter tops and in groups of at least two, separate from all other animals.

At the time of operation, the rats weighed between 260 and 392 g. Animals were treated preoperatively with subcutaneously applied 0.05 mg/kg buprenorphine (Bupaq, Richterpharma AG, Austria) and 4 mg/kg carprofen (Rimadyl, Zoetis Osterreich Gesm.b.H, Austria). Anesthesia was induced in an inhalation box with isoflurane (Forane, AbbVie Gesm.b.H, Austria) and anesthesia was maintained with 1.5-2.5% isoflurane/ oxygen by way of mask inhalation.

Once under stable anesthesia, a lateral approach was used to expose the right femur. After fixation with a four-pin, POM fixator (modified from the method described in Betz et al

(181) and Kunkel et al (182)), a defect of 5 mm was created with a Gigli wire saw. Constructs were placed into the defect and the muscle and skin were sutured surrounding the construct and the fixator, respectively. For each experimental group (SH and PO) and control (decellularized DCB), eights rats underwent implantation, with four rats operated on to confirm the critical-size defect. Analgesia was continued over four days post-implantation with 0.05 mg/kg buprenorphine and 4 mg/kg carprofen.

Animals were subjected to *in vivo* µCT scans at day 1, and at 3, 6, and 9 weeks post-implantation (see µCT section). Twelve weeks post-implantation, the rats were euthanized by an overdose injection of intracardially delivered thiopental sodium while under deep isoflurane anesthesia. The right femur of each animal was harvested for further investigation and study.

Micro-computed Tomography (µCT):

For *in vivo* µCT scans, a vivaCT 75 (Scanco Medical, Bruttisellen, Switzerland) preclinical scanner was utilized. Studied rats were anesthetized with 2% isoflurane throughout the duration of the scan. The right femur of each rat was scanned at an isotropic resolution of 50 µm at day one, 3 weeks, 6 weeks, and 9 weeks post implantation. Scans were reconstructed to provide 3D representations of the defect and graft.

After femur harvest at 12 weeks, µCT scans were performed on a µCT 50 (Scanco, Bruttisellen, Switzerland) at an isotropic resolution of 10 µm. Scans were reconstructed to provide 3D representations of the defects, as well as quantitative data for the bone volume and bone surface area to bone volume present within the defect.

Hard Bone Histology:

Femurs with attached fixation were immersed in 4% neutral-buffered formaldehyde solution, then dehydrated in ascending grades of ethanol and imbedded in light curing resin (Technovit 7200 VLC; Kulzer & Co., Wehrheim, Germany). Undecalcified thin ground sections along the longitudinal axis of the shaft oriented in a frontal plane were produced according to Donath (158) and stained with Levai-Laczko (159) dye. Histological specimens were digitized with the Olympus dotSlide 2.4, digital virtual microscopy system (Olympus, Japan, Tokyo) at a resolution of 0.32 µm per pixel. Semi-quantitative values for the amount of new bone deposited, the existing area of old bone, the area of fibrous tissue, the area of bone marrow, and the quantity and location of osteoclasts was determined on the stained samples within the defect area by two independent, blinded researchers on n=4 femurs per staining.

Immunohistochemistry:

Femurs not utilized for hard bone histology were submerged in 4% neutral-buffered formaldehyde solution for 24 hours, followed by extensive washing in PBS. Femurs were decalcified using Immunocal (StatLab, McKinney, TX), followed by extensive washing in PBS and graded ethanol dehydrations of the femurs. Sections of the femur were made 6 µm thick, and immunohistochemistry was performed following the published citrate buffer antigen retrieval methods. Vectastain rabbit antibody kit (PK-4001, Vector Laboratories, Burlingame, CA), and AbCam's mouse on mouse kit (ab127055 ,abcam, San Francisco, CA) were utilized to stain for CD206 (abcam, 0.1 µg/mL, ab64693), and CD163 (abcam, 1/500, ab182422).

Statistics:

Statistical significance of pre-implantation measurements was determined by using a Student's T-Test, $\alpha = 0.05$, with significance determined by $p<0.05$ (Prism Software, GraphPad, La Jolla, CA, USA). After harvest of implanted constructs, statistical significant was determined by using a one-way analysis of variance (ANOVA) followed by Tukey's post-test, $\alpha=0.05$, with significance determined by $p<0.05$.

Table 7S.1: Primers used in RT-PCR

Gene	Forward	Reverse
GAPDH	AAGGTGAAGGTCGGAGTCAAC	GGGGTCATTGATGGCAACAATA
RUNX2	CCGTCTTCACAAATCCTCCCC	CCCGAGGTCCATCTACTGTAAC
COL1A1	GATCTGCGTCTGCGACAAC	GGCAGTTCTTGGTCTCGTCA
MMP13	CCAGACTTCACGATGGCATTG	GGCATCTCCTCCATAATTTGGC
ALPL	GGGACTGGTACTCAGACAACG	GTAGGCGATGTCCTTACAGCC
IBSP	GAACCTCGTGGGGACAATTAC	CATCATAGCCATCGTAGCCTTG
COL10A1	CATAAAAGGCCCACTACCCAAC	ACCTTGCTCTCCTCTTACTGC
SOX9	AGCGAACGCACATCAAGAC	CTGTAGGCGATCTGTTGGGG
COL2A1	AGACTTGCGTCTACCCCAATC	GCAGGCGTAGGAAGGTCATC

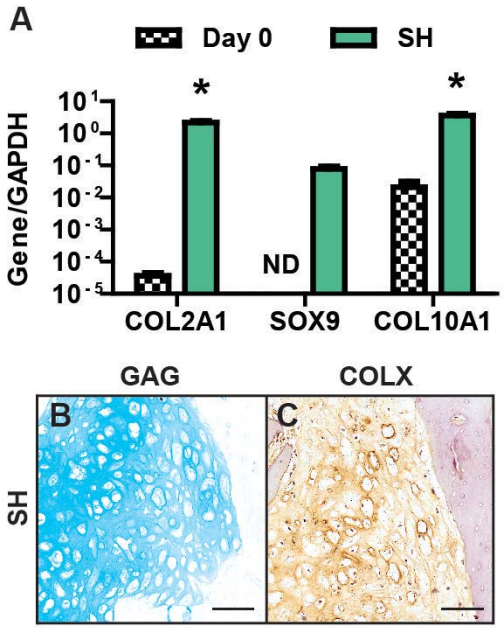

Figure 7S.2: Verification of the hypertrophic chondrocyte differentiation within the tissue engineered construct. *(7S.2A) Gene expression of key chondrogenic and hypertrophic genes were significantly increased at the culmination of differentiation, demonstrating a chondrocyte differentiation and then a hypertrophic maturation. (7S.2B) Histological sections of cultured SH constructs demonstrated glycosaminoglycan (GAG) deposition, indicating chondrocyte differentiation. (7S.2C) Immunohistochemistry demonstrated collagen type X deposition, strongly present surrounding the enlarged lacunae of the hypertrophic chondrocytes, indicating hypertrophic maturation. [n=3, Student's T-test with* = $p<0.05$ (7S.2A), Scale Bar = 100 µm(7S.2B-C)]*

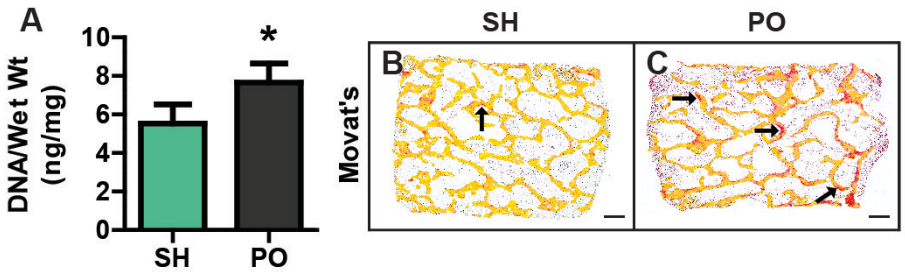

Figure 7S.3: Construct DNA content and osteoid formation. *Constructs were harvested after cultivation and before implantation. (7S.3A) DNA content was significantly higher in the PO constructs compared to the SH constructs. (7S.3B-C) Movat's Pentachrome was used to stain histological sections of the constructs and PO constructs had increased osteoid production (deposited red stain within the DCB scaffold, black arrows). [n=4, Student's T-test with* = p<0.05 (7S.3A), Scale Bar = 500 µm (7S.3B-C)]*

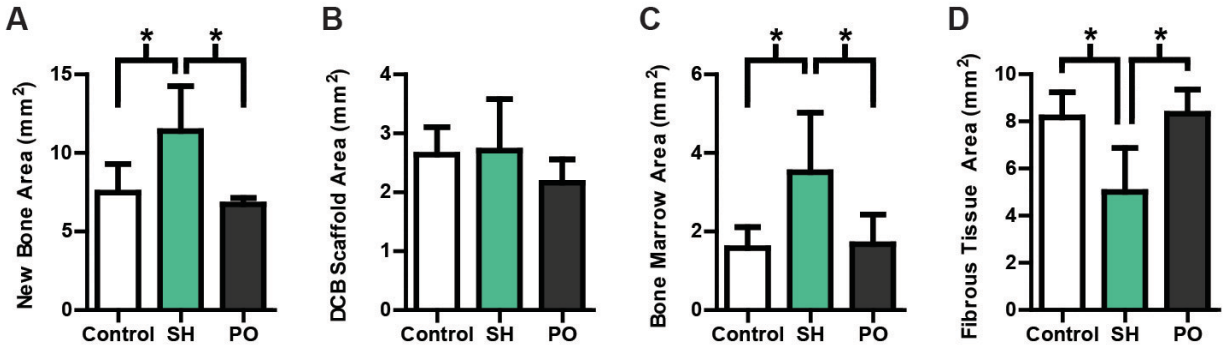

Figure 7S.4: Semi-quantitation of construct morphometry. *After harvest, hard bone histology was performed and constructs were stained with Levai-Laczko stain. (7S.4A) Quantitation of the different aspects of the regeneration demonstrated that SH produced significantly more new bone. (7S.4B) The amount of implanted DCB scaffold was not significantly different between the different constructs. (7S.4C) SH constructs had significantly more bone marrow within the constructs. (7S.4D) SH constructs had significantly less fibrous tissue within the defect area. [n=4, One-way ANOVA with Tukey post-test, with* = p<0.05, all quantitation was blindly conducted]*

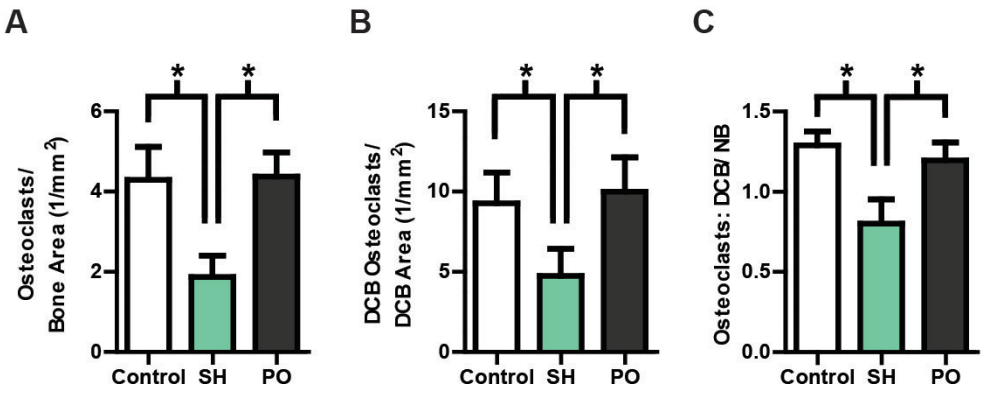

Figure 7S.5: Osteoclast presence and localization. *Osteoclasts were determined by their multinucleation and Howship's lacunae within the Levai-Laczko stains. (7S.5A) SH constructs had significantly less osteoclasts, normalized to the amount of bone present within the defect space. (7S.5B) Determining the number of osteoclasts that were digesting the implanted DCB scaffold, the SH constructs had significantly less osteoclasts than the other two constructs. (7S.5C) The ratio of osteoclasts digesting the implanted DCB versus the number of osteoclasts digesting newly produced bone was significantly less for the SH constructs. [n=4, One-way ANOVA with Tukey post-test, with* = p<0.05, all quantitation was blindly conducted]*

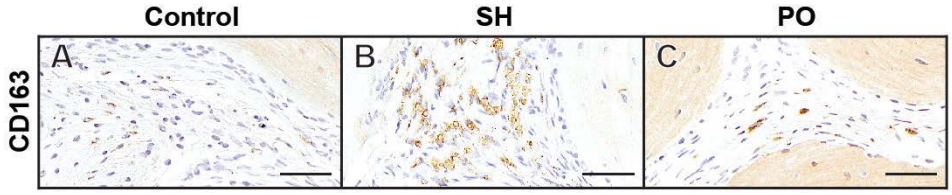

Figure 7S.6: CD163+ M2-polarized macrophages. *Serial sections of the immunohistochemistry samples allowed CD163+ to be closely correlated with CD206+ cells. Similar to the CD206 staining, CD163+ cells were more abundant in the SH constructs. [Scale Bars = 50 µm(S6A-C)]*

PART V

CONCLUSION

8 Conclusion

Bone tissue engineering has had difficulty in designing effective, clinically relevant grafts for long bone fracture repair. This dissertation attempted to enhance bone regeneration following a developmental paradigm, replicating native long bone repair processes by engineering endochondral ossification-mimicking grafts utilizing hypertrophic chondrocytes. The first aim examined the effects of oxygen tension on hypertrophic chondrocyte differentiation, demonstrating that a hypoxic environment similar to native, stable cartilage prevents hypertrophy, even when applied transiently. This aim suggests hypertrophic chondrocyte differentiation occurs in elevated oxygen tensions and that the increase in oxygen tension during endochondral ossification is not enough for hypertrophic maturation. The second aim measured the effect of advanced chondrogenic states in promoting enhanced hypertrophic differentiation. Whereas all samples studied contained hypertrophic chondrocytes and produced bone, advanced chondrogenic states resulted in improved hypertrophic maturation and a more widespread bone production, suggesting the importance of mirroring the native endochondral ossification for widespread bone production. The final aim evaluated the bone produced by hypertrophic chondrocytes and their ability to facilitate long bone repair. The hypertrophic chondrocytes rapidly produced voluminous, immature bone *in vitro,* and promoted extensive regeneration *in vivo* with mature bone bridging the defect. The results of this dissertation clearly demonstrate the feasibility and promise of hypertrophic chondrocyte-based tissue engineering strategies, and prompt its further investigation for clinical relevancy.

REFERENCES

1. Rodan GA (1992) Introduction to Bone Biology. *Bone* 13:S3-S6.

2. Sommerfeldt D & Rubin C (2001) Biology of bone and how it orchestrates the form and function of the skeleton. *European Spine Journal* 10(2):S86-S95.

3. Salgado AJ, Coutinho OP, & Reis RL (2004) Bone tissue engineering: State of the art and future trends. *Macromolecular Bioscience* 4(8):743-765.

4. Lenas P, Moos M, Jr., & Luyten FP (2009) Developmental Engineering: A New Paradigm for the Design and Manufacturing of Cell-Based Products. Part I: From Three-Dimensional Cell Growth to Biomimetics of In Vivo Development. *Tissue Engineering Part B-Reviews* 15(4):381-394.

5. Martin RB & Burr DB (1989) *Structure Function and Adaptation of Compact Bone* pp XII+275P-XII+275P.

6. Rodan GA & Martin TJ (2000) Therapeutic Approaches to Bone Diseases. *Science* 289(5484):1508-1514.

7. Hadjidakis DJ & Androulakis II (2006) Bone Remodeling. *Annals of the New York Academy of Sciences* 1092(1):385-396.

8. Parfitt AM (1976) Actions of Parathyroid-Hormone on Bone - Relation to Bone Remodeling and Turnover, Calcium Homeostasis, and Metabolic Bone Diseases .2. PTH and Bone-Cells - Bone Turnover and Plasma Calcium Regulation. *Metab.-Clin. Exp.* 25(8):909-955.

9. Clarke B (2008) Normal Bone Anatomy and Physiology. *Clinical Journal of the American Society of Nephrology : CJASN* 3(Suppl 3):S131-S139.

10. Wilson J, Clark AE, Hall M, & Hench LL (1993) Tissue response to Bioglass endosseous ridge maintenance implants. *The Journal of oral implantology* 19(4):295-302.

11. Willems NMBK, Langenbach GEJ, Everts V, & Zentner A (2014) The microstructural and biomechanical development of the condylar bone: a review. *The European Journal of Orthodontics* 36(4):479-485.

12. Marks SC, Jr. & Hermey DC (1996) *The structure and development of bone* pp 3-14.

13. Marks SC & Popoff SN (1988) BONE CELL BIOLOGY - THE REGULATION OF DEVELOPMENT, STRUCTURE, AND FUNCTION IN THE SKELETON. *American Journal of Anatomy* 183(1):1-44.

14. Ornitz DM & Marie PJ (2002) FGF signaling pathways in endochondral and intramembranous bone development and human genetic disease. *Genes & Development* 16(12):1446-1465.

15. Shapiro F (2008) Bone development and its relation to fracture repair. The role of mesenchymal osteoblasts and surface osteoblasts. *Eur. Cells Mater.* 15:53-76.

16. Martini F, Nath, J. L. (2009) *Funadmentals of anatomy and physiology* (Pearson/ Benjamin Cummings, San Francisco) 6th Ed.

17. Mackie EJ, Ahmed YA, Tatarczuch L, Chen KS, & Mirams M (2008) Endochondral ossification: How cartilage is converted into bone in the developing skeleton. *International Journal of Biochemistry & Cell Biology* 40(1):46-62.

18. Ai-Aql ZS, Alagl AS, Graves DT, Gerstenfeld LC, & Einhorn TA (2008) Molecular mechanisms controlling bone formation during fracture healing and distraction osteogenesis. *Journal of Dental Research* 87(2):107-118.

19. Goldring MB, Tsuchimochi K, & Ijiri K (2006) The control of chondrogenesis. *Journal of Cellular Biochemistry* 97(1):33-44.

20. Marsell R & Einhorn TA (2011) The biology of fracture healing. *Injury-International Journal of the Care of the Injured* 42(6):551-555.

21. Kronenberg HM (2006) PTHrP and skeletal development. *Skeletal Development and Remodeling in Health, Disease, and Aging*, Annals of the New York Academy of Sciences, ed Zaidi M), Vol 1068, pp 1-13.

22. Bahney CS, *et al.* (2014) Stem Cell- Derived Endochondral Cartilage Stimulates Bone Healing by Tissue Transformation. *J. Bone Miner. Res.* 29(5):1269-1282.

23. Maes C, *et al.* (2010) Osteoblast Precursors, but Not Mature Osteoblasts, Move into Developing and Fractured Bones along with Invading Blood Vessels. *Developmental Cell* 19(2):329-344.

24. Kronenberg HM (2003) Developmental regulation of the growth plate. *Nature* 423(6937):332-336.

25. Chan CKF, *et al.* (2009) Endochondral ossification is required for hematopoietic stem cell niche formation. *Nature* 457(7228):490-494.

26. Mescher AL, Junqueira, L.C.U (2013) *Junqueira's basic histology: Text and atlas* (McGraw Hill Medical, New York) Thirteenth Ed.

27. Bianco P, Cancedda FD, Riminucci M, & Cancedda R (1998) Bone formation via cartilage models: The "borderline" chondrocyte. *Matrix Biology* 17(3):185-192.

28. Gerstenfeld LC, Cullinane DM, Barnes GL, Graves DT, & Einhorn TA (2003) Fracture healing as a post-natal developmental process: Molecular, spatial, and temporal aspects of its regulation. *Journal of Cellular Biochemistry* 88(5):873-884.

29. Church V, Nohno T, Linker C, Marcelle C, & Francis-West P (2002) Wnt regulation of chondrocyte differentiation. *Journal of Cell Science* 115(24):4809-4818.

30. Minina E, Kreschel C, Naski MC, Ornitz DM, & Vortkamp A (2002) Interaction of FGF, lhh/Pthlh, and BMP signaling integrates chondrocyte proliferation and hypertrophic differentiation. *Developmental Cell* 3(3):439-449.

31. Zhong L, Huang X, Karperien M, & Post JN (2015) The Regulatory Role of Signaling Crosstalk in Hypertrophy of MSCs and Human Articular Chondrocytes. *International Journal of Molecular Sciences* 16(8):19225-19247.

32. Cancedda R, Cancedda FD, & Castagnola P (1995) CHONDROCYTE DIFFERENTIATION. *International Review of Cytology - a Survey of Cell Biology, Vol 159* 159:265-358.

33. de Crombrugghe B & Lefebvre W (2001) Regulatory mechanisms in the pathways of cartilage and bone formation. *Current Opinion in Cell Biology* 13(6):721-727.

34. Shen G (2005) The role of type X collagen in facilitating and regulating endochondral ossification of articular cartilage. *Orthodontics & craniofacial research* 8(1):11-17.

35. Carlevaro MF, Cermelli S, Cancedda R, & Cancedda FD (2000) Vascular endothelial growth factor (VEGF) in cartilage neovascularization and chondrocyte differentiation: auto-paracrine role during endochondral bone formation. *Journal of Cell Science* 113(1):59-69.

36. Gerber HP, *et al.* (1999) VEGF couples hypertrophic cartilage remodeling, ossification and angiogenesis during endochondral bone formation. *Nature Medicine* 5(6):623-628.

37. Maes C & Carmeliet G (2008) Vascular and Nonvascular Roles of VEGF in Bone Development. *VEGF in Development*, (Springer New York, New York, NY), pp 79-90.

38. Cruess RL & Dumont J (1975) Fracture healing. *Canadian Journal of Surgery* 18(5):403-&.

39. Bolander ME (1992) Regulation of fracture repiar by growth factors. *Proceedings of the Society for Experimental Biology and Medicine* 200(2):165-170.

40. Carano RAD & Filvaroff EH (2003) Angiogenesis and bone repair. *Drug Discovery Today* 8(21):980-989.

41. Carter DR, Beaupre GS, Giori NJ, & Helms JA (1998) Mechanobiology of skeletal regeneration. *Clinical Orthopaedics and Related Research* (355):S41-S55.

42. Wren TAL, Loboa EG, Beaupre GS, & Carter DR (2003) *Mechanobiology of skeletal tissue differentiation and regeneration* pp 1-10.

43. Kaderly RE (1991) PRIMARY BONE HEALING. *Seminars in Veterinary Medicine and Surgery-Small Animal* 6(1):21-25.

44. Thompson Z, Miclau T, Hu D, & Helms JA (2002) A model for intramembranous ossification during fracture healing. *Journal of Orthopaedic Research* 20(5):1091-1098.

45. Towler DA (2008) The osteogenic-angiogenic interface: novel insights into the biology of bone formation and fracture repair. *Current osteoporosis reports* 6(2):67-71.

46. Einhorn TA & Gerstenfeld LC (2015) Fracture healing: mechanisms and interventions. *Nat Rev Rheumatol* 11(1):45-54.

47. Arvidson K, *et al.* (2011) Bone regeneration and stem cells. *Journal of Cellular and Molecular Medicine* 15(4):718-746.

48. McKibbin B (1978) BIOLOGY OF FRACTURE HEALING IN LONG BONES. *Journal of Bone and Joint Surgery-British Volume* 60(2):150-162.

49. Chung U-i, Schipani E, McMahon AP, & Kronenberg HM (Indian hedgehog couples chondrogenesis to osteogenesis in endochondral bone development. *The Journal of Clinical Investigation* 107(3):295-304.

50. Phillips AM (2005) Overview of the fracture healing cascade. *Injury* 36(3, Supplement):S5-S7.

51. Ferguson C, Alpern E, Miclau T, & Helms JA (1999) Does adult fracture repair recapitulate embryonic skeletal formation? *Mechanisms of Development* 87(1-2):57-66.

52. Rodan GA (1998) Bone homeostasis. *Proceedings of the National Academy of Sciences of the United States of America* 95(23):13361-13362.

53. Sims NA & Martin TJ (2014) Coupling the activities of bone formation and resorption: a multitude of signals within the basic multicellular unit. *BoneKEy Rep* 3.

54. Franz-Odendaal TA, Hall BK, & Witten PE (2006) Buried alive: How osteoblasts become osteocytes. *Developmental Dynamics* 235(1):176-190.

55. Ali A, Douglas H, & Stanley D (2005) Revision surgery for nonunion after early failure of fixation of fractures of the distal humerus. *Journal of Bone and Joint Surgery-British Volume* 87B(8):1107-1110.

56. Flierl MA, *et al.* (2013) Outcomes and complication rates of different bone grafting modalities in long bone fracture nonunions: a retrospective cohort study in 182 patients. *Journal of Orthopaedic Surgery and Research* 8.

57. Gómez-Barrena E, *et al.* (2015) Bone fracture healing: Cell therapy in delayed unions and nonunions. *Bone* 70:93-101.

58. Jain A, Kumar S, Aggarwal AN, & Jajodia N (2015) Augmentation of bone healing in delayed and atrophic nonunion of fractures of long bones by partially decalcified bone allograft (decal bone). *Indian Journal of Orthopaedics* 49(6):637-642.

59. Jaiswal N, Haynesworth SE, Caplan AI, & Bruder SP (1997) Osteogenic differentiation of purified, culture-expanded human mesenchymal stem cells in vitro. *Journal of Cellular Biochemistry* 64(2):295-312.

60. Laurencin CT, Ambrosio AMA, Borden MD, & Cooper JA (1999) Tissue engineering: Orthopedic applications. *Annual Review of Biomedical Engineering* 1:19-46.

61. Mueller MB & Tuan RS (2008) Functional characterization of hypertrophy in chondrogenesis of human mesenchymal stem cells. *Arthritis and Rheumatism* 58(5):1377-1388.

62. Scotti C, *et al.* (2010) Recapitulation of endochondral bone formation using human adult mesenchymal stem cells as a paradigm for developmental engineering. *Proceedings of the National Academy of Sciences of the United States of America* 107(16):7251-7256.

63. Gawlitta D, *et al.* (2010) Modulating Endochondral Ossification of Multipotent Stromal Cells for Bone Regeneration. *Tissue Engineering Part B-Reviews* 16(4):385-395.

64. Simon MC & Keith B (2008) The role of oxygen availability in embryonic development and stem cell function. *Nat Rev Mol Cell Biol* 9(4):285-296.

65. Lee H-H, *et al.* (2013) Hypoxia Enhances Chondrogenesis and Prevents Terminal Differentiation through PI3K/Akt/FoxO Dependent Anti-Apoptotic Effect. *Scientific Reports* 3.

66. Leijten JCH, Teixeira LSM, Landman EBM, van Blitterswijk CA, & Karperien M (2012) Hypoxia Inhibits Hypertrophic Differentiation and Endochondral Ossification in Explanted Tibiae. *Plos One* 7(11).

67. Robins JC, *et al.* (2005) Hypoxia induces chondrocyte-specific gene expression in mesenchymal cells in association with transcriptional activation of Sox9. *Bone* 37(3):313-322.

68. Farnum CE, Lee R, O'Hara K, & Urban JPG (2002) Volume increase in growth plate chondrocytes during hypertrophy: The contribution of organic osmolytes. *Bone* 30(4):574-581.

69. Thompson EM, Matsiko A, Kelly DJ, Gleeson JP, & O'Brien FJ (2016) An Endochondral Ossification-Based Approach to Bone Repair: Chondrogenically Primed Mesenchymal Stem Cell-Laden Scaffolds Support Greater Repair of Critical-Sized Cranial Defects Than Osteogenically Stimulated Constructs In Vivo. *Tissue Engineering Part A* 22(5-6):556-567.

70. Johnstone B, Hering TM, Caplan AI, Goldberg VM, & Yoo JU (1998) In vitro chondrogenesis of bone marrow-derived mesenchymal progenitor cells. *Experimental Cell Research* 238(1):265-272.

71. Pelttari K, *et al.* (2006) Premature induction of hypertrophy during in vitro chondrogenesis of human mesenchymal stem cells correlates with calcification and vascular invasion after ectopic transplantation in SCID mice. *Arthritis and Rheumatism* 54(10):3254-3266.

72. Sekiya I, Vuoristo JT, Larson BL, & Prockop DJ (2002) In vitro cartilage formation by human adult stem cells from bone marrow stroma defines the sequence of cellular and molecular events during chondrogenesis. *Proceedings of the National Academy of Sciences of the United States of America* 99(7):4397-4402.

73. Claes L, Augat P, Suger G, & Wilke H-J (1997) Influence of size and stability of the osteotomy gap on the success of fracture healing. *Journal of Orthopaedic Research* 15(4):577-584.

74. Claes LE, *et al.* (1998) Effects of Mechanical Factors on the Fracture Healing Process. *Clinical Orthopaedics and Related Research* 355:S132-S147.

75. Schindeler A, McDonald MM, Bokko P, & Little DG (2008) Bone remodeling during fracture repair: The cellular picture. *Seminars in Cell & Developmental Biology* 19(5):459-466.

76. Saini S & Wick TM (2004) Effect of low oxygen tension on tissue-engineered cartilage construct development in the concentric cylinder bioreactor. *Tissue Engineering* 10(5-6):825-832.

77. Shang J, Liu H, Li J, & Zhou Y (2014) Roles of Hypoxia During the Chondrogenic Differentiation of Mesenchymal Stem Cells. *Current Stem Cell Research & Therapy* 9(2):141-147.

78. Baez A & Shiloach J (2014) Effect of elevated oxygen concentration on bacteria, yeasts, and cells propagated for production of biological compounds. *Microbial Cell Factories* 13:181.

79. Sheehy EJ, Buckley CT, & Kelly DJ (2012) Oxygen tension regulates the osteogenic, chondrogenic and endochondral phenotype of bone marrow derived mesenchymal stem cells. *Biochemical and Biophysical Research Communications* 417(1):305-310.

80. Murphy CL, Thoms BL, Vaghjiani RJ, & Lafont JE (2009) Hypoxia HIF-mediated articular chondrocyte function: prospects for cartilage repair. *Arthritis Research & Therapy* 11(1).

81. Gawlitta D, van Rijen MHP, Schrijver EJM, Alblas J, & Dhert WJA (2012) Hypoxia Impedes Hypertrophic Chondrogenesis of Human Multipotent Stromal Cells. *Tissue Engineering Part A* 18(19-20):1957-1966.

82. Schipani E, *et al.* (2001) Hypoxia in cartilage: HIF-1α is essential for chondrocyte growth arrest and survival. *Genes & Development* 15(21):2865-2876.

83. Studer D, Millan C, Ozturk E, Maniura-Weber K, & Zenobi-Wong M (2012) Molecular And Biophysical Mechanisms Regulating Hypertrpohic Differentiation In Chondrocytes And Mesenchymal Stem Cells. *Eur. Cells Mater.* 24:118-135.

84. Bosnakovski D, *et al.* (2004) Chondrogenic differentiation of bovine bone marrow mesenchymal stem cells in pellet cultural system. *Experimental Hematology* 32(5):502-509.

85. Adesida AB, Mulet-Sierra A, & Jomha NM (2012) Hypoxia mediated isolation and expansion enhances the chondrogenic capacity of bone marrow mesenchymal stromal cells. *Stem Cell Research & Therapy* 3(2):1-13.

86. Lee H-H, *et al.* (2013) Hypoxia Enhances Chondrogenesis and Prevents Terminal Differentiation through PI3K/Akt/FoxO Dependent Anti-Apoptotic Effect. *Scientific Reports* 3:2683.

87. Meretoja VV, Dahlin RL, Wright S, Kasper FK, & Mikos AG (2013) The effect of hypoxia on the chondrogenic differentiation of co-cultured articular chondrocytes and mesenchymal stem cells in scaffolds. *Biomaterials* 34(17):4266-4273.

88. Yodmuang S, Marolt D, Marcos-Campos I, Gadjanski I, & Vunjak-Novakovic G (2015) Synergistic Effects of Hypoxia and Morphogenetic Factors on Early Chondrogenic Commitment of Human Embryonic Stem Cells in Embryoid Body Culture. *Stem Cell Reviews and Reports* 11(2):228-241.

89. Talts JF, *et al.* (1998) Endochondral Ossification Is Dependent on the Mechanical Properties of Cartilage Tissue and on Intracellular Signals in Chondrocytesa. *Annals of the New York Academy of Sciences* 857(1):74-85.

90. Yu X, Guo Y, Kang Q, & Luo C (2013) Effects and mechanisms of mechanical stress on secondary fracture healing. *Frontiers in Bioscience-Landmark* 18:1345-1349.

91. Einhorn TA (1998) The cell and molecular biology of fracture healing. *Clinical Orthopaedics and Related Research* (355):S7-S21.

92. van der Stok J, *et al.* (2014) CHONDROGENICALLY DIFFERENTIATED MESENCHYMAL STROMAL CELL PELLETS STIMULATE ENDOCHONDRAL BONE REGENERATION IN CRITICAL-SIZED BONE DEFECTS. *Eur. Cells Mater.* 27:137-148.

93. Scotti C, *et al.* (2013) Engineering of a functional bone organ through endochondral ossification. *Proceedings of the National Academy of Sciences of the United States of America* 110(10):3997-4002.

94. Mueller MB, *et al.* (2010) Hypertrophy in Mesenchymal Stem Cell Chondrogenesis: Effect of TGF-beta Isoforms and Chondrogenic Conditioning. *Cells Tissues Organs* 192(3):158-166.

95. Scotti C, *et al.* (2012) Engineering a bone organ through endochondral ossification. *Journal of Tissue Engineering and Regenerative Medicine* 6:30-30.

96. Ronziere MC, Perrier E, Mallein-Gerin F, & Freyria AM (2010) Chondrogenic potential of bone marrow- and adipose tissue-derived adult human mesenchymal stem cells. *Bio-Medical Materials and Engineering* 20(3-4):145-158.

97. Somoza RA, Welter JF, Correa D, & Caplan AI (2014) Chondrogenic Differentiation of Mesenchymal Stem Cells: Challenges and Unfulfilled Expectations. *Tissue Engineering. Part B, Reviews* 20(6):596-608.

98. Lv H, *et al.* (2015) Mechanism of regulation of stem cell differentiation by matrix stiffness. *Stem Cell Research & Therapy* 6.

99. Park JS, *et al.* (2011) The effect of matrix stiffness on the differentiation of mesenchymal stem cells in response to TGF-beta. *Biomaterials* 32(16):3921-3930.

100. Duer MJ, Friščić T, Murray RC, Reid DG, & Wise ER (2009) The Mineral Phase of Calcified Cartilage: Its Molecular Structure and Interface with the Organic Matrix. *Biophysical Journal* 96(8):3372-3378.

101. Rey C, Beshah K, Griffin R, & Glimcher MJ (1991) Structural studies of the mineral phase of calcifying cartilage. *Journal of Bone and Mineral Research* 6(5):515-525.

102. Bhumiratana S, *et al.* (2011) Nucleation and growth of mineralized bone matrix on silk-hydroxyapatite composite scaffolds. *Biomaterials* 32(11):2812-2820.

103. Schlundt C, *et al.* (2015) Macrophages in bone fracture healing: Their essential role in endochondral ossification. *Bone*.

104. Wu AC, Raggatt LJ, Alexander KA, & Pettit AR (2013) Unraveling macrophage contributions to bone repair. *BoneKEy Rep* 2.

105. Street J, *et al.* (2002) Vascular endothelial growth factor stimulates bone repair by promoting angiogenesis and bone turnover. *Proceedings of the National Academy of Sciences of the United States of America* 99(15):9656-9661.

106. Chung UI (2004) Essential role of hypertrophic chondrocytes in endochondral bone development. *Endocrine Journal* 51(1):19-24.

107. Provot S & Schipani E (2005) Molecular mechanisms of endochondral bone development. *Biochemical and Biophysical Research Communications* 328(3):658-665.

108. Scott MA, *et al.* (2012) Brief Review of Models of Ectopic Bone Formation. *Stem Cells and Development* 21(5):655-667.

109. Viateau V, Logeart-Avramoglou D, Guillemin G, & Petite H (2008) Animal Models for Bone Tissue Engineering Purposes. *Sourcebook of Models for Biomedical Research*, ed Conn PM (Humana Press, Totowa, NJ), pp 725-736.

110. Grayson WL, *et al.* (2011) Optimizing the Medium Perfusion Rate in Bone Tissue Engineering Bioreactors. *Biotechnology and Bioengineering* 108(5):1159-1170.

111. Bhardwaj N, Devi D, & Mandal BB (2015) Tissue-Engineered Cartilage: The Crossroads of Biomaterials, Cells and Stimulating Factors. *Macromolecular Bioscience* 15(2):153-182.

112. Bhattacharjee M, *et al.* (2015) Tissue engineering strategies to study cartilage development, degeneration and regeneration. *Advanced Drug Delivery Reviews* 84:107-122.

113. Bauge C & Boumediene K (2015) Use of Adult Stem Cells for Cartilage Tissue Engineering: Current Status and Future Developments. *Stem Cells International*.

114. Bhumiratana S, *et al.* (2014) Large, stratified, and mechanically functional human cartilage grown in vitro by mesenchymal condensation. *Proceedings of the National Academy of Sciences* 111(19):6940-6945.

115. Mwale F, *et al.* (2006) Suppression of genes related to hypertrophy and osteogenesis in committed human mesenchymal stem cells cultured on novel nitrogen-rich plasma polymer coatings. *Tissue Engineering* 12(9):2639-2647.

116. Chen S, Fu P, Cong R, Wu H, & Pei M (2015) Strategies to minimize hypertrophy in cartilage engineering and regeneration. *Genes & Diseases* 2(1):76-95.

117. Grayson WL, *et al.* (2010) Engineering anatomically shaped human bone grafts. *Proceedings of the National Academy of Sciences of the United States of America* 107(8):3299-3304.

118. Aigner T, Greskotter KR, Fairbank JCT, von der Mark K, & Urban JPG (1998) Variation with age in the pattern of type X collagen expression in normal and scoliotic human intervertebral discs. *Calcified Tissue International* 63(3):263-268.

119. Ghone NV & Grayson WL (2012) Recapitulation of mesenchymal condensation enhances in vitro chondrogenesis of human mesenchymal stem cells. *Journal of Cellular Physiology* 227(11):3701-3708.

120. Bahney CS, Hsu C-W, Yoo JU, West JL, & Johnstone B (2011) A bioresponsive hydrogel tuned to chondrogenesis of human mesenchymal stem cells. *Faseb Journal* 25(5):1486-1496.

121. Buxton AN, Bahney CS, Yoo JU, & Johnstone B (2011) Temporal Exposure to Chondrogenic Factors Modulates Human Mesenchymal Stem Cell Chondrogenesis in Hydrogels. *Tissue Engineering Part A* 17(3-4):371-380.

122. Adesida AB, Mulet-Sierra A, & Jomha NM (2012) Hypoxia mediated isolation and expansion enhances the chondrogenic capacity of bone marrow mesenchymal stromal cells. *Stem Cell Research & Therapy* 3.

123. Malda J, Martens DE, Tramper J, van Blitterswijk CA, & Riesle J (2003) Cartilage tissue engineering: Controversy in the effect of oxygen. *Critical Reviews in Biotechnology* 23(3):175-194.

124. Buckley CT, Vinardell T, & Kelly DJ (2010) Oxygen tension differentially regulates the functional properties of cartilaginous tissues engineered from infrapatellar fat pad derived MSCs and articular chondrocytes. *Osteoarthritis and Cartilage* 18(10):1345-1354.

125. Cicione C, *et al.* (2013) Effects of Severe Hypoxia on Bone Marrow Mesenchymal Stem Cells Differentiation Potential. *Stem Cells International*.

126. Obradovic B, Carrier RL, Vunjak-Novakovic G, & Freed LE (1999) Gas exchange is essential for bioreactor cultivation of tissue engineered cartilage. *Biotechnology and Bioengineering* 63(2):197-205.

127. Co C, Vickaryous MK, & Koch TG (2014) Membrane culture and reduced oxygen tension enhances cartilage matrix formation from equine cord blood mesenchymal stromal cells in vitro. *Osteoarthritis and Cartilage* 22(3):472-480.

128. Khan WS, Adesida AB, Tew SR, Lowe ET, & Hardingham TE (2010) Bone Marrow-Derived Mesenchymal Stem Cells Express the Pericyte Marker 3G5 in Culture and Show Enhanced Chondrogenesis in Hypoxic Conditions. *Journal of Orthopaedic Research* 28(6):834-840.

129. Hirao M, Tamai N, Tsumaki N, Yoshikawa H, & Myoui A (2006) Oxygen tension regulates chondrocyte differentiation and function during endochondral ossification. *Journal of Biological Chemistry* 281(41):31079-31092.

130. Kawato Y, *et al.* (2011) Nkx3.2-induced suppression of Runx2 is a crucial mediator of hypoxia-dependent maintenance of chondrocyte phenotypes. *Biochemical and Biophysical Research Communications* 416(1-2):205-210.

131. Duval E, *et al.* (2012) Molecular mechanism of hypoxia-induced chondrogenesis and its application in in vivo cartilage tissue engineering. *Biomaterials* 33(26):6042-6051.

132. Olsen BR, Reginato AM, & Wang WF (2000) Bone development. *Annual Review of Cell and Developmental Biology* 16:191-220.

133. Karsenty G & Wagner EF (2002) Reaching a Genetic and Molecular Understanding of Skeletal Development. *Developmental Cell* 2(4):389-406.

134. Dennis SC, Berkland CJ, Bonewald LF, & Detamore MS (2015) Endochondral Ossification for Enhancing Bone Regeneration: Converging Native Extracellular Matrix Biomaterials and Developmental Engineering In Vivo. *Tissue Engineering Part B-Reviews* 21(3):247-266.

135. Rockwood DN, *et al.* (2011) Materials fabrication from Bombyx mori silk fibroin. *Nature Protocols* 6(10):1612-1631.

136. Farndale RW, Buttle DJ, & Barrett AJ (1986) IMPROVED QUANTITATION AND DISCRIMINATION OF SULFATED GLYCOSAMINOGLYCANS BY USE OF DIMETHYLMETHYLENE BLUE. *Biochimica Et Biophysica Acta* 883(2):173-177.

137. Reddy GK & Enwemeka CS (1996) A simplified method for the analysis of hydroxyproline in biological tissues. *Clinical biochemistry* 29(3):225-229.

138. Liu XS, Sajda P, Saha PK, Wehrli FW, & Guo XE (2006) Quantification of the roles of trabecular microarchitecture and trabecular type in determining the elastic modulus of human trabecular bone. *Journal of Bone and Mineral Research* 21(10):1608-1617.

139. Vortkamp A, *et al.* (1996) Regulation of rate of cartilage differentiation by Indian hedgehog and PTH-related protein. *Science* 273(5275):613-622.

140. Gerstenfeld LC & Shapiro FD (1996) Expression of bone-specific genes by hypertrophic chondrocytes: Implications of the complex functions of the hypertrophic chondrocyte during endochondral bone development. *Journal of Cellular Biochemistry* 62(1):1-9.

141. Mackay AM, *et al.* (1998) Chondrogenic differentiation of cultured human mesenchymal stem cells from marrow. *Tissue Engineering* 4(4):415-428.

142. Mello MA & Tuan RS (2006) Effects of TGF-β1 and triiodothyronine on cartilage maturation: In vitro analysis using long-term high-density micromass cultures of chick embryonic limb mesenchymal cells. *Journal of Orthopaedic Research* 24(11):2095-2105.

143. Miura M, *et al.* (2002) Thyroid hormones promote chondrocyte differentiation in mouse ATDC5 cells and stimulate endochondral ossification in fetal mouse tibias through lodothyronine deiodinases in the growth plate. *Journal of Bone and Mineral Research* 17(3):443-454.

144. Cheung JOP, *et al.* (2001) A novel cell culture model of chondrocyte differentiation during mammalian endochondral ossification. *Journal of Bone and Mineral Research* 16(2):309-318.

145. Zhou G, *et al.* (2015) Zbtb20 regulates the terminal differentiation of hypertrophic chondrocytes via repression of Sox9. *Development* 142(2):385-393.

146. Barry F, Boynton RE, Liu BS, & Murphy JM (2001) Chondrogenic differentiation of mesenchymal stem cells from bone marrow: Differentiation-dependent gene expression of matrix components. *Experimental Cell Research* 268(2):189-200.

147. Phinney DG (2012) Functional heterogeneity of mesenchymal stem cells: Implications for cell therapy. *Journal of Cellular Biochemistry* 113(9):2806-2812.

148. Chamberlain G, Fox J, Ashton B, & Middleton J (2007) Concise Review: Mesenchymal Stem Cells: Their Phenotype, Differentiation Capacity, Immunological Features, and Potential for Homing. *STEM CELLS* 25(11):2739-2749.

149. Albro MB, *et al.* (2013) Accumulation of Exogenous Activated TGF-beta in the Superficial Zone of Articular Cartilage. *Biophysical Journal* 104(8):1794-1804.

150. Albro MB, *et al.* (2016) Heterogeneous engineered cartilage growth results from gradients of media-supplemented active TGF-β and is ameliorated by the alternative supplementation of latent TGF-β. *Biomaterials* 77:173-185.

151. Basalo IM, *et al.* (2004) Cartilage Interstitial Fluid Load Support in Unconfined Compression Following Enzymatic Digestion. *Journal of biomechanical engineering* 126(6):779-786.

152. Karsenty G (2001) Minireview: Transcriptional control of osteoblast differentiation. *Endocrinology* 142(7):2731-2733.

153. Bruder SP, Jaiswal N, & Haynesworth SE (1997) Growth kinetics, self-renewal, and the osteogenic potential of purified human mesenchymal stem cells during extensive subcultivation and following cryopreservation. *Journal of Cellular Biochemistry* 64(2):278-294.

154. Meinel L, *et al.* (2005) Silk implants for the healing of critical size bone defects. *Bone* 37(5):688-698.

155. Grayson WL, *et al.* (2010) Engineering anatomically shaped human bone grafts. *Proceedings of the National Academy of Sciences* 107(8):3299-3304.

156. Jukes JM, *et al.* (2008) Endochondral bone tissue engineering using embryonic stem cells. *Proceedings of the National Academy of Sciences* 105(19):6840-6845.

157. Amini AR, Laurencin CT, & Nukavarapu SP (2012) Bone Tissue Engineering: Recent Advances and Challenges. *Critical reviews in biomedical engineering* 40(5):363-408.

158. Donath K (1988) Die Trenn-Dünnschliff-Technik zur Herstellung histologischer Präparate von nicht schneidbaren Geweben und Materialien. *Der Präparator* 34:197-206.

159. Levai JLG (1975) A simple differential staining method for semi-thin sections of ossifying cartilage and bone tissues embedded in epoxy resin. *Microscopy* 31(1-2):1-4.

160. Lian JB & Stein GS (2003) Runx2/Cbfa1: A Multifunctional Regulator of Bone Formation. *Current Pharmaceutical Design* 9(32):2677-2685.

161. Bousson V, *et al.* (2000) CT of the Middiaphyseal Femur: Cortical Bone Mineral Density and Relation to Porosity. *Radiology* 217(1):179-187.

162. Marion NW & Mao JJ (2006) Mesenchymal Stem Cells and Tissue Engineering. *Methods in Enzymology*, (Academic Press), Vol Volume 420, pp 339-361.

163. Ortega N, Behonick DJ, & Werb Z (2004) Matrix remodeling during endochondral ossification. *Trends in cell biology* 14(2):86-93.

164. Yang L, Tsang KY, Tang HC, Chan D, & Cheah KSE (2014) Hypertrophic chondrocytes can become osteoblasts and osteocytes in endochondral bone formation. *Proceedings of the National Academy of Sciences of the United States of America* 111(33):12097-12102.

165. Zhou X, *et al.* (2014) Chondrocytes Transdifferentiate into Osteoblasts in Endochondral Bone during Development, Postnatal Growth and Fracture Healing in Mice. *PLoS Genet.* 10(12):20.

166. Ilvesaro J, Metsikkö K, Väänänen K, & Tuukkanen J (1999) Polarity of Osteoblasts and Osteoblast-like UMR-108 Cells. *Journal of Bone and Mineral Research* 14(8):1338-1344.

167. Nakashima K, *et al.* (2002) The Novel Zinc Finger-Containing Transcription Factor Osterix Is Required for Osteoblast Differentiation and Bone Formation. *Cell* 108(1):17-29.

168. Paschalis EP, Betts F, DiCarlo E, Mendelsohn R, & Boskey AL (1997) FTIR microspectroscopic analysis of normal human cortical and trabecular bone. *Calcified Tissue International* 61(6):480-486.

169. Carlevaro MF, Cermelli S, Cancedda R, & Descalzi Cancedda F (2000) Vascular endothelial growth factor (VEGF) in cartilage neovascularization and chondrocyte differentiation: auto-paracrine role during endochondral bone formation. *Journal of Cell Science* 113(1):59-69.

170. Harper J & Klagsbrun M (1999) Cartilage to bone[mdash]Angiogenesis leads the way. *Nat Med* 5(6):617-618.

171. Bishop JA, Palanca AA, Bellino MJ, & Lowenberg DW (2012) Assessment of Compromised Fracture Healing. *Journal of the American Academy of Orthopaedic Surgeons* 20(5):273-282.

172. Hak DJ, *et al.* (2014) Delayed union and nonunions: Epidemiology, clinical issues, and financial aspects. *Injury* 45, Supplement 2:S3-S7.

173. Albee FH (Evolution of bone graft surgery. *The American Journal of Surgery* 63(3):421-436.

174. Langer R & Vacanti JP (1993) TISSUE ENGINEERING. *Science* 260(5110):920-926.

175. Caplan AI (2007) Adult mesenchymal stem cells for tissue engineering versus regenerative medicine. *Journal of Cellular Physiology* 213(2):341-347.

176. Jukes JM, *et al.* (2008) Endochondral bone tissue engineering using embryonic stem cells. *Proceedings of the National Academy of Sciences of the United States of America* 105(19):6840-6845.

177. Grayson WL, *et al.* (2008) Effects of Initial Seeding Density and Fluid Perfusion Rate on Formation of Tissue-Engineered Bone. *Tissue Engineering Part A* 14(11):1809-1820.

178. Chan CKF, *et al.* (2009) Endochondral ossification is required for haematopoietic stem-cell niche formation. *Nature* 457(7228):490-U499.

179. Boccaccio A & Pappalettere C (2011) *Mechanobiology of Fracture Healing: Basic Principles and Applications in Orthodontics and Orthopaedics* (INTECH Open Access Publisher).

180. Colnot C (2009) Skeletal Cell Fate Decisions Within Periosteum and Bone Marrow During Bone Regeneration. *Journal of Bone and Mineral Research* 24(2):274-282.

181. Betz OB, *et al.* (2010) The Repair of Critical-Sized Bone Defects Using Expedited, Autologous BMP-2 Gene-Activated Fat Implants. *Tissue Engineering Part A* 16(3):1093-1101.

182. Kunkel N, *et al.* (2015) Are Tendon-derived Stem Cells a Better Source for Bone Regeneration? *Tissue Engineering Part A* 21:S121-S121.

183. Strem BM, *et al.* (2005) Multipotential differentiation of adipose tissue-derived stem cells. *The Keio Journal of Medicine* 54(3):132-141.

184. Estes BT, Wu AW, & Guilak F (2006) Potent induction of chondrocytic differentiation of human adipose-derived adult stem cells by bone morphogenetic protein 6. *Arthritis & Rheumatism* 54(4):1222-1232.

185. Hennig T, *et al.* (2007) Reduced chondrogenic potential of adipose tissue derived stromal cells correlates with an altered TGFβ receptor and BMP profile and is overcome by BMP-6. *Journal of Cellular Physiology* 211(3):682-691.

PART VI

APPENDIX

A Hypertrophic Chondrocyte Differentiation of Adipose Derived Stem Cells

A.1 Hypothesis

Hypertrophic chondrocytes derived from adipose derived stem cells behave similarly to bone marrow stem cells.

A.2 Rationale

Over the course of this dissertation, the source of adult stem cells switched from bone marrow to adipose tissue. Though bone marrow stem cells (BMSCs) have been exclusively used in hypertrophic chondrocyte differentiation, adipose derived stem cells (ADSCs) exhibit similar morphology and multi-lineage potential and are more abundant and easier to access than BMSCs (183). To justify this switch from BMSCs to ADSCs, the differentiation and matrix production capabilities were compared between hypertrophic chondrocytes derived from these sources. The goal of the project was to demonstrate that hypertrophic chondrocytes could be successfully derived from ADSCs, and that they behaved similarly to BMSC-derived hypertrophic chondrocytes.

A.3 Methods

Bone marrow stem cells were obtained from Lonza (Basel, CH) from two different donors and adipose derived stem cells were obtained from two different donors at the Austrian Red Cross (Linz, AT). Cells were passaged to p4 in expansion medium containing high-glucose Dulbecco's Modified Eagle Medium (DMEM, ThermoFisher, Waltham, MA) supplemented with 10% FBS (Atlanta Biologicals, Flowery Branch, GA), 1% penicillin streptomycin (ThermoFisher,

Waltham, MA), and 1 ng/mL basic fibroblast growth factor (ThermoFisher, Waltham, MA). Cells were pelleted by placing 250,000 cells into 96 U-bottom well plates (ThermoFisher, Waltham, MA) and centrifuging at 300g for 5 minutes. During the first two weeks, pellets were cultured in chondrogenic medium consisting of high glucose DMEM, 1% penicillin streptomycin, 1% ITS+ (Corning, Corning, NY), 100 nM dexamethasone, 50 µg/mL L-proline, 100 µg/mL sodium pyruvate, 10 mM HEPES buffer (Corning, Corning, NY) 50 µg/mL ascorbic acid 2-phosphate, 10 ng/mL TGF-β3 (Peprotech, Rocky Hill, NJ). BMP6 was added to ADSC chondrogenic medium at a concentration of 10 ng/mL to improve pellet chondrogenesis (184, 185). After two weeks of chondrogenic differentiation, pellets were cultured in hypertrophic medium for three additional weeks. Hypertrophic medium had a similar recipe as chondrogenic medium, except for the reduction in dexamethasone concentration to 1 nM, removal of TGF-β3, addition of L-thyroxine at 50 ng/mL, and the addition of 5 mM sodium β-glycerophosphate. Pellets were harvested at weeks two and five of culture and analyzed for matrix composition, gene expression, and mineral deposition by µCT.

A.4 Results and Discussion

The behavior across all studied donors and time points was relatively similar. As has been previously noted, there is high donor variability for stem cells and that was evident within the samples studied in this experiment. Induced maturation to hypertrophic chondrocytes resulted in a decrease in cell number, a trend that was matched in all studies (Figure A.1).

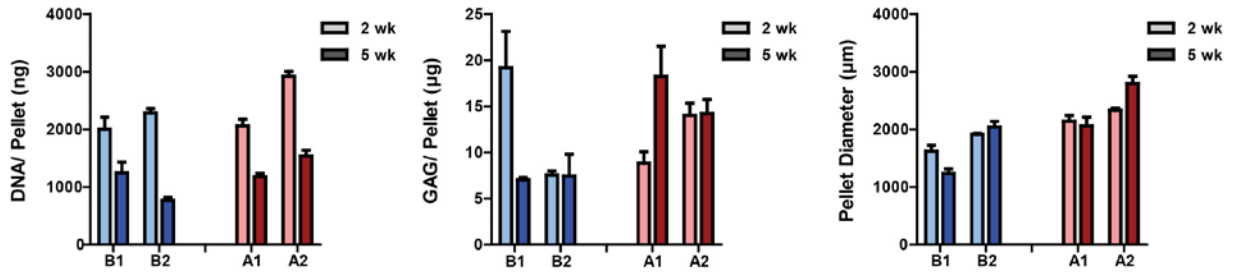

Figure A.1: Biochemical quantitation of the different cell sources and donors*. The DNA/ pellet seemed relatively similar, with the same dramatic decrease in DNA content upon the completion of hypertrophic maturation. Donor variability appeared to affect GAG content per pellet, with unusual behavior occurring in each cell source. In general, the ADSCs appeared to generate larger cell pellets per 250,000 cells. n=4.*

The amount of GAG deposition varied based on the donor, but in general, the ADSCs contained higher GAG content. The ADSCs also were generally larger in diameter than the BMSCs. Mineral deposition was something that also fluctuated more based on the donor than on the specific cell type, as was demonstrated by the three-dimensional micro computed tomography reconstructions (Figure A.2). Quantifying the amount of mineral within the pellet showed similar amounts and densities of mineral deposited.

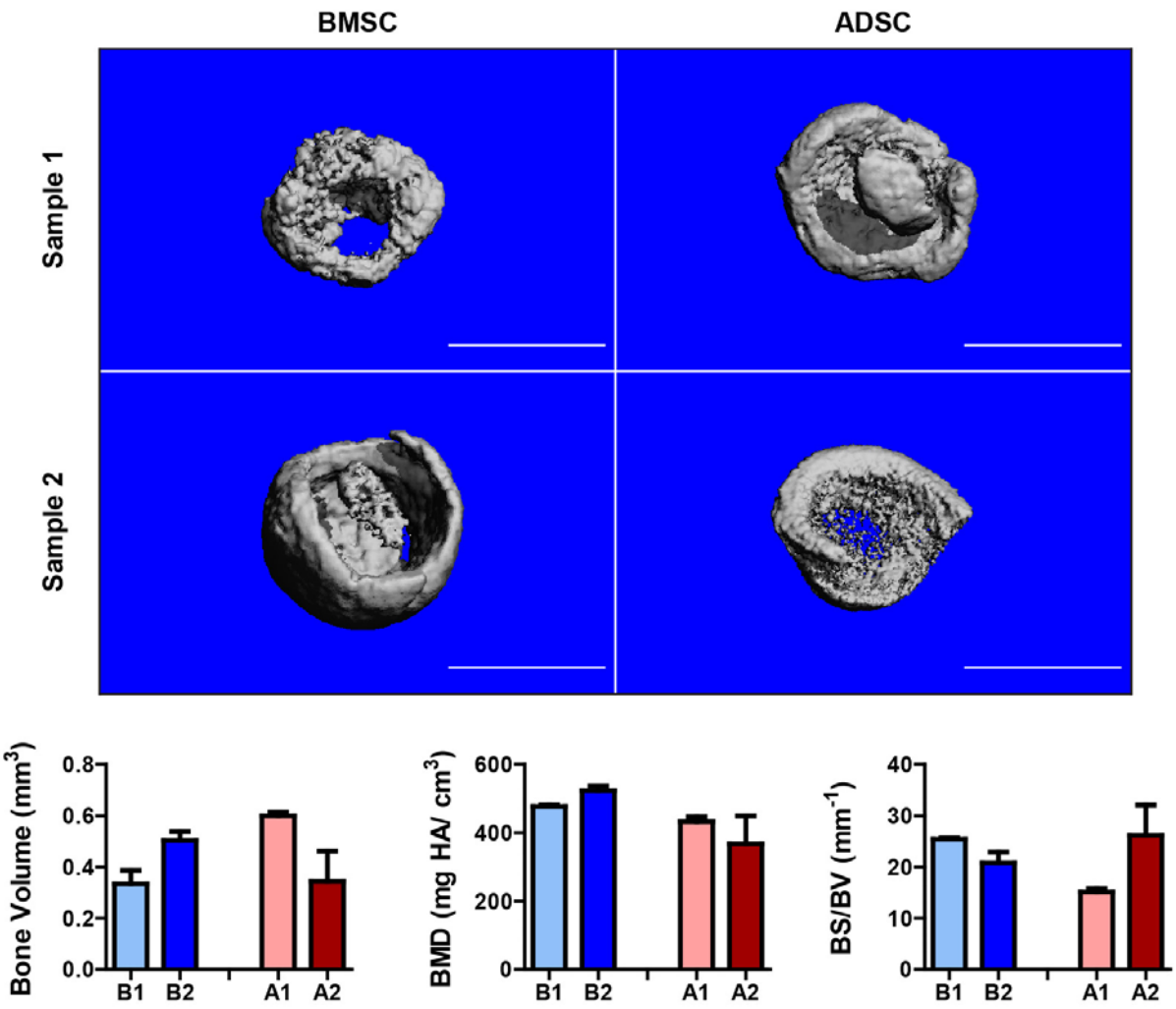

Figure A.2: Hypertrophic chondrocyte deposition of mineral*. The amount of mineral deposited appeared to be highly dependent upon the donor, but the volume and pattern of deposition appeared similar between the cell sources. Through quantitation, it appeared that the BMSCs deposit a slightly denser mineral than the ADSCs. n=4.*

Analyzing the gene expression at post-chondrogenic and post-hypertrophic medium showed no apparent differences in the expression of key chondrocyte and hypertrophic markers (Figure A.3). Expression of key genes for cartilage formation (SOX9 and COL2A1) was relatively the same with all groups. The genes utilized to gauge hypertrophic differentiation consisted of the unique hypertrophic chondrocyte collagen, collagen type X (COL10A1), a master regulator of bone production (RUNX2), and a degradative enzyme, alkaline phosphatase, that prepares

phosphates for mineral formation (ALPL). Compared to the analysis of chondrogenesis, there was more variability in hypertrophic chondrocyte expression. However, this variability appeared to be based more on donor differences than the actual stem cell source.

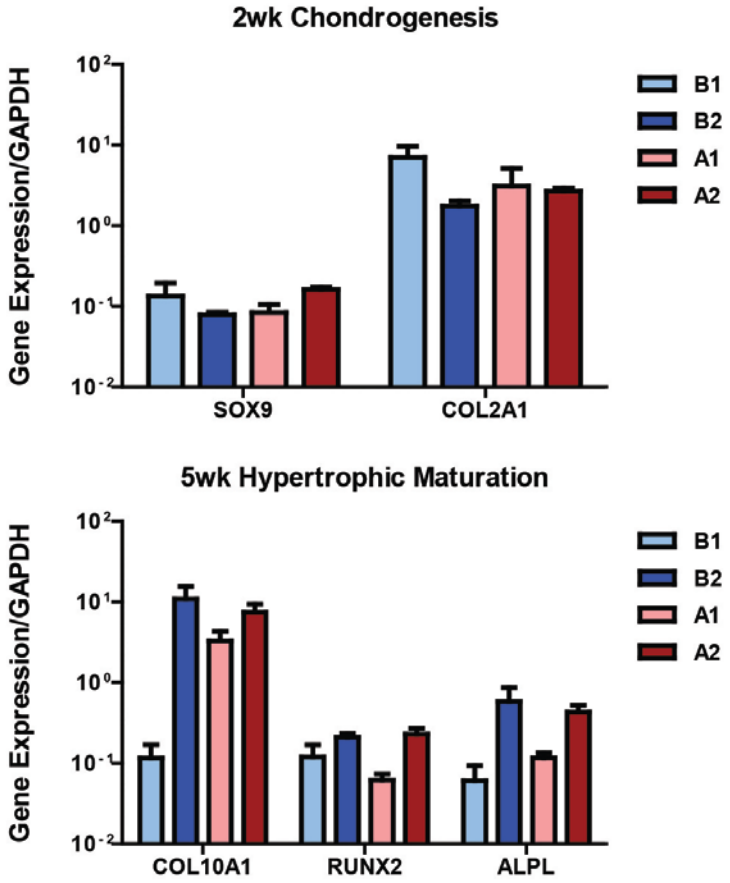

Figure A.3: Expression of chondrocyte and hypertrophic genes*. At the culmination of chondrogenic culture, the expression of key genes (SOX9 and COL2A1) was relatively similar between the cell sources and donors, without extensive variability. At the culmination of hypertrophic culture, there was much larger variability within the cell sources and amongst the donors. However, there appeared to be no consistent trends with regards to key hypertrophic chondrocyte genes (COL10A1, RUNX2, ALPL). n=4.*

A.5 CONCLUSION

Hypertrophic chondrocytes were differentiated form ADSCs, behaving in a similar manner to BMSCs. Like BMSCs, there was noticeable donor variability in the differentiation ability and matrix production, but overall trends seemed to match between the BMSCs and ADSCs. Therefore, this study demonstrates the suitability of this clinically-relevant, widely available stem cell source (ADSCs) for hypertrophic chondrocyte differentiation and bone graft formation.